EPFL

Thèse n° 7971

Accelerated Discovery of Metal-Organic Frameworks (MOFs) For Energy Related Applications

Présentée le 22 mai 2020

à la Faculté des sciences de base
Laboratoire de simulation moléculaire
Programme doctoral en chimie et génie chimique

pour l'obtention du grade de Docteur ès Sciences

par

Arunraj CHIDAMBARAM

Acceptée sur proposition du jury

Prof. A. Züttel, président du jury
Prof. B. Smit, Dr K. Stylianou, directeurs de thèse
Prof. M. van der Veen, rapporteuse
Prof. S. Garcia, rapporteuse
Prof. K. V. Agrawal, rapporteur

École polytechnique fédérale de Lausanne

2020

Acknowledgements

I would like to thank my supervisors Prof. Berend Smit and Prof. Kyriakos Stylianou for giving me this opportunity to do PhD under their tutelage.

I am thankful to the professors - Prof. Jeffrey A. Reimer and Prof. Jorge A. R. Navarro with whom I had the opportunity to collaborate and work during my PhD. I would like to thank Pete and Mohammad from the computational group for the collaboration. I am pleased to have shared the office space with my colleagues – Mish, Pelin, Alina, Bardiya, Samantha, Andrzej, Chris, Tu and Serhii. I am thankful to Pascal and Richard for their contribution. I would like to thank Evelyn, our group secretary and Constance, former group secretary for their administrative help.

I am always thankful to Liza for her guidance and constant encouragement. Last but not least, I would like to thank and acknowledge my parents, Raphael, Varsha, Manju, Trinath and Sindhuja for all their moral support, motivation, love and care.

Abstract

Metal-Organic Frameworks (MOFs) are an emerging class of materials that consist of metal ions which are linked with organic ligands *via* coordination bonds to form extended networks. MOF structures consists predominantly of open voids which makes them amongst the most porous materials synthesized to date.

The aim of this thesis is to contribute to the development of a platform for a systematic study of the influence of synthetic conditions on MOFs and thereby, assess how this can affect the surface area of MOFs. To achieve this aim, a platform that utilises high-throughput robotic synthesis guided by genetic algorithm and machine learning was devised. This led to a rational synthesis of a MOF with the highest surface area reported to date.

MOFs are considered as promising adsorbents for carbon capture from flue gasses emitted from fossil fuel fired power plants. Whilst there are many MOFs that are optimised for separation of CO_2 from N_2, their separation capability is detrimentally affected when they are subjected to realistic flue gas conditions that contains H_2O vapour. This is due to the competition between CO_2 and H_2O for the same adsorption sites. To address this, through close collaboration with computational scientists, we discovered a new class of materials for CO_2/H_2O separations.

Keywords
Metal-organic frameworks, MOFs, porous, surface area, high-throughput robotic synthesis, genetic algorithms, carbon capture, flue gas, CO_2, H_2O

Résumé

Les structures métal-organique (MOF) constituent une classe émergente de matériaux constitués d'ions métalliques liés aux ligands organiques via des liaisons de coordination pour former des réseaux étendus. Les structures MOF sont principalement composées de vides ouverts, ce qui les classe parmi les matériaux les plus poreux synthétisés à ce jour.

Le but de cette thèse est de contribuer au développement d'une plate-forme pour une étude systématique de l'influence des conditions de synthèse sur les MOF, et de ce fait, évaluez comment cela peut affecter la aire de surface des MOF. Pour atteindre cet objectif, une plate-forme utilisant une synthèse robotique à haut débit guidée par un algorithme génétique et un apprentissage automatique a été conçue. Ceci a conduit à la synthèse rationnelle d'un MOF avec la plus grande surface rapportée à ce jour.

Les MOFs sont considérés comme des adsorbants prometteurs pour la capture du carbone des gaz de combustion émis par les centrales à combustibles fossiles. Bien que de nombreux MOFs soient optimisés pour la séparation du CO_2 du N_2, leur capacité de séparation est compromise si ils sont soumis à des conditions réalistes de gaz de combustion contenant de H_2O vapeur. Cela est dû à la concurrence entre CO_2 et H_2O pour les mêmes sites d'adsorption. Pour remédier à cela, grâce à une étroite collaboration avec des scientifiques en informatique, nous avons découvert une nouvelle classe de matériaux pour les séparations CO_2/H_2O.

Mots-clés
Les structures métal-organique, MOF, poreux, aire de surface, synthèse robotique à haut débit, algorithme génétique, capture du carbone, gaz de combustion, CO_2, H_2O

Table of Contents

List of figures

List of tables

Chapter 1 Introduction

1.1. Climate change – CO_2 emissions

The ever spiralling emission levels of carbon dioxide is one of the pressing environmental concerns of ours and for the future generations to come due to its potential effects linked to global warming and climate change[1]. The United Nations Framework Convention on Climate Change (UNFCC) and the Intergovernmental Panel on Climate Change (IPCC) has recognized the necessity for the immediate reduction in fossil fuel consumption[2]. Through their regular scientific assessment reports and conventions they emphasize that anthropogenic activities of combustion of fossil fuels and emissions of greenhouse gases like CO_2 as one of the primary causes for global warming of Earth and climate change.

The rapid boom in civilization and the surge in economic development through industrialization has led to the heavy dependence on fossil fuels resulting in an acceleration of the worldwide energy demands[3]. The release of greenhouse gases is steadily increasing and are seeing new highs which were never seen before. The recent 2019 atmospheric measurement of CO_2 concentration shows that there is 414.8 ppm of CO_2 concentration which is in stark contrast with the value of 280 ppm measured from the pre-industrial era[4].

In parallel, the global temperatures which are being registered periodically shows that global warming is on its course with little slowdown in sight for the 21st century[5]. The far reaching consequences of global warming was further echoed in global mean sea level rises. Driven by the current carbon emissions, the global sea level has been projected to exceed 2 m in the case of early instability of Antarctic ice sheet. Recent studies indicated the tripling of the global vulnerability of several low lying cities and countries to sea level rise and the flooding of the coastal area[6].

These factors has led the governments both on national and international level in joint collaboration with research communities, industries and think tanks to come up with strategies for abating the emissions of greenhouse gasses and in effect, for ways to tackle the climate change. The climate talks in 2015 in Paris, COP21 agreement organized by the UNFCC is a recent example of global and collective accountability. The leaders of 195 countries pledged to reduce the greenhouse gas emissions and limit the rise in global temperature to below 2°C by the year 2100 in order to avoid serious and far reaching consequences for biodiversity and humankind. However, in 2018, the IPCC through their special report which is a summary for policy makers underlined that a global warming of 1.5°C could also result in drastic consequences. Furthermore, a net emission balance of zero has to be attained sooner than 2100[7].

Several climate action demonstrations and protests erupted across the world demanding actions and accountabilities in light of a global realization of the political inaction to curb CO_2 emissions. In response to it, many countries have revised their emission reduction targets of 2015 with Switzerland being the latest country to respond with The Swiss Federal Council aiming to transform Switzerland as a climate

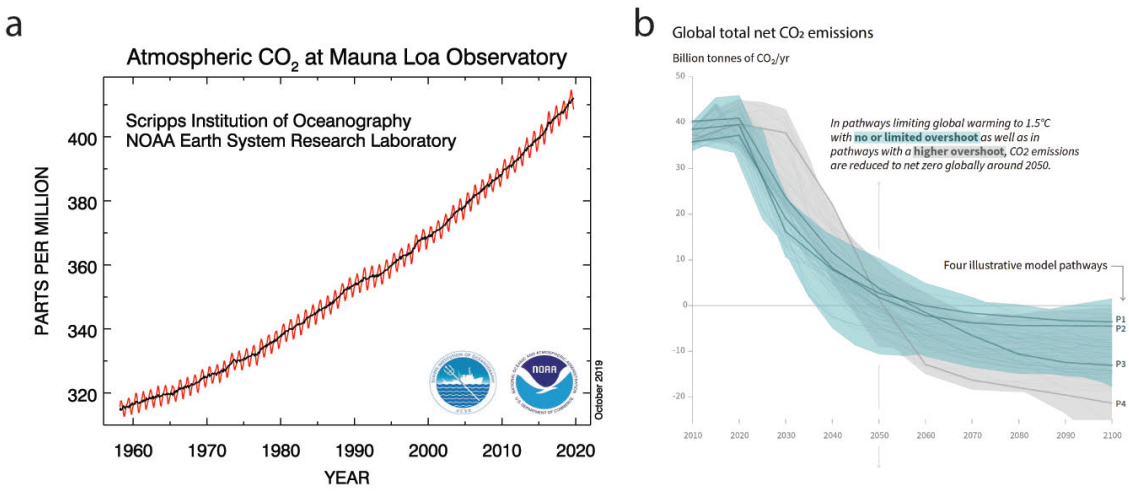

Figure 1.1: Anthropogenic CO_2 emissions

a, A graph showing the atmospheric CO_2 concentration as recorded at Mauna Loa Observatory in Hawaii. b, Global net anthropogenic CO_2 emissions in four pathways that is projected to limit the global warming to 1.5℃ with no or limited overshoot and higher overshoot; From IPCC's 2018 scientific report

neutral county by 2050. For which, use of natural CO_2 sinks such as forests, soil and technologies that can remove CO_2 from atmosphere and sequester them will be developed[8].

1.2. Carbon capture and storage (CCS)

The CO_2 emissions can be classified based on the emissions sources, i.e. distributed sources (ex. transportation) and stationary or point sources such as fossil fuel-based power plants, industrial sectors like cement, iron and steel etc. The augmented efforts in reducing the CO_2 emissions is promoted through a two-way approach of preventive and remediation methods. The former is related to the promotion of new alternative renewable energies sources such as solar, wind, biomass. Whereas, remediation approach relies on the curbing of carbon emissions in stationary sources such as thermal power plants, industrial facilities that discharges massive amounts of CO_2. In the case of remediation measures, Carbon capture and storage (CCS) is the central focus for several reasons[9-11].

CCS represents a group of technologies for CO_2 capture[12]. Following which, CO_2 is compressed, transported and permanently stored or utilized to make value-added chemicals. CCS offers the prospects to cater to the increasing energy demands for fossil fuels in the present and immediate future whilst abating the emissions of greenhouse gas which is in line with the global targets[13]. This is particularly important as in the near future, there appears to be a little probability of a global slowdown of CO_2 emissions[14]. The other reason is the highly challengeable development of alternative clean energy sources. For instance, hydrogen has been widely acknowledged as the energy carrier of the future which is believed as the long-

term answer for the question of what could be the alternative global energy supply. However, the current infrastructure for the production and storage of hydrogen is challenging[15].

Proposed by IPCC, CCS is a technology that is essential to curtail the growth of CO_2 concentration in the atmosphere. It is considered as one of the very attractive options in the mitigation portfolios of IPCC as it has number of advantages to its credit[11]. First, the integration of CCS into the existing energy systems without the necessity for large changes to the system itself is possible. Thus, retrofitting of CCS to large stationary sources such as fossil fuel based power stations, cement plants is feasible. In addition, CCS is a workable option for accelerating the drive towards decarbonisation of energy sector and emission intensive industries. The decarbonisation of the industrial sectors which account for 25% of the global CO_2 emissions including cement, iron and steel manufacturing, petrochemicals are vital to meet the CO_2 emissions targets by IPCC[16]. In this regard, CCS is considered as a cost effective option to abate the CO_2 industrial emissions. And thirdly, CCS can be combined with negative emission technologies for phasing in the use of low-carbon or carbon-neutral bioenergy systems (BECCS)[17].

Furthermore, CCS occupies an advantageous position on comparison with intermittent renewable energy sources (IRES) such as photovoltaic (PV) and wind power. The three main factors that are considered to restrain the deployment of IRES are 1) Lack of displacement of firm capacity on an one for one basis by IRES[18], 2) intermittent output based on a seasonal conditions and the relatively unpredictable factor associated with their output demand, 3) market cannibalization – the effect of decreasing market value that happens with the increased production of IRE[11]. This is due to the offset between the supply and demand. For example, highest production of energy from IRES does not necessarily correlate with the peak electricity requirement which could lead to the reduction in their market value. Thus, to achieve the decarbonisation targets of energy sector, it is increasingly being recognized that IRES in the system should be balanced with firm capacity technologies like fossil CCS, nuclear. This way dependable low or neutral carbon electricity can be generated. In additional, other options such as geothermal, reservoir hydro power, solar plus energy storage facility in an expected sunny climate are expected to be competing with the CCS to provide firm capacity and not IRES on their own.

Though CCS technologies are regarded as an essential approach in reducing carbon emissions, we are yet to see rapid commercial large-scale deployment of CCS projects. There are only 43 major large scale CCS projects in different stages of deployment. Of the 43, only 18 are in operational stage. Whereas, 5 of them are in construction phase and the reminder of them are in various stages of development[19]. Amongst the 43 projects, the majority of the projects are located in The United States.

Deployment of CCS involves a collaborative effort that requires effective contributions from various stakeholders such as governments, policy makers, venture capitalists, scientists, engineers. Factors such as safe financial funding as well as support through policies and legislative frameworks are the essentials for CCS projects to reach the operational phase[20]. And, the availability of safe geological storage is fundamentally essential for any CCS project to be successful[21]. These factors explain on why the capture of CO_2 is considered as one of the biggest challenges for the 21st century[1]. This was confirmed by a study

by the International Energy Agency (IEA) wherein they assessed the progress of CCS over the past two decades and concluded that the current progress rate is not in line of what is required for climate goals achievement[22].

Other studies tend to explain this little deployment of CCS from the perceived notions concerning its safety. The slow deployment is further exacerbated by the fear that CCS will tend to extend the reliance on fossil fuels. Thus, it could be an obstacle to larger implementation and utilization of renewable power[23]. However, the future looks promising for the CCS technology. A study presented by Koelbl et al.[24], find that the share in primary energy for CCS is mostly bound to be higher in the second half of this century compared to the first half. According to their studies, the authors report through their integrated assessment models (IAMs) CCS can consistently capture a minimum of 600 Gt of CO_2 until 2100 which could be fulfilling the 2°C target.

It is evident that the various components of the process chain of CCS such as the transport and storage of CO_2 with on-shore and off-shore pipelines are technologically mature with a technology readiness level (TRL) of 9[11]. Whereas, CO_2 storage in depleted oil and gas fields or utilisation for enhanced oil recovery are at the demonstration phase (TRL 7). Herein, TRL refers to a 9-point scaling system which is a qualitative assessment of the maturity level of a technology. The technology readiness of transport and storage required for CCS thus shifts the focus toward the capture phase that represents nearly two-thirds of the total cost for the CCS[25].

Whilst, majority of the capture technologies are either in pilot plant or demonstration steps, the reason for them being not commercialized yet could be attributed to two reasons. The capture cost which is interconnected with the regeneration energy (energy required to strip the CO_2 from the capture material) and the separation efficiency of the capture material for CO_2 over other components of the gas mixture. The enhancement of the separation efficiency and establishment of the technologies that are low in electrical energy requirements for regeneration is considered as the utmost essential for significantly reducing the overall cost associated with the carbon capture phase. This thesis focusses entirely on the carbon capture component of the CCS technology.

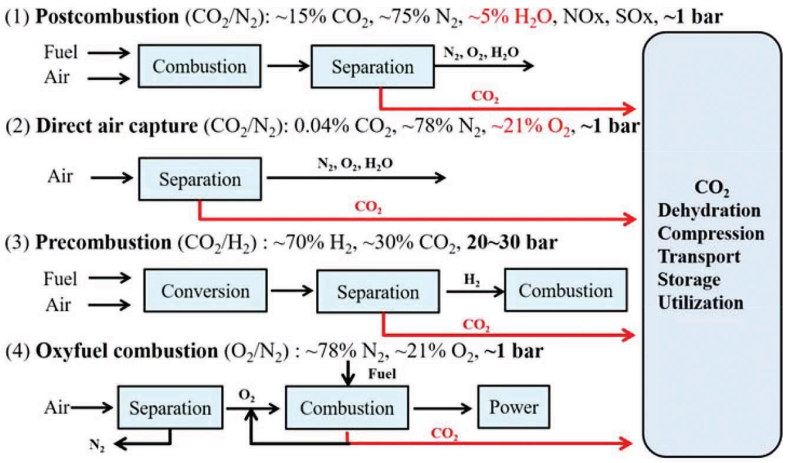

Figure 1.2: A schematic illustration of different carbon capture processes.

The image is adapted from [26]

1.3. Carbon capture processes

The carbon capture processes are primarily directed towards the large stationary sources such as fossil fuel fired power plants. The IPCC through their estimates based on their IAMs suggest that the carbon emissions could be reduced by 80-90% for a conventional power plant equipped with CCS [11,27]. The significance of CCS is understood when the lifetime of a fossil fuel fired power plant is considered as it can have a lifetime of 40 years. In general, depending on the combustion of fossil fuel such as coal or natural gas for power generation, the carbon capture processes can be classified as: postcombustion capture, precombustion capture, oxyfuel combustion capture.

Postcombustion capture is currently the most matured carbon capture process. It involves the separation of CO_2 from N_2 which is predominantly present in the flue gas after the fuel combustion. The CO_2 concentration in flue gas varies depending on whether natural gas or coal is combusted. It is ~4 vol% for a natural gas power plant and 10-15 vol% for a coal fired combustion plant[28]. This process allows the provisions for a number of carbon capture technologies to be utilized as the existing facilities for combustion need not be modified. Thus, the benefit of directly using it in current power plants by retrofitting is possible. The flue gas is typically in atmospheric pressure range with CO_2 capture occurring at lower partial pressures. Normally, the flue gas is treated for desulphurization as it is obligatory by law in several countries.

Hitherto, large-scale postcombustion CO_2 separation processes have mainly been with absorption technology with liquid amine as the absorbent[29]. The amine scrubbing technology have been well developed over the past 50 years and it is commercialized with the TRL value of 9. In recent years, there has been a significant efforts in finding an alternative to amine scrubbing such as adsorption, cryogenic separation, and membrane based separation technologies.

Precombustion capture involves a series of conversions of the fossil fuel into various gases before combustion. They are typically used when the starting fuel is natural gas. The process involves a three step conversion wherein, the methane rich fuel is reacted at high pressure and temperature to give synthesis gas or syngas stream containing CO, CO_2 and H_2. The CO is subsequently converted in a water-gas shift reactor to produce H_2 and CO_2. Subsequently, the CO_2 is separated prior to the combustion stage to produce high purity H_2 devoid of any CO_2.The advantage of precombustion process is that the CO_2 capture is easier in this process compared to postcombustion process as CO_2 concentration ranges from 15-60% with elevated pressures[30]. The technologies that are used for this process are physical solvents and they are favoured over chemical solvents especially when there is high concentration of acid gas. In addition, membrane separation technology is preferred for this process for their scalability, low energy cost, easier operation although sorption based technology is feasible[31].

Another option to reduce CO_2 emission is through oxyfuel combustion. They form the basis for zero emission cycle that are regarded as more promising for new installations than the existing postcombustion power plants[32]. The process here involves the burning of coal or natural gas in pure oxygen to yield a flue gas consisting principally of CO_2 (>90%) and some water vapour along with small amounts of NO_x and SO_x. In addition, part of the combustion gases is normally recirculated. The complete removal or the reduction of the inert gas content (N_2) in the inlet stream to the furnace increases the thermal efficiency of the boiler unit. Through this process, CO_2 capture is not needed as it facilitates the easy condensation of water vapour from the flue gas. The drawback of this process is the operating cost of cryogenic air separation units to remove N_2 and the energy efficiency needed to get pure O_2. However, it is expected that this cost could be mitigated by the elimination of the necessity for CO_2 capture. Oxygen selective membranes are considered as an alternative technology to cryogenic air separation.

The IPCC and the COP21 Paris agreement have identified the necessity for negative carbon emissions such as bioenergy based carbon capture and storage (BECCS) and direct air capture (DAC). In DAC, CO_2 of 0.04 vol% is directly extracted from air in ambient conditions[33]. Sorbent based technologies are widely used for this process. The potential of mitigating CO_2 emissions from distributed and point sources is regarded as the biggest merit of DAC. This is in direct contrast to the carbon capture processes from stationary large point sources as described above. In addition, DAC processes are not location specific as the DAC facility can be set up anywhere and they do not encounter the possibilities of facing the SO_x, NO_x, contaminants in flue gas. The prevailing possibility of higher cost in removing CO_2 compared to flue gas processes has to be allayed for DAC to be developed and deployed commercially. This is owed to the very low CO_2 content in atmosphere.

1.4. Carbon capture technologies

The aim of this section is to give a broad literature overview of the carbon capture technologies that are researched and developed for the above described carbon capture processes. They are solvent absorption with amines, adsorption technology explained with solid sorbents such as zeolites, activated carbons and

metal-organic frameworks (MOFs). Furthermore, MOFs are introduced and described elaborately as this thesis focussed solely on MOF materials. Other technologies such as membrane separation, cryogenic fractionation, chemical looping etc. and sorbents such as ionic liquids, mesoporous silica, hydrotalcites etc. are not discussed here as they are beyond the scope of this PhD thesis.

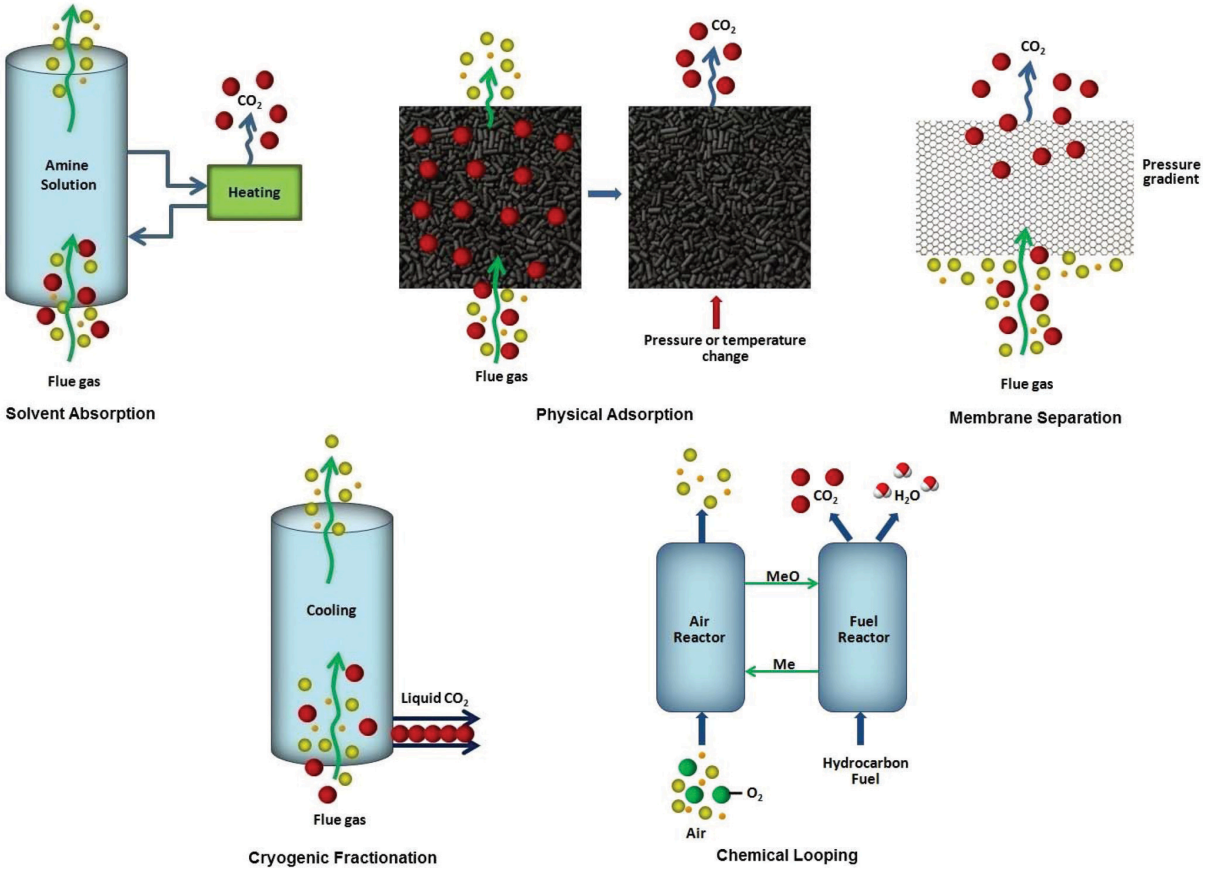

Figure 1.3: A schematic illustration of different carbon capture technologies

The image was reproduced from[34] - Published by The Royal Society of Chemistry

1.4.1. Solvent absorption

a. Amine aqueous solvents

The benchmark CO_2 capture technology for postcombustion process is 20-30 wt% aqueous monoethanolamine (MEA), the classical chemical absorbent. In 1930, it was proposed in a patent to separate acidic gasses[35]. The MEA based liquid phase chemisorption technology is the only carbon capture technology that is industrially matured, commercialized and have been employed for over 50 years. Based

on this technology, many plants currently remove CO_2 from natural gas, hydrogen, and other gasses which has minimal oxygen.

In a typical process, the aqueous amine solution passes from the top of an absorption tower. Whilst, the flue gas stream containing CO_2 (10-15 kPa) is introduced at the bottom at 40 °C with the aid of a blower. The process results in 90% of CO_2 removal from the flue gas through the formation of carbamate. Then,

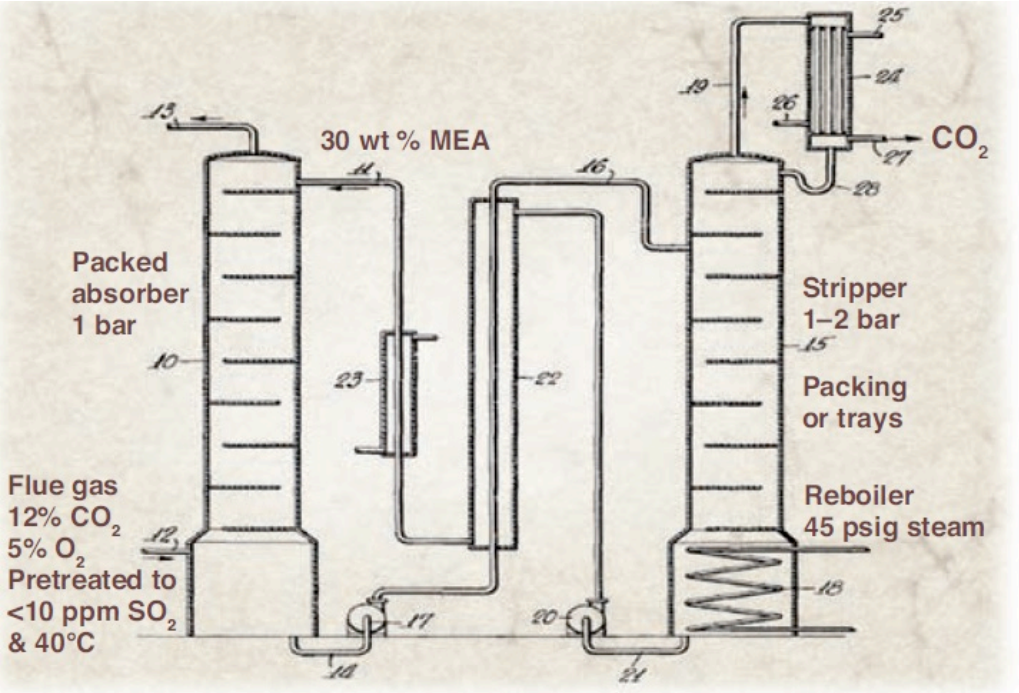

Figure 1.4: The scrubbing process

Invented by Bottoms[35]. From [29]. Reprinted with permission from AAAS

the CO_2 rich aqueous amine solution passes to the stripping tower wherein, the mixture is heated with steam to liberate the absorbed CO_2 by breaking the covalent bond at temperatures of 100-140°C. Subsequently, the regenerated amine solution is recycled back to the absorption tower for CO_2 absorption. The high heat of formation (100 kJ mol^{-1}) for the carbamate production results in a significant energy penalty for the regeneration of the absorbent. The typical minimum stripper reboiler duties being 3.6-4.0 GJ per ton of captured CO_2[36].

Estimates shows that an energy penalty of 20-30% of the output will be incurred by the power plant if MEA based amine scrubbing is retrofitted for carbon capture. This can be up to 70% of the total operating costs[29]. It has led to the ongoing research of finding alternative chemical or physical absorbents, adsorbents. The primary objective being the reduction in the regeneration energy requirements and thereby, limiting the costs of electricity production[26,37]. In addition, MEA suffers from oxidative and

thermal degradation due to the presence of residual oxygen in the flue stream. The corrosivity and the reasonable levels of toxicity are some of the other characteristics of MEA which are considered as major limitations.

To date, many aqueous solutions of primary, secondary and tertiary amines have been tested and or employed such as diethanolamine (DEA), methyldiethanolamine (MDEA), ethylenediamine (EDA), piperazine (PZ)[38]. Primary and secondary amines mainly react with CO_2 to give a carbamate or bicarbonate as reaction product. Whereas, tertiary amines do not form a carbamate.

b. Inorganic and physical solvents

Inorganic chemical absorbents such as aqueous potassium carbonate, aqueous sodium carbonate, and aqueous ammonia are also considered and researched as alternatives for MEA. The aqueous ammonia solutions react with CO_2 to form bicarbonate and ammonium ions[39,40]. Unlike the conventional amine solvents, they are thermally and oxidatively stable, non-corrosive and has comparatively lower reboiler energy requirements for stripping (2-3.0 GJ per ton of captured CO_2). However, the challenges are associated with tackling the solid formation as ammonium carbamate or ammonium bicarbonate precipitate out at low temperatures of 0-10°C. Although, it has lower reboiler duty than MEA, the considerable changes in the process design to include solid separation equipment, heat exchangers are seen as additional complications[38]. Aqueous potassium carbonate solutions differ from the ammonia solutions with their higher operating temperatures[41]. But, here the major challenge is the observation of poor CO_2 mass transfer with pilot plant studies indicating an absorption of only 20-25% of the CO_2 from the flue gas.

Physical solvents such as Selexol (mixture of dimethyl ethers of polyethylene glycol, operating temperature of 5-40°C), Rectisol (cold methanol at -40°C) are considered as alternatives to chemical absorbents[42,43]. They possess the advantage of commercial availability and industrially maturity with applications in natural gas sweetening, synthesis gas treatment at higher feed gas pressure. Their physical absorption of CO_2 also explains their reduced capacity at lower feed gas pressures compared to chemical amine solvents. Consequently, lesser electrical energy is required for regeneration than the amine scrubbing processes. Owing to the high solubility of water in the Selexol solvent, the partial pressure of water vapour in the feed gas has to be kept minimal as possible in order to avoid the impairment of CO_2 absorption capacity.

Overall, many new generation of chemical and physical absorbents are being developed at the bench scale. They are benchmarked against the MEA for their characteristics with special emphasis on their electrical energy requirements for the regeneration. This ongoing research and development for number of decades has enabled the identification of new absorbents whose performance characteristics are better than MEA in some or all.

1.4.2. Adsorption

Significant efforts are directed in researching and establishing new materials in lieu of conventional solvent absorbents that are held back by the energy intensive regeneration step and of chemical degradation issues[44-47]. The adsorption technology for carbon capture were considered in the early 1990's[48,49]. Solid physical adsorbents either in packed or fluidized bed configuration with pressure and/or temperature swing cyclic adsorption processes are considered as an alternative to solvent absorption processes for carbon capture. Traditional adsorbents such as zeolites, activated carbons are industrially mature and relevant with widespread applications in petrochemical industries in separation, purification, production, catalysis, etc. This is reflected on the estimate for adsorbent materials in global markets with roughly $11.1 billion in 2019, a 38% increase than in 2013[26].

Adsorption technology is considered to be more attractive for the following reasons[11]. They possess significant advantages for energy efficiency compared with absorption. Although, there is no straightforward and comprehensive way to ascertain the energetics and economics of adsorption and absorption, many performance metrics indicate cost reduction by adsorption. The technology offers the flexibility of a wide range of process operating conditions which ensures the utilization of low, medium and high temperature adsorbents for precombustion and postcombustion processes. This facilitates the research and development of plethora of adsorbents for targeted applications. On comparison with amine based solvents, adsorbents possess minimal environmental footprint with negligible chances of decomposition and forming corrosive and/or toxic compounds.

The fundamental working difference between absorption and adsorption is that in the former, CO_2 molecules dissolve in the bulk of the solvents in absorption. Whereas, in adsorption, it is either physisorption - van der Waals interactions or chemisorption with covalent bond formations between the CO_2 molecules and the surface of the material. The regeneration of the CO_2 loaded solid sorbent is performed by the application of temperature, pressure or vacuum swing cycles to remove the CO_2.

1.4.2.1. Cyclic adsorption processes

In an adsorbent based CO_2 capture process, regeneration of the adsorbent after each adsorption cycle is a must. Typically, regeneration is achieved by Pressure Swing Adsorption (PSA), Vacuum Swing Adsorption (VSA), Temperature Swing Adsorption (TSA) or some combination of these processes[50]. In all of them, the solid adsorbent is expected to be packed into a column and the adsorbed CO_2 from the flue gas would be desorbed by increasing the temperature or decreasing the pressure of the bed. These processes are considered as industrially established technologies and they have been employed for a number of gas separation applications.

The maturity and advancement in cyclic processes is considered to step up the commercialization potential of adsorption technology for carbon capture. In general, the regeneration processes are tailored to match

the properties of the adsorbent which requires the optimization of the process parameters such as temperature for desorption, inlet or outlet pressure. The purity of the CO_2 and the recovery value are the metrics that suggests the efficiency of these processes for carbon capture. The CO_2 purity is highly dependent on the regeneration temperature or blown down pressure in the case of PSA.

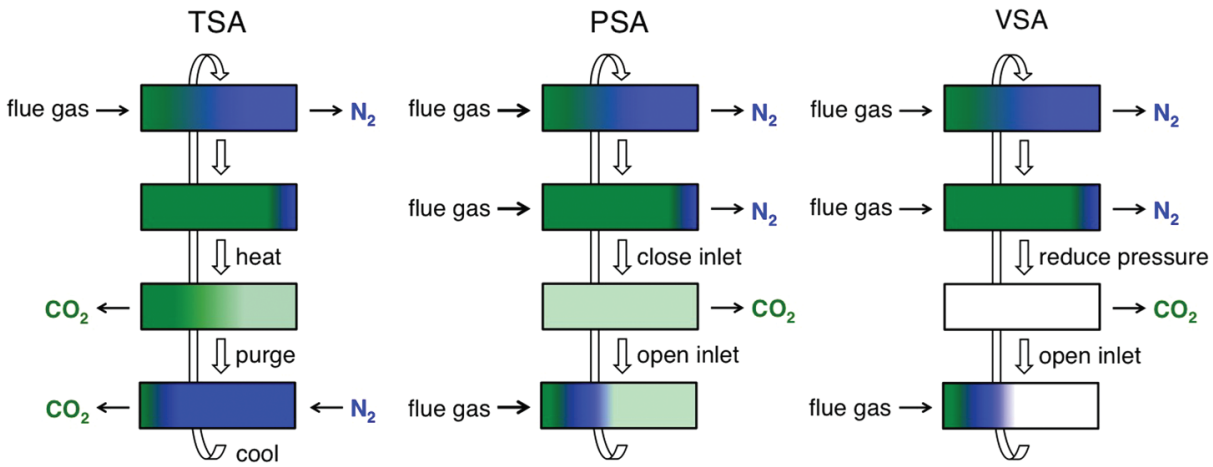

Figure 1.5: The different cyclic adsorption processes

Reprinted (adapted) with permission from[47]. Copyright (2012) American Chemical Society

a. Temperature swing adsorption (TSA)

It has been widely used in air separation units (ASU) to remove water and CO_2 from air and in dehydration of natural gas prior to liquefaction. Numerous studies have been reported for a lab-scale demonstration[51-53]. It is considered as promising due to the availability of low grade heat from power plants that could be used to thermally regenerate the CO_2 laden sorbent bed[54]. In a typical TSA cycle, the saturated bed is heated to the optimal desorption temperature of the sorbent material employed which causes the adsorbed gas molecules to desorb. A purge is used after the attainment of equilibrium at the desorption temperature and after no more of adsorbed gas leaves the column. The purge fills the void spaces of the bed and it is continued until the purity of the eluted gas drops below a certain level. Then, the sorbent bed is cooled and the next adsorption cycle commences.

Packed bed is the conventional TSA configuration. They have long cycle times because of long heating and cooling requirements which is a significant penalty[11]. As an alternative, fluidized bed configurations are tested. Herein, the heat transfer limitations of packed bed configuration are dealt by strong mixing that facilitates rapid heat transfer. Studies also show that this leads to lower CO_2 uptakes. SARC, swing adsorption reaction cluster is proposed as a variant of the fluidized bed process in which several fluidized bed adsorbers with counter-current operation are employed[55].

b. Pressure swing adsorption, Vacuum swing adsorption

In PSA, the inlet gas stream is pressurized (8 to 28 bar) and fed to the column until saturation of the sorbent bed. Then, the inlet feed gas valve is closed which reduces the column pressure to ambient pressure. This change in pressure causes significant quantities of adsorbates to desorb and elute from the column. In a similar manner, VSA applies sub-atmospheric pressure after adsorption which desorbs the adsorbates. The energy requirements for VSA or PSA process such as vacuum pump or that of a compressor are expected to increase the energy penalty and the cost of the captured CO_2. Overall, it is more likely that these processes will be applied for gasses which have higher CO_2 partial pressures like precombustion, cement, steel processes[56].

1.4.2.2. Metrics for adsorbent evaluation

Carbon capture with adsorption is prominent field as the number of potential adsorbent materials that are reported for carbon capture is enormous. However, only some of them have reached the demonstration stage and none are commercialized yet. There are many plausible reasons for this gap. First, it is an uphill challenge to synthesize and test all the adsorbents. It is further complicated by the lack of industrial maturity for certain adsorbents. Third, not all the adsorbents that are reported are evaluated for the vast number of performance parameters. It makes it insufficient for acquiring the technical confidence that is essential for a lab scale technology to move to higher technology readiness levels (TRLs). This explains the large scale screening complexity that these adsorbents possess.

In addition, the knowledge and the knowhow on mass transfer resistance and diffusional limitations encountered by CO_2 and other gases in solid adsorbent materials are scarce. This increases the complexity further as these information is required to model a complete adsorption process. This calls for a multi-disciplinary combinatorial approach through which researchers can combine the experimental data, knowledge with molecular simulation and process modelling. This should facilitate the inclusion of multiple objective optimization for a quantitative comparison of adsorbents for a number of performance evaluation criteria which are discussed below.

a. CO_2 adsorptive capacity and working capacity

The CO_2 capture by the adsorbent material is reported in terms of the adsorptive capacity from CO_2 adsorption isotherm. It is the most widely used evaluation tool for CO_2 capture in literature. Adsorptive capacity serves as the initial screening tool and there are two different ways in reporting them. Through gravimetric CO_2 uptake (mmol/g or mol/kg), the information on the quantity of the CO_2 adsorbed within a unit mass of the adsorbent is obtained. Similarly, the volumetric capacity (mol/m^3) refers to how densely CO_2 can be adsorbed within a unit mass of the adsorbent material. They crucially influence the mass and the volume of the adsorbent bed required. Both the parameters are crucial in designing the adsorption

separation applications. Overall, an adsorbent with higher Brunauer-Emmett-Teller (BET) surface area (m^2/g) leads to a higher CO_2 uptake capacity, but not essentially a higher adsorptive selectivity over other components of the feed gas.

Working capacity is an important metric that indicates the separation capabilities of the adsorbents when employed in a real PSA, VSA cyclic processes. It is defined as the difference in the amounts of CO_2 that is adsorbed at the adsorption pressure and the desorption pressure. It corresponds to the actual amount of CO_2 that can be captured in one full cycle of adsorption and desorption. Higher the working capacity, larger is the amount of the feed gas that can be treated with a given amount of adsorbent and certain period of time. Ideally, it should be calculated using mixture adsorption data to get the accurate value of working capacity.

b. Enthalpy of adsorption (Q_{st})

The design of the regeneration process is highly dictated by the quantitative interactions between the adsorbate and the adsorbent. Ascertaining it is highly essential as finding alternatives with lower regeneration energy requirements than the conventional MEA solvent is one of the main driving forces. The magnitude of the enthalpy of adsorption displays the affinity of the sorbent towards CO_2 and the adsorptive selectivity. In other words, it gives an indication of the strength of CO_2 binding. For instance, if the magnitude of the enthalpy of adsorption is too high it suggests that the sorbent has strong interactions with CO_2 and that it will require large amount of energy to break the sorbent-CO_2 interactions. To the contrary, if the value is lower it indicates that the material would be easily regenerated. However, the purity of the captured CO_2 would be lowered due to the decreased adsorptive selectivity and it warrants the increase of volume of adsorbent beds.

The enthalpy of adsorption is often expressed as Isosteric heat of adsorption (Q_{st}) as a function of the quantity of the adsorbed CO_2 (kJ/mol). It describes the average enthalpy of adsorption for an adsorbing CO_2 molecule at a specific surface coverage. It is evaluated using the Clausius-Clapeyron equation with two or more CO_2 adsorption isotherms collected inside 10 K of each other. The Q_{st} calculated at zero coverage is of further interest as it gives the strength of the strongest binding sites for CO_2 within the adsorbent.

c. Adsorption selectivity

A sorbent exhibiting high selectivity for CO_2 over the other components of the (flue) gas mixture is highly essential in CO_2 capture applications. It is another key assessment tool in screening the adsorbent materials. The adsorption selectivity of sorbent for component 1 (CO_2) over component 2 (N_2 or CH_4) is defined as the ratio of their uptakes at equilibrium conditions to the ratio of their molar fractions of the bulk phase. The adsorptive selectivity, a thermodynamic separation arises because of the differences in affinity for their adsorption on the pore surface. The most primary method for determining the adsorptive

selectivity is the calculation of the selectivity factor from the experimental single component adsorption isotherms of CO_2 and N_2. The key factor that has to be considered is the balance between the strong affinity for removing the required component from the gas mixture like CO_2 and the energy consumption required for regenerating the CO_2 laden sorbent.

There are different mechanisms for adsorptive separation which include 1) the molecular sieving effect, distinguishing capability of the sorbent materials based upon the size or shape of certain components of the gas mixture; 2) the preferential interactions between the adsorbate and the surface which induces the thermodynamic equilibrium effect; 3) differences in the diffusion rates induced separation called as the kinetic effect. In practice, adsorptive selectivity from experimental single component isotherms is not an ideal adsorbent evaluation criterion as it does not reflect the reality like that of a cyclic PSA or VSA processes wherein, a mixture of different components will be present. However, as the experimental method of obtaining the multi component isotherms is difficult, many research groups use the single component gas isotherms for selectivity calculations that is less accurate.

d. Regenerability

The ratio of the working capacity and the amount adsorbed at the adsorption pressure is defined as regenerability. Given, the enormous magnitude of the global CO_2 emissions, any chemical that is employed to capture CO_2 will rapidly deplete its global reserves and supplies if it is used for one-time. Thus, it underlines the obligation that the capture materials must be regenerable. Therefore, the energy required to regenerate the material is highly essential in ascertaining the efficiency and the cost.

e. Robustness – Thermal, Chemical, hydrolytic

The study of structural rigidity - chemical and thermal stability of the adsorbents is highly essential as they highly correlate to the cyclic stability (recyclability) when employed for thousands of cycles in separation process. For example, designing a TSA process for an adsorbent with low thermal stability could be problematical. Equally important is the mechanical robustness of these separation materials as few perturbations to the structural or chemical features under high mechanical pressure could affect their performance. This is particularly important for fixed bed configuration which requires a dense packing of the adsorbent bed. The water stability of the adsorbent materials is required for applications like postcombustion where significant amount of water is present in the incoming flue gas stream. Though the primary challenge of carbon capture from a postcombustion process is to separate CO_2 from N_2, the flue gas is saturated with 5-7 vol% of water. Studies suggest that the dehydration of the flue gas prior to carbon capture is not a feasible option for large scale adsorption. As addition of new column invites additional costs by adding 2-3 GJ per t_{CO_2} to the energy requirement[11]. Therefore, it is highly indispensable for the lab scale assessment of CO_2 capture performance of the adsorbents in the presence of water vapour.

f. Breakthrough measurements

In a real world CO_2 capture system, under practical fluid flow conditions, the flue gas mixture will pass through the packed adsorbent bed. Henceforth, dynamic column breakthrough experiments can provide information on the gas separation capabilities of the adsorbents in a laboratory demonstration prior to scale up and designing of the processes. Principally, the coupling of volumetric or a gravimetric apparatus with a gas chromatograph or mass spectrometer enables the measurement of co-adsorption of the components of the gas mixture. Owing to the lack of readily and commercially available breakthrough equipment such tests are performed with in-house fabricated setups.

Herein, the gas mixture of desired flue gas conditions flows through the column packed with the adsorbent material. The downstream composition of the gas stream is monitored which will consist predominantly of the gas component that has low affinity for the adsorbent like N_2 until the bed is saturated with strongly and preferentially adsorbed CO_2. Consequently, the breakthrough of CO_2 occurs with the downstream composition eventually correlating with the inlet, upstream composition. Many factors influence the breakthrough experiments such as the multicomponent adsorption capacities, the size and shape of the column, flow rates of the gas, packing of the adsorbent, mass and height of the adsorbent bed, operating pressure and temperature, etc.

g. Parasitic energy

Parasitic energy is a computational tool to screen large databases of crystalline adsorbent materials for identifying the most energy efficient materials for CO_2 separation from flue gas[57,58]. The objective here is to identify the material that has the minimal energy load which is additionally imposed on a power plant when integrated with CCS facility. It is calculated based on the energy required to remove the CO_2 gas from the material through thermal regeneration process and the energy needed to compress the CO_2 to transportation conditions. The generated steam from the power plants is assumed as the heat source and the electricity that is produced is utilized for the compressors. It requires the values such as Q_{st}, selectivity and working capacities of gas mixtures which is computationally calculated. This is a pragmatic approach as synthesizing, characterizing and testing the adsorbents for CO_2 separation through breakthrough studies is a tedious and daunting process. This computational performance metric is applicable and limited to only crystalline adsorbents such as zeolites and metal-organic frameworks (MOFs).

An ideal, hypothetical adsorbent can be defined as the one with large adsorption capacity, highly robust with infinite regenerability, and a flexible operating conditions. However, in reality, all adsorbents have trade-offs. Thus, an adsorbent which is practical and works effectively within an efficient carbon separation process is considered as a winning adsorbent.

1.4.2.3. Adsorbents for carbon capture

This section focusses on the various CO_2 adsorbents which can be categorized into the following groups of zeolites, activated carbons and metal-organic frameworks (MOFs). Their characteristics, strengths and weaknesses in the context of CO_2 capture are summarized.

a. Zeolites

Literature review suggests that the zeolites are amongst the most extensively reported adsorbents for CO_2 capture. They are a class of crystalline and porous aluminosilicate minerals built of a periodic array of TO_4 octahedra (T = Si or Al). The International Zeolite Association (IZA) has indexed 248 unique zeolites[59] with a structure code to identify each one of them. In addition, there are 40 naturally occurring zeolites.

Zeolites interact primarily with CO_2 through the exchangeable cations present in the pore space. These exchangeable cations are introduced in the pores to charge compensate the negative framework charges. The CO_2 adsorption in zeolites is identified to take place through physisorption as the dominant process. It is heavily influenced by the electric field that is generated by the charge compensating cations in the pore spaces. Therefore, in this sense, CO_2 adsorption properties of zeolites is directed by the framework structure, the Si/Al ratio and the location of cations in the framework[60-62]. In particular, the contribution of aluminium content and the type of cation is more as studies show that the zeolite with the maximum aluminium amount and the cations with highest base strength exhibiting the maximum CO_2 adsorption. In addition, to explore further on the cation based interactions with CO_2, two phenomena have been reported such as dual cation site[61] and cation gating effect[63]. In the former, CO_2 adsorption is favoured by enabling simultaneous interaction with two cation sites and whereas, in the case of latter, only molecules that are able to interact with the cations at the entrance of the pore channel can permeate through further and be adsorbed.

The porous characteristics of zeolites also influence the CO_2 adsorption. From a comparative study of zeolites of varying pore diameter and volume, zeolite 13X was observed to have the highest adsorption capacity[64]. The synthetic zeolite 13X is considered as the benchmark material of CO_2 adsorbents from the class of zeolites. It has an uptake capacity of about 3 mmol g^{-1} at 0.15 bar and 313 K. A screening study that evaluated different synthetic zeolites based on their CO_2 isotherms for their CO_2 uptake capacity revealed that the zeolites exhibited a wide range of capacities from 1.2 to 4.5 mmol g^{-1} at 295 K and 1 bar. It was credited to the composition and the type of cations[65]. Thus, it can be concluded [66]that in order to develop practical zeolite as adsorbents for CO_2 capture applications, the composition (Si/Al ratio) and the pore structure of the framework should be considered.

Zeolites possess the advantage of industrial maturity as the knowhow of zeolite manufacturing and their gas separation applications is well established. There are many commercially available zeolites such as 4A, 5A, 13X, HiSiv-1000, HiSiv-3000 etc. In addition, many of them are available as structured adsorbents which

is very important for sorbent solid handling on a larger or commercial scale. The crystallinity of zeolites is another advantage as it makes the computational modelling and screening studies relatively easier[57].

The important weakness of zeolites is their sensitivity to moisture in the feed gas as zeolites shows strong affinity for water, thereby reducing the CO_2 uptake greatly over a few adsorption/desorption cycles. This reduction in the CO_2 adsorption is due to the competitive adsorption between CO_2 and H_2O for the same adsorption sites. Wherein, the highly polar H_2O molecules are preferentially adsorbed on the cations which leads to the reduction in the electric field generated by the cations[67]. As a consequence, it necessitates very high temperatures for regeneration to strip the CO_2 which is considered as a significant disadvantage from an energy perspective[46,66].

b. Activated carbons

Activated carbons are from the class of carbonaceous materials which represents a plethora of unique materials whose structure is predominantly composed of C atoms. Beside activated carbons, the class is inclusive of materials such as charcoal, carbon molecular sieves, carbon nanomaterials like graphene, carbon nanotubes etc. As with zeolites, the CO_2 adsorption in these materials depends mostly on physisorption. Hence, the surface properties such as surface area, pore structure and size play a decisive role. The carbonaceous structures are either meso- or microporous with majority of them being microporous[68].

Amongst the several carbonaceous adsorbents that are reported[69], activated carbons are discussed here. Activated carbons are well established adsorbent materials for a multitude of applications and it is natural that they have also been studied in CO_2 separations[68]. They exhibit wide variations in their surface or textural properties which causes their adsorption characteristics as highly variable. This variation is attributed to the raw material from which they are produced and the activation procedure that is followed. Their raw material sources are diverse that ranges from coal, wood to biomass. Typically, the preparation of activated carbons consists of two steps: carbonization and activation. The first step is the pyrolysis of the raw materials in an inert atmosphere to obtain a char which is devoid of most of the non-carbon elements. Subsequently, the char is either physically or chemically treated to produce the material with improved surface properties. The latter is known to make activated carbons with well-developed porosity[70,71].

In general, it is known that the CO_2 adsorption capacity of activated carbons are lower than that of zeolites at lower pressures or ambient conditions. However, at higher pressures, the CO_2 adsorption capacities are reported to be larger than that of zeolites. Several researchers through their comparative studies have demonstrated this characteristic of activated carbons[72-74]. This was attributed to the higher N_2 BET surface areas although the surface affinity of activated carbons for CO_2 was comparatively lower to those of zeolites. It makes the activated carbons more attractive for high pressure applications like precombustion CO_2 capture over low pressure flue gas applications.

As in the case of zeolites, activated carbons has the similar industrial maturity and commercial availability that they benefit from. The other key advantage is in terms of the raw materials and the cost. The availability of diverse raw material sources makes the industrial production relatively straight forward and low cost. Activated carbons owing to their moderate adsorption of CO_2 and lower values of heat of adsorption shows that CO_2 are weakly adsorbed on the carbons. This is evident with excellent reversibility of their adsorption capacities and with lesser energy intensive requirements for adsorbent regeneration compared to zeolites.

The other characteristic that activated carbons have over zeolites is their inherent hydrophobic nature as their CO_2 adsorption capacities are negatively affected by the presence of H_2O. In some cases, the effect is less drastic as compared with zeolites[75]. However, repeated cycling/storage under humid conditions causes a reduction of adsorption capacity compared to their performance under dry conditions which is considered to be caused due to the slow oxidation of the carbon surface. An active subject of research has been initiated due to the aforementioned hydrolytic limitations with the objective of overcoming it and improving the adsorption properties of activated carbons. The research is primarily focused on modifying the surface of activated carbons[76-78].

Overall, zeolites and activated carbons are the class of physisorbent materials with several attractive properties to their credit such as, industrial maturity, low cost, rapid adsorption kinetics. However, typically, they are strongly affected by the presence of water in the feed gas, often in negative ways. This highlights the necessity of overcoming the water challenge for these adsorbents with respect to carbon capture from wet flue gasses.

c. Metal-Organic Frameworks (MOFs) - Introduction

MOFs are a class of materials that are crystalline and porous. The past two decades have witnessed the fuelling interest in these materials for numerous reasons such as their porosity, tunability, crystallinity, versatility[79-81]. This has led to an enormous progress in the development of the field of MOFs in their design, synthesis, characterization and applications. Typically they are three-dimensional (3D) frameworks whose synthesis involves the self-assembly of metal ions or clusters and organic ligands that are connected together with the coordination bonds[82].

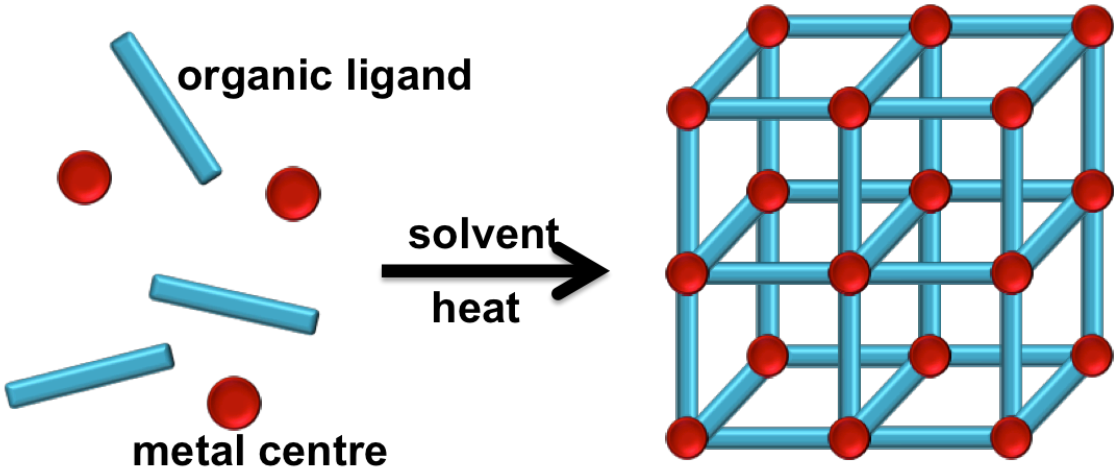

Figure 1.6: An illustration depicting the formation of Metal-Organic Frameworks (MOFs)

1. MOF synthetic techniques

MOF synthesis proceeds with the nucleation and crystal growth. The nucleation is typically initiated by providing energy - heating to a higher temperature. Subsequently, growth is initiated by cooling the reaction mixture down to lower temperature. Several synthetic routes for MOF synthesis have been established and reported[83,84]. They differ based on how the energy is introduced to the reaction mixture.

(1) Room temperature (RT) synthesis,
(2) conventional electric heating (CEH) – heat (energy) transfer from an oven,
(3) microwave heating (MW) – electromagnetic microwaves,
(4) electrochemistry (EC) – electric potential,
(5) mechanochemistry (MC) and ultrasonic (US) – mechanical waves

The establishment of several synthetic routes not only shows the maturity of MOF synthesis and also it can be seen as a route to obtain novel MOFs that cannot be synthesized otherwise. In addition, the variation in the energy transfer to the reaction mixture results in MOFs with different sizes and morphologies which can influence the structure-property relationships in immense diverging ways.

MOFs are typically synthesized through solvothermal synthetic conditions wherein the reaction occurs in closed vessels like Teflon lined reactors under self-induced pressure above the boiling point of the solvent. Whereas, non-solvothermal MOF synthetic reactions occurs at or below the boiling point under atmospheric pressure conditions which can be further classified based on the temperature at which occurs – room temperature (RT) synthesis or elevated temperature synthesis like reflux synthesis.

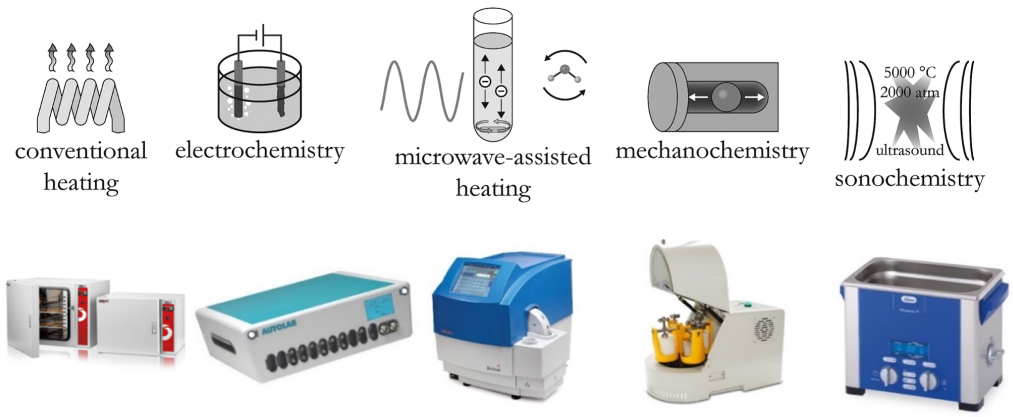

Figure 1.7: *The different established synthetic techniques for the formation of Metal-Organic Frameworks (MOFs)*

Figure adapted, modified from [84] with permission from the Royal Society of Chemistry

Literature review suggests that majority of the MOF synthetic conditions are based on the conventional electric heating procedure that requires several hours to days for synthesis and the body of work performed in the early stages were based on low-temperatures. The strategy in the case of low temperature reactions was to use highly concentrated starting solutions which will induce the precipitation much faster followed by the recrystallization and/or slow evaporation of the solvent mixture. The energy barrier required for crystallisation is surmounted by implementing high temperature reactions which offers the flexibility of starting the reactions with clear solutions rather than precipitated solutions. This way the critical nucleation concentration is outdone and it results in obtaining of comparatively larger crystals which are suited for structure determination.

Alternatively, microwave reactors are employed for MOF synthesis. Overall, microwave synthesis offers faster synthetic route (few minutes to maximum an hour) to obtain smaller crystals compared to CEH procedure (several hours to days). Herein, there is direct interaction of the electromagnetic microwave radiation with the starting reaction mixture. Since, polar solvents are used typically in MOF synthesis they tend to align in the applied electromagnetic field which leads to the collisions amongst them resulting in increased kinetic energy. As a direct consequence of this, comparatively higher heating rates and homogenised heating throughout the starting reaction mixture is possible. Due to the aforementioned reasons, microwave assisted synthesis accelerates the crystallisation reaction with enhanced nucleation rate.

Electrochemical synthesis is also explored for MOF synthesis where the main objective is large industrial scale production in a continuous process rather than in a batch process. It is achieved by the introduction

of the metal ions in a continuous manner through the dissolution of the anode into the reaction medium that is primarily comprised of the ligand in dissolved state along with a conducting salt.

The interest in using solvent free synthesis from an environmental point of view could be attributed to the exploration of mechanochemical synthesis. As in this synthetic route, reactions are carried out at room temperature without any solvents for shorter reaction times. The products are primarily formed by the breaking of intermolecular bonds under mechanical conditions leading to a chemical transformation. Likewise, through the application of ultrasound waves to reaction mixture at high energy. This mechanical vibrations which are larger than the dimensions of the molecules of the starting reaction mixture upon interaction with solvents, through cyclic alteration of pressure creates several bubbles. The bubbles grow and accumulate ultrasonic energy and as they expand further leading to their collapse which is called as cavitation. It causes the formation of higher temperature, pressures and shear forces leading to the formation of molecules.

2. MOF synthetic parameters and optimization

Irrespective of the synthetic technique that is followed for the synthesis of MOFs, there exists a prime objective which is to identify the optimum synthetic conditions which would enable to

(1) isolate crystals or a micro crystalline (long range order),
(2) get phase pure,
(3) porous framework whose porosity is in agreement with the theoretically calculated maximum value.
The porosity is particularly important if the MOF is targeted for porosity based applications like gas storage, separation etc.

The synthesis of MOFs requires the optimisation of several synthetic parameters that includes both process and compositional such as

(i) temperature,
(ii) power,
(iii) reaction time,
(iv) pressure,
(v) metal(s),
(vi) ligand(s),
(vii) molar ratio of metal and ligand,
(viii) solvent(s),
(ix) solvent ratio,
(x) volume of the solvent(s),
(xi) pH,

(xii) modulator/additives;
(xiii) commercial supplier of ligand,
(xiv) purity of the starting materials
(xv) availability of the chemicals
(xvi) headspace of the reactor etc.

In general, the optimization of the aforementioned parameters should facilitate the formation, breakage and reformation of metal-ligand bonds to provide structure propagation. The optimization can be challenging as some parameters are independent to each other and some are dependent on each other. They all have an influence on the crystallization of MOFs making MOF synthesis less straightforward[84]. The intricacy of MOF synthesis is explained as follows.

In order to attain the desired crystallinity and reaction rate, an increase of the reaction temperature is necessary. However, this might influence the crystal morphology, porosity and in some cases might promote the degradation of the MOF. Other parameters such as concentration, metal salt source etc. is proven to influence the crystallization of MOFs. The higher concentration of ligand will lead to the formation of over coordination thus slowing the crystal growth. In addition, to influencing the phase formation synthetic parameters also influence the crystal morphology.

Similarly, the choice of solvents is one of the most important synthetic parameter in the synthesis of MOFs. High-boiling point solvents are typically chosen for synthesis as they are suitable for high temperature solvothermal synthesis. Normally, solvent molecules do not directly interact with the framework. However, they act as void-filling molecules in MOF structures which often poses challenges later in the activation stage as removal of them from the voids without collapsing the framework is a challenging process. This is attributed to the high surface tension (dynes/cm) and capillary forces exerted by the high boiling point solvents on the structure. This explains the synthetic maneuvering that a MOF chemist might possess.

In other instances, usage of modulator is required when the metal-ligand bond formation is very strong as it prevents the formation of amorphous material. They are non-structural and tends to form dynamic bonds with the metal source by competing with organic ligands which slows the formation of structural bonds. Benzoic acid, acetic acid, oxalic acid, hydrochloric acid are some of the commonly used modulators. The addition of acidic modulators will influence the MOF synthesis as it is extremely sensitive to minute variations in the reaction mixture. For instance, HCl might dissolve the MOF that is forming and influence the crystal growth. The presence of modulator could decrease the nucleation rate that could result in fewer nuclei and larger crystal particle sizes. One of the other parameters which has an effect on the final particle size is pH. With higher pH, deprotonation of the organic ligand is promoted which causes an increase in the rate of nucleation and might lead to decreased particle size. This gives an overview of the challenges associated with the parameters such as ligands, modulators, pH and their concentrations. It shows the complications that each of the MOF synthetic parameters poses for MOF chemists to optimize them.

3. Requirement for the development of a synthetic platform for MOFs

Typically, the synthetic conditions and the chemistry of a particular MOF is almost exclusive and not entirely transferrable to synthesize other new MOFs. This non-transferability or non-applicability of synthetic conditions warrants the establishment of the optimal synthetic condition by optimizing the several synthetic parameters and performing several partially successful and failed experiments for every new MOFs. Thus, it has prompted the MOF chemists to approach MOF synthesis case by case mostly through trial and error method of several rounds of optimization cycles to obtained the desired crystallinity and phase purity. That requires the fine tuning of the various synthetic parameters which is exacting, time consuming and expensive from financial and human resources point of view. In addition, after such arduous optimization attempts, there exists the possibility of not obtaining the optimal synthetic conditions. It is therefore very evident that there is lack of a general synthetic scheme for the synthesis of MOFs.

Overall, this can be regarded as the major impediment which prevents us from fully realizing the vast potential of MOFs in two ways. First, as in principle, it is possible to have infinite number of structures by judicious combination of different metals and ligand. In this context, many computationally designed MOFs which are envisioned for targeted applications are either considered as synthetically non-viable or very challenging to synthesis. Second, many MOF research groups envision the commercial usage of the MOFs which they report. For which, ideally reactions that are faster in duration, facile and with the clear understanding of the contribution of various synthetic parameters are considered to be essential and advantageous for large scale production. However, this is not observed in reality.

Thus, there exists the necessity for development of a synthetic platform or tool which can optimize and improve the MOF synthesis efficiently. Through which, a better comprehension of the influence of the various synthetic parameters of MOFs can be gained. Ultimately, the synthetic tool should pave the way for acceleration of the synthetic discovery of MOFs and in addition, accelerate the synthesis of MOFs by upscaling and cutting down the duration of synthesis. It defines the first research objective of this doctoral thesis.

3.1. High-throughput experimentation

To explore the vast synthetic parameter space and to systematically vary the synthetic parameters various industrial laboratories like pharmaceuticals apply high-throughput (HT) methods. HT methods are considered as a powerful tool to accelerate the discovery of new materials and optimize their challenging synthetic procedures efficiently. Commercially, HT methods are deployed primarily to cut down the time taken for the novel or improved products to reach the market. Although HT experimentation studies are capable of executing as many reactions within a certain duration they are typically not intended for such

application. Rather, the focus is on selecting the parameters with care and extracting the maximum possible information from the experiment.

It is based on the concepts of miniaturization and parallel workflow in combination with automation. These HT methods have the features of performing several synthesis in parallel or in series with reactors which can hold few milliliters of reaction mixture. Depending on the application to be executed, the workflow is programmed accordingly with an algorithm. The algorithm is essentially instructions for the robotic platform to execute.

It comprises of automation for robotic handling, dispensing of the reactants and also for characterization of the products. This approach gives a major boost to perform and screen several synthetic reactions simultaneously thus overcoming the difficulties of trial and error optimization method. It can greatly facilitate the exploration of the vast chemical space with lesser human resources. HT robotic synthesis provides greater precision and control over the synthetic parameters and thereby, resulting in the decrease of variations in synthesis due to no human errors and greater reproducibility of the generated data. The large amounts of data that are produced helps in the establishment and extraction of the reaction trends. From which, role of the various and individual synthetic parameters on MOF formation is obtained leading to a better understanding.

Figure 1.8: *The high-throughput (HT) robotic synthesizer platform from Chemspeed Technologies AG and the work flow for a HT microwave synthesis of MOF*

3.2. Literature review of HT experimentation to MOF synthesis

The application of HT experimentation to MOF synthesis is less commonly observed. The major objective of such studies are as follows:

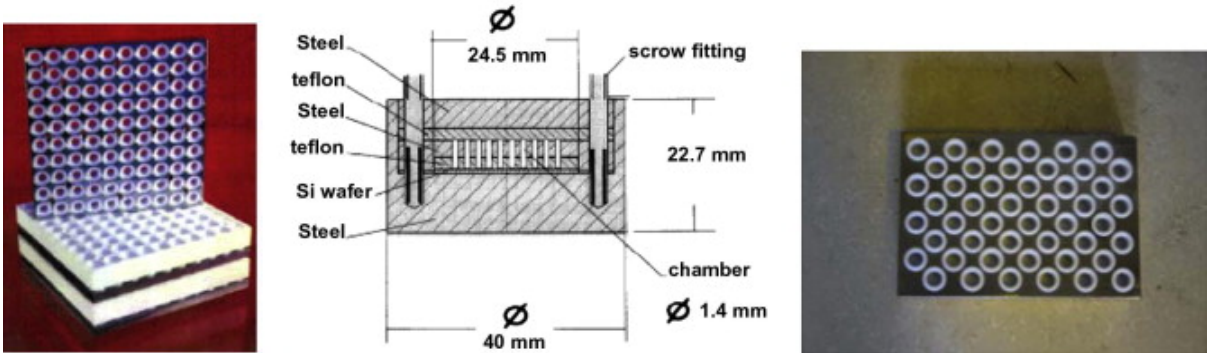

Figure 1.9: *The high-throughput Teflon-based reactors for solvothermal MOF synthesis.*

The image is reproduced from[85]

1) to accelerate the discovery of new MOFs
2) to efficiently optimize the synthetic conditions
3) to discover the reactions trends from the dense amounts of generated data
4) to elucidate the structure-property relationships based on the reaction trends

HT experiments is made of four elements, namely

1) design of experiments
2) preparation of reaction mixtures
3) synthesis
4) isolation
5) characterization
6) data evaluation
7) new design of experiments

Steps 1 and 6, 7 require the use of software. It is highly essential that this step is executed with great care as a poorly designed experiments can be inefficient and drain the resources. To this end, computational methods are developed and utilised. However, a good working knowledge of computational methods alone is not sufficient to reduce the synthetic parameter space. In addition to it, one has to have chemical intuition which is the knowledge gained and acquired from conducting previous experiments and that is available in publications.

Whereas, the other steps can be implemented with varying degrees of automation. The step 2 and 3 involves the dispensing of metals, organic ligands, solvents, homogenization, and pH adjustment. The step 4 involves filtration and washing of the MOF product with solvents and drying of the MOF. Step 5 typically involves the measurement of crystallinity and/or crystal size as the primary evaluation step for assessing the synthetic conditions based on the X-ray diffraction patterns. The obtained XRD patterns are then compared to the simulated powder patterns. MOFs of varying crystallinity with presence of different crystalline phases will complicate the evaluation step. This warrants the development or availability of a reliable method for identification of crystallinity and phase purity from PXRD patterns.

The first ever study to report HT experimentation to MOF synthesis was published in 2008 and it focused on zeolitic imidazolate frameworks, ZIFs[86]. A total of 9600 reactions were performed in several batches with a 96-well plate reactor placed in an oven. The influence of molar ratios of metal to ligand and the various concentrations of the solvents on the crystallization of ZIFs were studied. They reported the discovery of 16 new ZIFs and 5 new topologies. Furthermore, through HT methods they scaled up the synthesis of 7 ZIFs. Owing to the use of oven, the optimized synthetic condition had a longer reaction time of 72 h.

The other publication that reported the HT experimentation in the same year was the study on amino functionalized Fe-MIL-53 MOF[87]. A range of synthetic parameters - reaction temperature, solvents, concentration of the solvent, molar ratio of metal and ligand, pH and their influence on crystallization of ZIF MOFs was studied. The authors of the papers also demonstrated the scaling up of the MOF synthesis. They identified the nature of the reaction medium to have the intense impact on the MOF formation.

Majority of the work on HT experimentation to MOF synthesis was performed by the research group of Prof. Stock. As a follow-up to the above described work, they reported three other publications with further investigations aided by HT synthesis. The synthesis of MOFs that were investigated and optimized in a HT method are Al-MIL-53-NH_2[88], MIL-121[89], CAU-4[90]. The HT methods facilitated the authors to discover MIL-121 which is the analogue of Al-MIL-53-NH_2. The MOF was discovered when the authors performed a detailed investigation of the influence of pH and concentration. Not only, HT investigations along with synthesis-structure correlations led them to discover MIL-121, it also enabled them to establish the synthetic conditions of two other compounds namely MIL-118, MIL-120. These studies exhibit on how HT methods enables the acceleration of discovery of MOFs from the systematic investigation and the density of data that is generated.

The other example is the isolation of isoreticular compound of Cr-MIL-101[91]. The authors led by Professor Stock employed a HT reactor system with 24-well plate with which individual reactions of more than 600 were performed. They studied the influence of several synthetic parameters and from which temperature, the choice of solvents and the source of the metal were identified to play an important role.

Another HT investigation report from Professor Stock involving microwave synthesis that focused on the influence of the different individual organic ligands and the combination of them on the formation of MOFs

with Nickel paddlewheel unit was reported[92]. The employed strategy of establishing the synthetic conditions of the Ni analogue version of Cu-HKUST-1 with BTC ligand was successful. They replaced the BTC ligand with BTB resulting in the discovery of Ni-MOF-14. Overall, these HT studies made them discover and report 6 new compounds with four porous Ni based MOFs and two layered MOF structures.

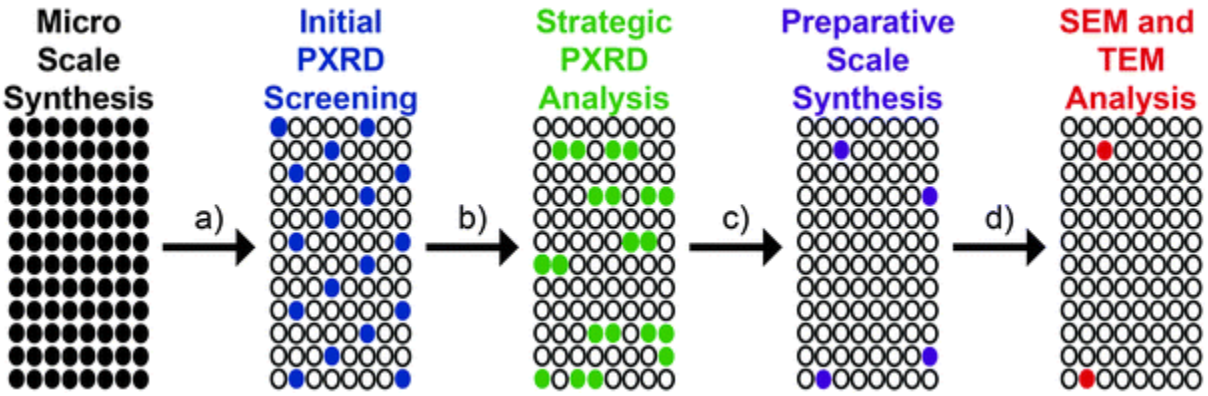

Figure 1.10: *Schematic outline of a high-throughput screening method*

Each oval represents one set of reaction conditions in a 96-well plate. (a) 96 unique solvothermal reactions are prepared per run, and a PXRD pattern is collected for 1 in 6 reactions. (b) When a reaction is determined by rapid PXRD analysis to be crystalline, PXRD data are collected for surrounding reactions. (c) Reaction conditions determined by PXRD analysis to give pure-phase crystalline products are used in preparative-scale reactions. (d) Preparative-scale reactions that are determined by PXRD analysis to give pure-phase crystalline products are characterized by electron microscopy to determine size scale and dispersity. The image[94] *is reproduced with permission from the Royal Society of Chemistry*

A completely HT automated robotic methodology for the synthesis optimization of Fe-BTT, an isostructural version of Cu and Mn-BTT was reported[93]. Though, it was isostructural, the synthesis of phase pure Fe-BTT required several cycles of optimization. In addition, it was observed that the final optimized synthetic conditions of Fe-BTT to differ considerably from Cu and Mn-BTT. This clearly demonstrates the non-transferability of the optimized synthetic conditions from one MOF to the other even though are closely related.

Nanoscale versions of porphyrin, zirconium based MOFs - MOF-525, MOF-545, PCN-222 were synthesized through HT screening methodology that employs microwave synthesis and rapid PXRD analysis[94]. The liquid dispensing was programmed and automated with a syringe that prepared 96 reaction mixtures in parallel. A total of 1036 reactions were executed to identify the optimal synthetic reactions that yielded nanocrystals of the desired MOFs. The authors extended the HT experimentation to PXRD characterization.

4. Outlook and first research objective

From the literature, the trend of publishing only the synthetic reaction that is identified as successful from several hundreds or thousands of partially successful or failed reactions can be observed. In addition, the observed reaction trends is not elucidated well. Thus, the captured chemical intuition is non-transferred. Besides which, majority of HT methods has been applied to solvothermal synthesis which doesn't reduce the synthetic duration of MOFs which is essential for the commercial scalability.

It is also evident from the literature review on how HT experimentation is highly beneficial and powerful in discovery of several new compounds not only in industrial labs but also in academia by optimizing the synthetic conditions and studying the reaction trends. Especially, discovering several new MOFs by studying the reaction trends is often not observed in experiments performed without HT methodology. In spite of such merits, HT methodology is less commonly used in academia research. This is reflected by the observation of less number of publications that report HT methodology to MOF synthesis compared to the enormous publications without HT methodology. This disparity can be explained based on two possible reasons.

First, the initial high capital investments that are required for purchasing HT robotic synthesizer platform or parts of it like automated dispensers. Second, the requirement of the technical knowhow of a robust optimization technique to optimize MOF synthesis and guide us to the optimal synthetic condition with less experiments to perform. Furthermore, working knowledge of a robust data extraction and data learning technique is required that can study the reaction trends from volumes of data and establish the relations between the structure and properties. Eventually, it should result in capturing a MOF chemist's chemical intuition and make the synthesis process rational and efficient. This gap in literature calls for computations and HT experiments to come together and development of a synthetic platform for MOFs. The synergy of which should result in a powerful and efficient synthetic platform which can optimize, improve MOF synthesis, accelerate the discovery of MOFs and learn the reaction trends. It defines the first outline of this doctoral thesis.

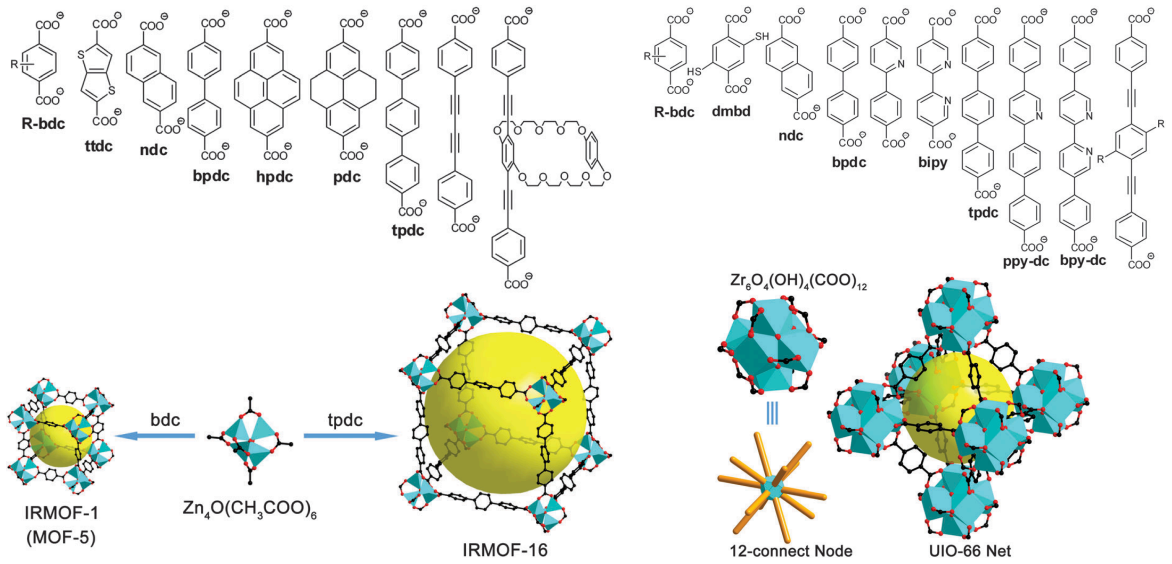

Figure 1.11: *Tunability of MOFs*

MOFs offers the opportunity to systematically alter the pore space by changing the length and functionality of the ligand. Tunability is illustrated with IRMOF series and UiO-66 series as examples. Image is reproduced from[95] *with permission from the Royal Society of Chemistry*

5. Salient features of MOFs

The ever increasing interests for MOFs and the resultant publications and patents can be attributed to certain salient features of MOFs. They are

1) Crystallinity
2) Versatility
3) Tunability and
4) Porosity

MOFs are highly versatile and it is reflected in the extraordinary variations in their structure and composition that the synthesis could bring about. The different combinations of metals and the ligands facilitates a myriad of MOF structures of diverse physical and chemical properties. The typical organic ligands used in synthesis of MOFs include compounds with a specific functional group like for example, carboxylate or imidazolate and the metal represent a substantial range of the periodic table (ex. Al^{3+}, Cu^{2+}, Cr^{3+}, and Zn^{2+}). This diversity in MOF reticular chemistry is evident with the ever increasing number of MOF crystal structures deposited in the Cambridge Crystallographic Data Centre (CCDC)[96]. Furthermore, the highly ordered crystalline structure of MOFs allows the structural characterization, establishing the structure-property relationships and also makes them ideal for simulation and modelling studies.

The tunability feature offers the ability to systematically modulate the crystal structure, pore dimensions, surface chemistry within the MOFs. The tunability of structural features is reflected in their properties. For instance, the variation of pore features of a MOF will influence the gas separation properties such as adsorption capacity, selectivity, Q_{st} etc.

The majority of the as-synthesized materials have the void spaces within the pores that are occupied by the solvent molecules which are involved in the synthesis. Through the experimental procedure named as activation/desolvation, vacuum and/or heat is applied to the as synthesized MOF. Alternatively, if the structure collapses due to activation, the high boiling point solvents are first exchanged with low boiling point solvents like acetone. Subsequently, they are activated. During which the solvent molecules are removed thus making their surface areas accessible to guest molecules with wide range of porosity properties. Thereby, making porosity as the foremost attribute of MOFs which makes them highly attractive for gas storage and separation applications.

MOFs exhibit unprecedented internal surface areas and pore volumes. For example, in 2018, the researchers from Dresden University of technology reported a mesoporous MOF, DUT-60[97] with the highest BET area reported till date of 7839 m^2g^{-1} with a pore volume of 5.02 cm^3 g^{-1}. This surpassed the previous highest BET area (7140 m^2g^{-1} and pore volume of 4.40 cm^3g^{-1}) of NU-110 MOF[98] reported by the researchers from the Northwestern University. These MOFs have their surface areas which are greater than that of a football field or that of The White House which reflects the sheer magnitude of the porosity display. In addition, many of the MOFs display permanent porosity. Furthermore, the distinguishing feature of MOFs from other porous materials like activated carbons is the observation of monodispersity in the crystalline array of pores. In combination with the porosity features, MOFs also exhibit high void volumes and ultralow densities. This has resulted in the use of MOFs in a variety of lab-scale adsorption tests.

6. MOFs for CO_2 capture

The aforementioned properties of MOFs have led researchers and scientists from MOF research community to investigate and demonstrate the applicability of MOFs for CO_2 separation applications such as postcombustion process, precombustion, direct air capture and natural gas sweetening processes[15,47,99-104]. A broad literature classification of MOFs for CO_2 capture based on their specific structural features can be made and it results in the following sub-sets-

1) MOFs which contain open metal sites;
2) Surface functionalized frameworks;
3) Frameworks with exposed anions;
4) Catenated frameworks and
5) Flexible frameworks

Amongst which, MOFs with open metal sites and/or CO_2 affinity functional groups are demonstrated to exhibit promising performances.

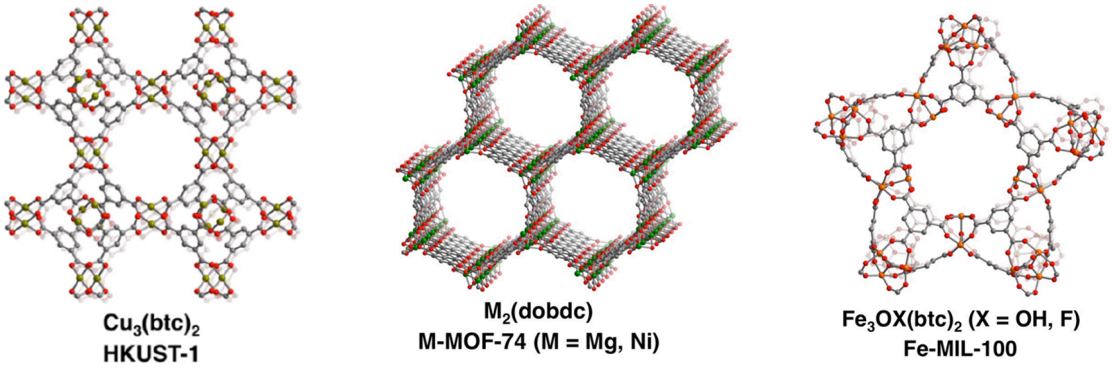

Figure 1.12: *The crystal structures of MOFs with open metal sites*

Gray, red, blue, dark-yellow, orange, dark green spheres represent C, O, N, Cu, Fe, Mg, Ni atoms, respectively; H atoms have been omitted for clarity

6.1. MOFs with open metal sites

This strategy involves the generation of structures that bears the metal cation sites which are exposed on the pore surface[47,104]. They are generated through the desolvation/activation of the MOF. The solvent molecule in the coordination sphere of the metal is removed thus exposing them as open metal sites with Lewis acidity that originates from their partial positive
charge. Through which, the affinity, interactions and selectivity of the MOF for the guest CO_2 molecule is enhanced over other guest molecules like N_2 of the feed gas at low pressures. The CO_2 gas molecules with their quadrupole moment and polarizability makes them strongly bind to the charge-dense open metal sites through electrostatic interactions compared with N_2. This strong affinity of CO_2 for open metal sites is reflected in the single component CO_2 isotherms with very steep uptake at low pressures.

HKUST-1 $[Cu_3(btc)_2]$[105], the archetype MOF is one of the well-studied MOFs. It is one of the foremost examples of MOFs with open metal sites. Majority of the studies focused predominantly on utilizing the open Cu^{2+} adsorption sites that it affords upon removal of the solvent molecules from the framework. In the context of CO_2 separation, these Cu^{2+} sites interact strongly with CO_2 due to the strong charge density of the cation with an end-on coordination between CO_2 and the metal centre. The MIL series of MOFs such as MIL-100[106], MIL-101[107] reported by the researchers from the Matériaux Institut Lavoisier are the other prime examples for open metal sites MOFs with end-on coordination with CO_2. They exhibit coordinatively unsaturated Fe^{3+} sites which are obtained following the removal of H_2O molecules that are bound to the metal centres.

The other well-studied MOF that bears open metal sites is the MOF-74 or CPO-27 family of M_2(dobdc) structure type where M = Ni, Co, Zn, Mg, Mn; H_4dobdc = 2,5-dihydroxyterephthalic acid[108]. They are characterized by their honeycomb, hexagon like channels that are 12 A° in diameter and have a very high concentration of open metal sites. The benchmark material in this family is MOF-74(Mg)[109]. The MOF-74(Mg) and MOF-74(Ni) are shown to outperform the benchmark adsorbent Zeolite 13X under dry separation conditions of CO_2/N_2 mixtures.

However, these materials have to be carefully handled due to the inclination of the exposed sites to become hydrated on exposure to atmosphere moisture even for short duration. In the context of postcombustion process, it is reported that MOFs with open metal sites tend to lose their CO_2 capacity (measured under dry conditions) significantly as the CO_2 binding sites are likely to be blocked or adsorbed by H_2O molecules[110,111]. Here, the real challenge is to overcome the competitive coordination of water to the open metal sites. Hence, for realistic postcombustion CO_2 separation applications, this strategy of MOFs with open metal sites seems non-applicable except in the cases of tethering functionalities to the open metal sites which is discussed in the ensuing sub-section.

6.2. Surface-functionalized frameworks

The objective of surface functionalization in MOFs is to enhance the framework's affinity for CO_2 through suitable pore surface properties. Typically, functionalization leads to the reduction in the surface area of the framework after the introduction of functional groups. Whereas, enhancements for the CO_2 capacities with increased uptakes in the low pressure region is observed. The intensity of such interactions relies significantly on the nature of that particular functional group. Correspondingly, the affinity for CO_2 is also reflected in the increased adsorptive selectivities of the framework for CO_2 over other components of the feed gas. Ideally, functionalization is expected to minimize the regeneration energy.

The synthetic strategy of preparation of surface functionalized MOFs for tuning their CO_2 affinity is pursued through several ways. Amongst which, the most intensively studied is the introduction of nitrogen containing organic groups. This approach of introducing nitrogen functionality can be performed and it can be outlined furthered: aromatic amine frameworks, heterocyclic frameworks, alkyl amine bearing frameworks. The introduction of aromatic amines as a pendant functionality is one of the most widely investigated strategies for CO_2 separation applications. This significant interest could perhaps be explained owing to the commercial availability of ligands with aromatic amines such as the 2-aminoterephthalic acid or amino-benzene dicarboxylic acid (NH_2-BDC). Here the amine functionality is covalently attached to the main structural ligand.

There are numerous examples to elucidate this approach. The popular example is the very well-studied UiO-66 MOF reported by the research group from the University of Oslo[112]. The UiO-66 is a microporous MOF with a 3D structure whose zirconium-oxo clusters are coordinated with benzene dicarboxylate (BDC) ligand. The functionalized version of the UiO-66 is UiO-66-NH_2. Wherein, an amino functionalized ligand

(NH_2-BDC) is incorporated into the framework[113,114]. The latter exhibits the expected affinity of amino groups towards CO_2 with adsorption properties better than the parent, non-functionalized UiO-66. Likewise, CAU-1 MOF[115] from Christian Albrecht University is a framework consisting of aluminium hydroxide clusters connected together by the NH_2-BDC ligand that exhibited a moderate CO_2 uptake and CO_2/N_2 selectivity with high initial Q_{st} value.

The other approach to enhance the CO_2 uptake is by using the heteroatomic sites that are present within the framework. Heteroatomic amines whose nitrogen atoms that are non-coordinated but are part of the aromatic ring have been investigated for CO_2 sorption. In this context, a cobalt and adeninate based three-dimensional (3D) bio-MOF-11 was reported for increased CO_2 uptake with pore surfaces which are considerably polarized [116]. The affinity of bio-MOF-11 for CO_2 was attained through the combination of structural features such as the presence of free aromatic and heteroatomic amine from the adeninate decorating the internal surfaces of the pores and their small pore size.

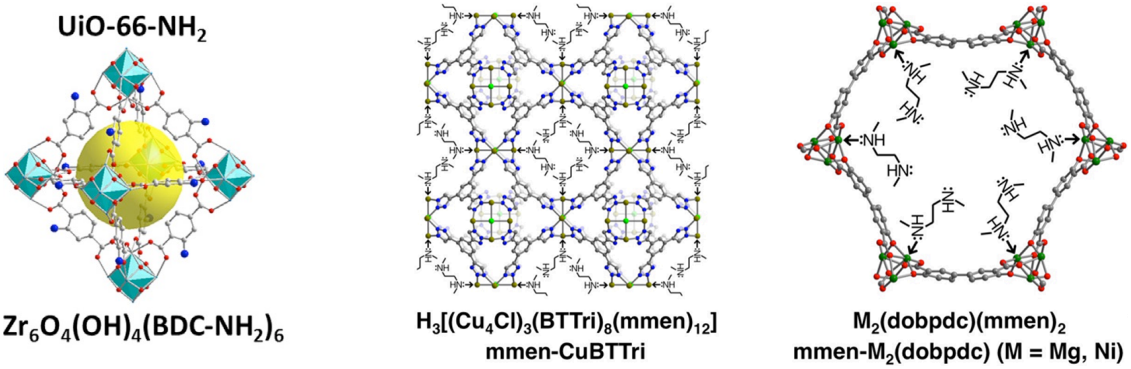

Figure 1.13: The crystal structures of surface functionalized MOFs

pendant amine in the UiO-66 structure through a functionalized ligand, alkylamines tethered to the Cu^{2+} metal sites of CuBTTri framework; Mg^{2+} or Ni^{2+} of the Mg_2(dobpdc) framework

Through these approaches of aromatic amine and heterocycle amine based frameworks, the CO_2 adsorption is still physisorptive. The regenerative conditions are very mild for stripping the CO_2 from the functionalized pore surface of the MOF. The drafting of alkyl amines to MOFs is the other promising methodology to increase their low pressure CO_2 capture performance. With this incorporation technique of more basic amines, the aqueous amine scrubber chemistry of very strong chemisorption of CO_2 is mimicked in MOFs. The performance in such cases is typically characterized by the formation of covalent bonds between the alkyl amine functionalized frameworks and the CO_2. Furthermore, the Q_{st} values are typically very high indicating chemisorptive process with high values of uptake and selectivity at low pressures that are relevant for carbon capture like postcombustion. The key to this approach, lies with increasing the density of alkylamines inside the framework. For this approach of tethering alkylamines,

the pioneering and cutting edge developmental work has been performed by the research group of Prof. Long from the University of California, Berkley.

Their earliest studies were with $H_3[(Cu_4Cl)_3(BTTri)_8]$; (BTTri = 1,3,5-tris(1*H*-1,2,3-triazol-4-yl) benzene) whose parent structure was modified by grafting of ethylenediamine (en) on to the exposed Cu^{2+} metal sites of the framework[117]. The en-functionalized framework displayed superior CO_2 uptake compared to the pristine CuBTTri parent framework with 1.6 wt% uptake and -90 kJ mol^{-1} Q_{st}. This was in stark contrast to the Q_{st} of unfunctionalized framework (-20 $kJmol^{-1}$). They followed their work with grafting of a secondary amine, N, N-dimethylethylenediamine (mmen) onto the Cu(II)[118]. This produced a further enhancement of CO_2 uptake with 15.4 wt% at 298 K and 1 bar which is 15% higher than the unfunctionalized parent framework.

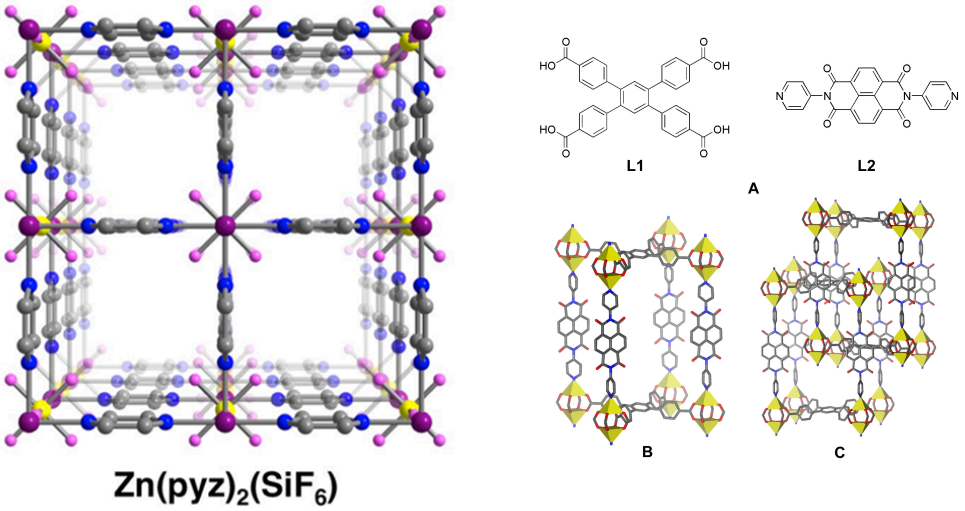

Figure 1.14: The crystal structure of MOF with exposed anion and interpenetrated structure

$Zn(pyz)_2(SiF_6)$ MOF with exposed F^- ions protruding into the pore space. grey, red, blue, dark-yellow, orange, purple, pink, yellow, and bright-green spheres represent C, O, N, Cu, Fe, Zn, F, Si, and Cl atoms, respectively; H atoms have been omitted for clarity. Purple tetrahedra represent Zn atoms. A) A two fold interpenetrated framework is represented with the chemical structure of ligands used in synthesis L1 and L2. B) The crystal structure of catenated MOF, one level of catenation is omitted to illustrate connectivity. Yellow polyhedra represent zinc ions; gray, carbon; blue, nitrogen; red, oxygen. Hydrogens omitted for clarity. C) Catenation of the MOF. The image is reproduced from[119]

The work of grafting the mmen was extended to the Mg_2(dobpdc), a variant of the previously described CPO-27/MOF-74, Mg_2(dobdc); ($dobpdc^{4-}$ = 4,4'-dioxidobiphenyl-3,3'-dicarboxylate; $dobdc^{4-}$= 2,5-dioxidobenzene-1,4-dicarboxylate or 2,5-dihydroxyterephthalic acid)[120]. The mmen was appended to the coordinatively unsaturated metal sites of Mg_2(dobpdc) which led

to the exhibition of high CO_2 capacity of 14.5 wt% at very low pressures of 0.1 bar and 298 K with a Q_{st} of -71 $kJmol^{-1}$. The authors in their follow-up work demonstrated that by replacing Mg^{2+} with other divalent ions such as Mn^{2+}, Fe^{2+}, Co^{2+}, Zn^{2+} facilitates the adsorption of CO_2 to be adjusted in accordance to the metal-mmen (M-N) bond strength[121]. They elucidated a reversible insertion mechanism of CO_2 into the M-N bond resulting in the formation of ammonium carbamate units which propagates along the pore length.

The grafting of amines in MOFs which leads to the chemical mode of interaction with CO_2 has some limitations that are analogous to that of aqueous amine solvents such as the high energy penalty for activation. In addition, there are questions pertaining to the stability of such materials that could potentially lead to the chemical leaching, given the lability of the bond and affect the recyclability. Comparatively, the pendant aromatic amine bearing frameworks offer greater stability whereas they have reduced interactions with CO_2 as the drawback. Overall, the challenge here is to design bespoke MOFs rather than the functionalization of the MOF. The synthetic challenge and costs makes their applicability for bulk CO_2 removal as difficult.

6.3. MOFs with exposed anions

There exists a class of MOFs whose mode of interaction with CO_2 is neither through positively charged open metal sites, unsaturated metal centres nor through the surface functionalities that have high affinity for CO_2. Instead, they interact strongly with the electropositive C atom of CO_2 through their exposed anionic sites that protrudes into the channels of the framework leading to strong CO_2 adsorption at low pressures. This is exhibited by the family of SIFSIX-3-M (M = Cu, Ni, Zn) frameworks with their uptake being the highest reported to date for MOFs which lacks any open metal sites or amine functionalities[122,123]. Through the combination of very small pores and the exposed F^- anions that protrude into the corners of the channels there is a strong adsorption of CO_2 at low pressures.

6.4. Catenated framework

Interpenetrated or catenated frameworks refers when more than two individual networks made of same or different components are entangled with each other. Depending on the nature of entanglement[124], it can be sub-divided into two classes – homo interpenetrated and hetero interpenetrated MOFs. In the case of former, the structure has identical networks whereas in the latter, it contains different networks in one structure. The entanglement occurs due to the presence of supramolecular interactions between the networks which endows it various features like enhanced stability, lower surface areas and enhanced pore surface interactions with the guest molecules. This observation has led to the exploration of interpenetration in MOFs as a strategy for gas storage, separation studies.

In the context of CO_2 capture, catenated frameworks exhibit enhanced CO_2 adsorption owing to specific electrostatic interactions with the pore surfaces. This is observed with the stepwise filling of CO_2 molecules

within the pore channels. Furthermore, their selectivity for CO_2 over N_2 or over CH_4 is ascribed to their smaller pore sizes which does selective molecular sieving of gas molecules based on their kinetic diameter.

Catenation promoted separation is the least explored strategy amongst all the other structural features driven strategies for CO_2 separation. This is due to the accidental discovery of majority of interpenetrated frameworks thus offering less space for design of such MOFs.
In addition, although they exhibit enhanced interactions the capacities are often inferior when compared with other MOFs.

6.5. Flexible frameworks

This class of MOFs exhibit flexible structures which is in contrast to the most commonly observed rigid frameworks. Rigid frameworks display the retainment of porosity upon adsorption and desorption of gas (guest) molecules in the pore spaces. However, flexible or dynamic frameworks collapse on removal of gas

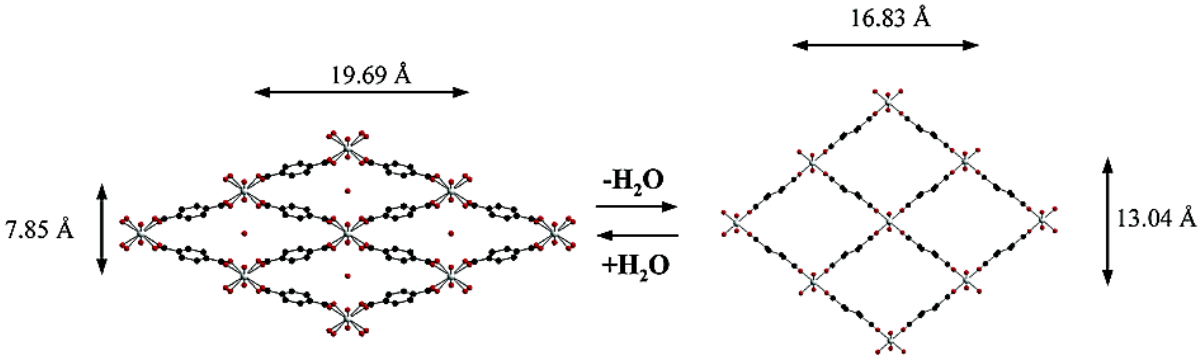

Figure 1.15: View of the pore systems of MIL-53(Cr) MOF which exhibits the flexible, breathing mechanism upon hydration and dehydration

Reproduced (adapted) from[125]. Copyright (2002) American Chemical Society

molecules but their porosity and porous structure is retained on adsorption of the same gas molecules at certain (higher) pressures. They operate through a mechanism labelled as gate opening mechanism meaning they are non-porous until a certain pressure. However, on attainment of that pressure, the structure becomes porous and uptakes the guest molecules which is reflected as distinct step in their adsorption isotherms. The external pressure induced stimuli leading to gate opening mechanism is alternatively described as breathing mechanism. This is predominantly and exclusively observed in certain class of MIL MOFs-MIL-53 developed and reported in literature by the researchers from the Matériaux Institut Lavoisier, France.

The MIL-53 family of flexible MOFs is comprised of MIL-53(Al), MIL-53(Cr), MIL-53(Fe) and their surface functionalized counterparts namely MIL-53(Al)-NH_2, MIL-53(Cr)-Cl, MIL-53(Cr)-Br etc. This family of MOFs has been extremely investigated for CO_2 separation applications.
It is formed by corner sharing $MO_4(OH)_2$ where M = Al or Cr or Fe octahedra which are coordinated to the BDC ligands. The MIL-53 MOF in its hydrated version exists in narrow pore form with negligible or less uptake of guest molecules. On dehydration (activation), it transits to the large pore structure due to the absence of hydrogen bond interactions. It is reflected with the observation of structure transition in their single component CO_2 adsorption behaviour when the framework turns in to its large pore form from narrow pore form at high CO_2 pressure of 15 bar.

Although, they exhibit promising CO_2 separation applications, their performance is however impacted when separation applications are performed in the presence of water. In which case, for post combustion separations, the amount of adsorbed CO_2 decreases with increasing amount of water that was adsorbed. And, in low water loadings, water was strongly adsorbed over CO_2 which indicates the strong competition that exists for the adsorption sites amongst water and CO_2.

7. Water impediment for MOFs for CO_2 capture and the second research objective

The previous sections give us a lucid picture on how MOFs has captivated the imagination of scientists for CO_2 capture which is displayed through the various foundational works and the subsequent rapid developments that were made in the field. This is evident as the field has amassed wide range of knowledge regarding the CO_2 adsorption performance of diverse number of MOFs from both experiments and computations. And, it is reflected through the ever increasing number of publications in this area of research. However, the field is witnessing the transition in the area of focus from fundamental aspects, proof of concept establishment to practicality considerations.

It is crucial to underscore that academia research and studies on the feasibility of MOFs as CO_2 sorbents under more realistic, real-world conditions have not received the full due consideration that is required. Literature review suggests that majority of the studies have overlooked the effect of H_2O and relied on single component CO_2, N_2 isotherms for the assessment which makes it challenging for identifying the best sorbent materials from a realistic flue gas mixture that has H_2O[126,128].

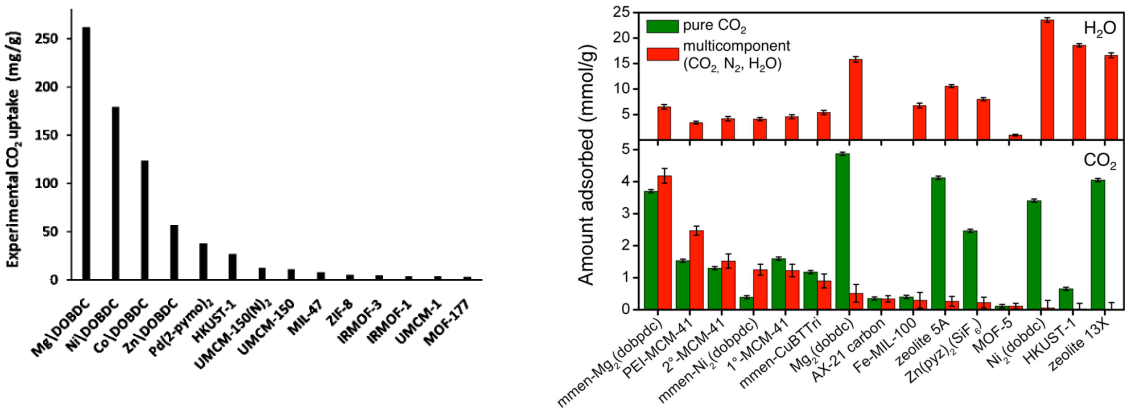

Figure 1.16: The evolution of screening processes for (postcombustion) carbon capture with MOFs

14 MOFs were screened for the experimental uptake of CO_2 at 0.1 bar from single component CO_2 isotherms. The influence of other components of the postcombustion flue gas such as H_2O was not considered. Image reproduced from[126]. Copyrights (2009) American Chemical Society. Whereas, the figure on right shows the summary of multicomponent adsorption measurements performed in this work for mixtures of CO_2, N_2, and H_2O at 40°C and equilibrium conditions representative of a coal-fired power plant flue gas. The green bars represent the amount of CO_2 adsorbed in a single-component isotherm at the same CO_2 partial pressure as the multicomponent experiment. The red bars in the bottom pane represent the amount of CO_2 adsorbed in the multicomponent experiment. The red bars in the upper pane represent the amount of H_2O adsorbed in the multicomponent experiment. Image reproduced from[127]. Copyrights (2015) American Chemical Society. The MOF Mg/DOBDC is identified as the top performing MOF from the study on the left whilst when H_2O is included the performance of the MOF drastically decreases as observed in the other study. This clearly illustrates the necessity of assessment in more realistic conditions which includes H_2O in the feed stream

Much of the other studies presented to date involves the obtainment of the single component CO_2 adsorption isotherms after exposure of the MOFs to precise amounts of H_2O which is confined inside the pores[129,130]. This approach of pre-adsorption of H_2O in the channels of the materials is promising as it gives information on whether H_2O can significantly increase or decrease the adsorption of CO_2. However, it has to be emphasized that it is difficult to achieve and is not always clear why. It is further complicated when studies report the analysis of MOFs for only certain (low) relative humidities. In addition, this strategy does not completely reflect the realistic flow of flue gas conditions that an adsorbent will experience when employed in a CO_2 separation process.

Further, ever since breakthrough experiments were first described in 2009[109] for the evaluation of MOFs under dynamic conditions, it has gradually become the standard tool to evaluate the postcombustion CO_2 separation capabilities from a binary or ternary mixture of CO_2, N_2 and H_2O vapour. In this regard, it is noteworthy to mention that many computational, experimental or combinatorial efforts are made. In

2015, Jeff Long and co-workers reported the first of its kind lab-scale postcombustion carbon capture through a multicomponent equilibrium adsorption of CO_2, N_2 and H_2O for 15 different MOFs, zeolites, activated carbons and mesoporous silicas with their in-house high-throughput analyser[127]. It is important to mention that in reality, no CO_2 separation process will operate under equilibrium conditions. It is interesting to observe that some of their results contradicted with dynamic measurements that was previously reported.

To counter the water challenge, it is proposed that these moisture sensitive sorbent materials can be employed for carbon capture in a commercial process but at the expense of drying the flue gas which is prohibitively expensive. Thus, exposure to water is inevitable and it can affect the stability and the performance of MOFs. There is a two-way impact of H_2O vapour molecules to MOF materials that has to be considered to overcome the vulnerability towards H_2O. First, the metal-ligand coordination bonds can be disrupted leading to the disintegration of the structure[131].

For example, the prototypical MOF-5 or IRMOF-1 reported by Omar Yaghi et al. in 1998 is considered as a breakthrough in the field of MOFs for obtaining permanent micro porosity[132,133]. The compound MOF-5, $Zn_4O(BDC)_3$ serves as an example for a family of MOFs termed as iso-reticular MOFs (IRMOFs)[134], wherein the zinc tetrahedral are connected to the BDC ligand resulting in a cubic structure. The material has been investigated for a wide range of sorption studies. Conversely, its crystallinity is lost on exposure to small amounts of humidity due to hydrolysis. The water directly attacks the zinc tetrahedral and thereby leading to the displacement of the bound ligand which causes the total collapse of the framework. This susceptibility to hydrolysis was further observed in other zinc-carboxylate based MOFs such as MOFs from the IRMOF series and MOF-177[135].

To tackle the hydrolytic stability problem, the MOF scientific community has substantially invested synthetic efforts in improving the water stability of MOFs and they can be classified as following [47]: (i) MOFs with metals that possess high valence ions – tri or tetravalent metal ions such as Cr^{3+}, Al^{3+}, Fe^{3+}, and Zr^{4+}; (ii) azolate based ligands with greater basicity rather than carboxylate ligands leading to higher metal-ligand bond strengths and stability; for example, the series of zeolitic imidazolate frameworks (ZIFs); (iii) MOFs functionalized with hydrophobic functional groups.

The second limitation is that the H_2O vapour molecules can compete with CO_2 for the same adsorption sites in MOFs. Therefore, any amount of H_2O present in the feed gas will drastically affect the CO_2 uptake capacity, selectivity, and other adsorption properties for materials which exhibit this behaviour. Then, some MOFs exhibit the so called intermediate behaviour of H_2O and CO_2 being preferentially adsorbed in different adsorption sites until a certain level of relative humidity. In this case, it would seem that uptake of CO_2 is increased for a certain amount of adsorbed H_2O. But, beyond which, there is a significant decrease in CO_2 uptake with increasing relative humidity owing to the competition[136].

There are also studies which shows for certain MOFs that the CO_2 adsorbed is almost unaffected irrespective of whether water is adsorbed or not which could lead us to certain hypothesis[137]. In this case,

it could be either that the H_2O and CO_2 molecules occupy different sites with no competition amongst them or it could be that the CO_2 displaces the adsorbed H_2O. However, MOFs which display such performances are scarce and limited. Thus, there is an ongoing research for MOFs whose CO_2 adsorption properties are affected limitedly or unaffected or even improved by H_2O.

It highlights the lacuna that exists which in turn offers the space and potential for developing MOFs that can capture CO_2 efficiently from wet flue gasses. The importance of it should be seen in the context of climate change and rising CO_2 emissions. To combat such catastrophic effects, every possible way of curbing CO_2 emissions is valuable and MOFs offers one of the most promising solutions. This defines the second research objective of this doctoral thesis – to design, synthesis, characterize and demonstrate MOFs can capture CO_2 efficiently in the presence of water.

8. Thesis Outlook

The remainder of this thesis will address the two research objectives that are discussed in this introduction chapter. First, devising an efficient synthesis platform for accelerating the discovery and synthesis of MOFs and more importantly for comprehending the contribution of the diverse synthetic parameters is explained in chapter 2 of this thesis. By combining three components: high-throughput robotic experimentation for synthesis; genetic algorithms for guiding the synthesis through optimization; and machine learning for quantifying and studying the relative importance of synthetic parameters, an efficient synthesis platform was developed. Through this methodology, as a proof of concept the synthesis and surface area of HKUST-1 MOF was optimized. The obtained HKUST-1 MOFs from more than 120 experiments were characterized and ranked based on an assessment methodology that was developed for this work. It included the assessment of crystallinity, phase purity and BET surface area. The robustness of this platform facilitated in achieving the optimal synthetic condition of HKUST-1 MOF with the highest surface area reported to date. The learning of the importance of the synthetic parameters for Cu-HKUST-1 synthesis facilitated the acceleration of the synthesis of Zn-HKUST-1 MOF.

The chapter 3 of this thesis illustrates how the research objective of designing, synthesising and demonstrating that MOFs can capture CO_2 in the presence of H_2O was achieved. In this work, two MOFs, Al-PMOF and Al-PyrMOF which are water stable and contains the most hydrophobic adsorbaphore were synthesized. The MOFs were synthesized based on a structural feature termed as adsorbaphore that offers strong CO_2 binding and continuing selectivity for CO_2 over N_2 in the presence of H_2O. It is a parallel layer of aromaticity separated by interatomic distance of 6.5-7 A°. Following the solvothermal synthesis of the designed MOFs, Al-PMOF and Al-PyrMOF were characterized for the crystallinity, phase purity, porosity with several characterization techniques - PXRD, TGA, FTIR, SEM, BET, CO_2 and H_2O single component adsorption isotherms. Furthermore, experiments such as in situ gas loading and localization with PXRD, solid state ^{13}C NMR were performed to demonstrate that H_2O and CO_2 do not compete for the adsorbaphore site. In addition, the MOFs were assessed for their carbon capture performance by collecting breakthrough curves with wet post combustion flue gas like feed stream. Their CO_2 separation

and capture performance was minimally influenced by H_2O and on benchmarking, it was identified that their performance is better than some of the commercially available adsorbent materials like zeolite 13X and activated carbon and water stable UiO-66-NH_2 MOF.

Overall, this thesis displays on how the synthesis discovery of the very promising and emerging MOF materials for several of its attributes and energy applications like carbon capture can be accelerated through a newly devised efficient synthesis methodology. In the context of their application to carbon capture in realistic conditions, this thesis shows on how the particular shortcoming of water influencing the CO_2 sorption was addressed effectively through design, synthesis, and characterizations.

Chapter 2 Acceleration of the discovery and synthesis of metal-organic frameworks (MOFs)

Abstract

We developed a synthetic platform that affords the acceleration of synthesis optimization and discovery of metal-organic frameworks. The methodology is driven by the optimization of synthetic conditions with genetic algorithm, synthesis by high-throughput robotic synthesizer and comprehension of the importance of synthetic variables through machine learning of the data. Through which, we performed a successful search of the optimal synthetic conditions of HKUST-1 MOF which yielded the highest surface area reported to date. We illustrated the importance of capturing and quantifying chemical intuition that is identical to that of an experimental MOF chemist.

2.1. Introduction

There exists a necessity for the development of a synthetic platform for acceleration of the discovery and synthesis of MOFs as described and emphasized in the introduction chapter of this thesis. It forms the first research objective. In this context, the introduction chapter further explains on how high-throughput (HT) automated robotic synthesizer can be a valuable addition to the desired synthetic platform providing the required experimental impetus. Furthermore, the importance of having a robust design of experiments to complement HT experiments was highlighted in the introduction chapter.

For instance, the commonly used factorial design for synthesis strategy involves the systematic variations of synthetic variables[85]. A three time systematic variation of nine MOF synthetic parameters can result in 9^3 = 729 experiments to perform. The cost of both performing such experiments and assessing the generated data increases exponentially. Herein, HT synthesis has the potential to perform such dense experiments and subsequently generate dense amount of reaction data for analysis. The literature review of application of HT experimentation to MOF synthesis that is included in the introduction chapter gives an overview of publications which reports thousands of HT experiments that were performed to discover new MOFs. To this end, it was decided that for this work presented in this chapter, acceleration in the synthesis and discovery is fundamental. Thereby, to address this, three things were considered and implemented.

First, this work applies HT to microwave synthesis of MOFs which is in contrast to the majority of the previous studies which applied HT to solvothermal synthesis. The drawback of such strategy is with the synthesis duration (several hours to days). In order to reduce the synthesis duration a microwave synthesis reactor was affixed to the HT robotic platform thus guaranteeing the acceleration of synthesis and discovery of MOFs with short synthesis durations. The description of the principle behind microwave synthesis, solvothermal synthesis etc. is explained in the section of MOF synthetic techniques of the introduction chapter.

Second, we chose genetic algorithm (GA), a robust and global optimization algorithm[4,138]. The optimal synthetic condition of a MOF should exist in the global optimum which can be attained by using GA as the optimization tool. This eliminates the high possibility of winding up in the local optimum if the optimization was performed otherwise with gradient based algorithms. As a consequence, the number of synthesis and optimizations reactions that are required to be performed will reduce considerably. It offers high probability for accelerating the discovery and synthesis.

Third, we chose machine learning regression model to learn and quantify the relative importance of the synthetic variables involved in the MOF synthesis. This is highly beneficial as HT synthesis and GA in combination is expected to produce dense amount of data which is ideal from machine learning point of view.

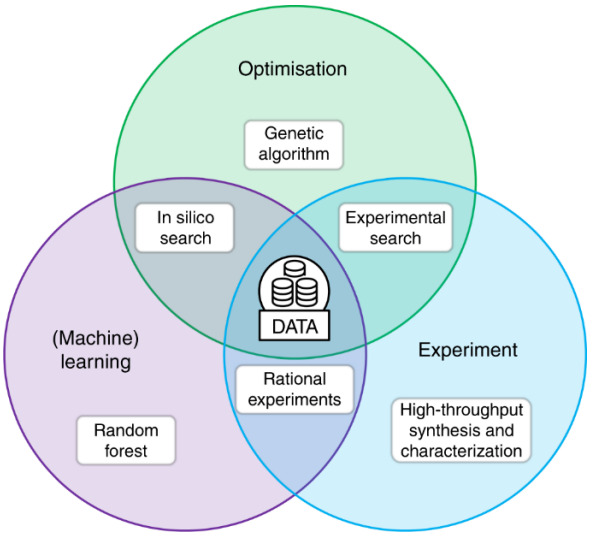

Figure 2.1: The scheme of the developed synthetic platform

Furthermore, machine learning of the dense amount of generated data consisting of partially successful and failed synthetic conditions and the resultant MOFs will facilitate the capture and validation of chemical intuition. The captured chemical intuition should be equivalent to the chemical intuition that an experimental MOF chemist will acquire on what parameters weighs the most for a particular MOF synthesis. This empirical knowledge is however gained and developed after performing several hundreds to thousands of challenging MOF synthetic reactions.

Thus, the developed synthetic platform consists of three components – (1) synthesis with HT automated robotic synthesizer affixed with a microwave reactor; (2) synthesis optimization with GA and (3) studying the reaction trends and comprehension of the relative importance of synthetic variables with machine learning. At the intersection of these three components lies the rational experiments that should accelerate the synthesis and discovery of new MOFs. The scheme of the MOF synthetic platform is illustrated as a venn diagram in Figure 1.
In this work, we demonstrate the robustness and applicability of the developed synthetic platform through two case studies. First, we optimize the synthetic conditions of a benchmark MOF and from which we capture the chemical intuition. Second, we show on how the captured chemical intuition when reused accelerates the discovery of a polymorph version of the benchmark MOF.

2.2. Optimization of the synthetic conditions of HKUST-1

HKUST-1 MOF is considered as one of the benchmark MOFs. It is one amongst the few MOFs to be commercially available from BASF chemicals under the trade name Basolite^{TM} C300. It was reported in 1999 by the researchers from the Hong Kong University of Science and Technology which explains the acronym HKUST[105]. HKUST-1 consists of copper (Cu) paddlewheel units coordinated to the trimesic acid, otherwise known as btc = 1,3,5-benzenetricarboxylate ligands.

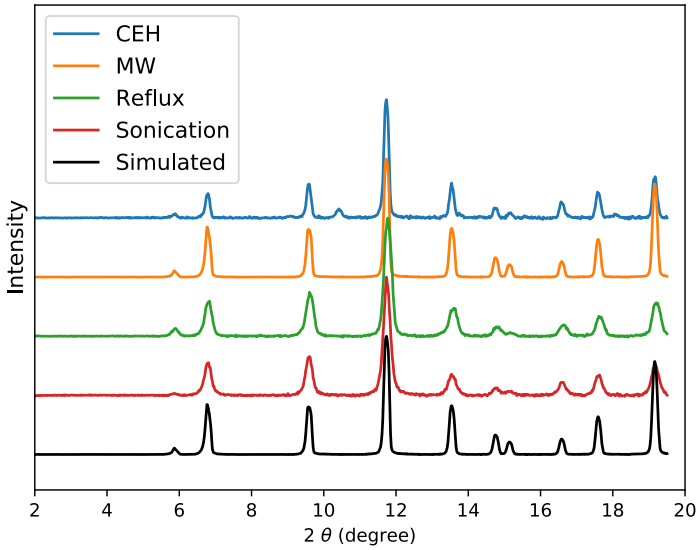

Figure 2.2: The PXRD of crystalline HKUST-1 synthesized using different methods.

These samples have a wide range of BET surface areas: 389 m^2 g^{-1} for CEH; 1228 m^2 g^{-1} for MW, 900 m^2 g^{-1} for reflux, 1036 m^2 g^{-1} for sonication

Thus, it is alternatively referred as Cu-BTC MOF in literature. Some of solvent molecules that are involved in the synthesis will be present on the axial sites of the paddlewheels in the as synthesized HKUST-1. Upon removal of solvent molecules through activation, the void spaces of HKUST-1 can be accessed.

It can be considered as a workhorse MOF as different research groups have utilized HKUST-1 to demonstrate the applicability of their methodology. In addition to it, several investigations of HKUST-1 for its structure-property relationships and the consequential applications can be observed in the MOF chemical literature. The extensive utilization of HKUST-1 explains the establishment of wide variety of synthetic techniques (see the literature review summary in appendix). This ensued in the exploration of vast synthetic parameters by each of these publications.

Interestingly, the reported BET surface area of HKUST-1 MOF varies drastically with values as low as 300 to values as high as 2000 m^2g^{-1}. The first publication to report HKUST-1 MOF mentions a BET surface area of 629 m^2g^{-1}. These values are in stark contrast to the theoretical maximum of 2153 m^2g^{-1}. To verify this disparity, we synthesized HKUST-1 with different established synthetic techniques – CEH, MW, US, Reflux and conditions. The obtained HKUST-1 MOFs were crystalline and phase pure as their powder X-ray diffraction (PXRD) patterns were in concordance with the simulated pattern. The HKUST-1 MOFs were then activated under similar conditions and following which, the N_2 isotherms were collected at 77 K. The BET surface areas were in line with the literature values. The reasoning behind the observed disparity is unclear.

Synthesis variable	Optimisation constraints	Notes
Water (H_2O)	$0 - 6$ ml	The total solvent volume is constrained to be between 1ml to 6 ml.
Dimethylformamide (DMF)	$0 - 6$ ml	
Ethanol (EtOH)	$0 - 6$ ml	
Methanol (MeOH)	$0 - 6$ ml	
Isopropyl alcohol (iPrOH)	$0 - 6$ ml	
Reactants ratio	$0.8 - 1.8$	Molar ratio of Cu nitride to BTC ligands
Temperature	$100 - 200$ °C	
Microwave power	$150 - 250$ W	
Reaction time	$2 - 60$ mins	

Table 2.1: The synthesis variables constructing the chemical phase space, and their corresponding optimisation range

As emphasized in the introduction chapter, the prime objective of any MOF synthesis is to establish the optimal synthetic condition which should yield the MOF with highest crystallinity, phase purity and the porosity value in concordance with the theoretical maximum. The latter is essential if the MOF were to be applied for porosity based applications like gas storage, gas separation studies. This is of high importance from a practical point of view for a MOF like HKUST-1 which is considered as one of the promising MOFs for methane storage applications[8,139]. Thus, HKUST-1 offers the space for bridging such disparity in the BET surface area through synthesis and optimization. This makes HKUST-1 as an ideal candidate to be tested for assessing the applicability of our developed synthetic platform.

The selection of synthetic variables to optimize the synthetic conditions of HKUST-1 has to be carefully exercised as it directly influences the number of experiments taken to attain the optimal synthetic condition. Therefore, the selection of synthetic variables is the first scientific challenge of this work. In this regard, we chose nine different synthetic parameters – solvents such as water, dimethylformamide, ethanol, methanol, isopropyl alcohol, reactant ratio of Cu salt to BTC ligand, microwave power and

reaction duration and temperature. These variables were imposed with optimization constraints that was due to the experimental limitations. For instance, the volume of the solvent used for the microwave vial cannot exceed above 6 millilitres due to safety concerns. Likewise the constraints for the temperature and power of the microwave reaction were capped accordingly.

Priority was given to select polar solvents as it is established that in principle more the polarity of the solvent more beneficial it is for microwave synthesis. The temperature is the other variable which is fundamental for attaining the desired highest crystallinity and phase purity and this is dependent on microwave power for microwave chemistry. The other variable that was given due attention and included for optimisation is the reactant ratio. It is recognised that higher concentration of the ligand will result in an over coordinated species tending in lower crystal growth.

Having selected the synthetic variables which constitutes the chemical space to be explored by GA, we then proceeded to perform the experiments. The second scientific challenge is to fix the number of experiments per optimization cycle as GA works by generating a population of solutions in each iteration. This differs from the other algorithms as they function by the generation of a single solution. As per GA parlance, an iteration is called as generation. Our HT robot can perform thirty experiments per day and hence, we chose the number of synthetic conditions for HKUST-1 optimisation to be generated by GA as thirty. This is in contrast to typical functioning of GA as the population will consist of several hundreds or thousands of solutions and limiting it to thirty due to technical limitation of robot is a scientific challenge.

The evaluation of the solution domain – HKUST-1 synthetic conditions was performed by an assessment method which was developed for this particular work. The synthesis was performed for each of the thirty synthetic conditions generated by GA. The resultant HKUST-1 samples were measured for their crystallinity, phase purity from PXRD patterns collected at room temperature and BET surface area from N_2 isotherms collected at 77 K.

Crystallinity and phase purity of samples were assessed by the full-width at half maximum (FWHM) of the diffraction peaks of the PXRD patterns, and with a penalty in fitness for every additional peak that appears in the experimental PXRD pattern compared to the simulated pattern. A Gaussian function is fitted to the peak which give us the FWHM with the following set of equations:

$$f(x) = \frac{1}{\sigma\sqrt{2\pi}} \exp\left[-\left(\frac{(x - x_0)^2}{2\sigma^2}\right)\right], \quad (1)$$

$$\mathrm{FWHM} = 2\sqrt{2\ln(2)}\sigma, \quad (2)$$

where variable x is the 2θ of the diffraction angle. The average FWHM of all the peaks of the PXRD is taken as the measure of crystallinity. Lorentzian, Pearson, and combined Lorentzian, Pearson and Gaussian distributions were also considered, and no considerable differences were observed in the ranking.

It was decided to collect the PXRD patterns for all the HKUST-1 samples of each generation whereas the collection of isotherms was limited to only the highly crystalline and phase pure samples. This was due to

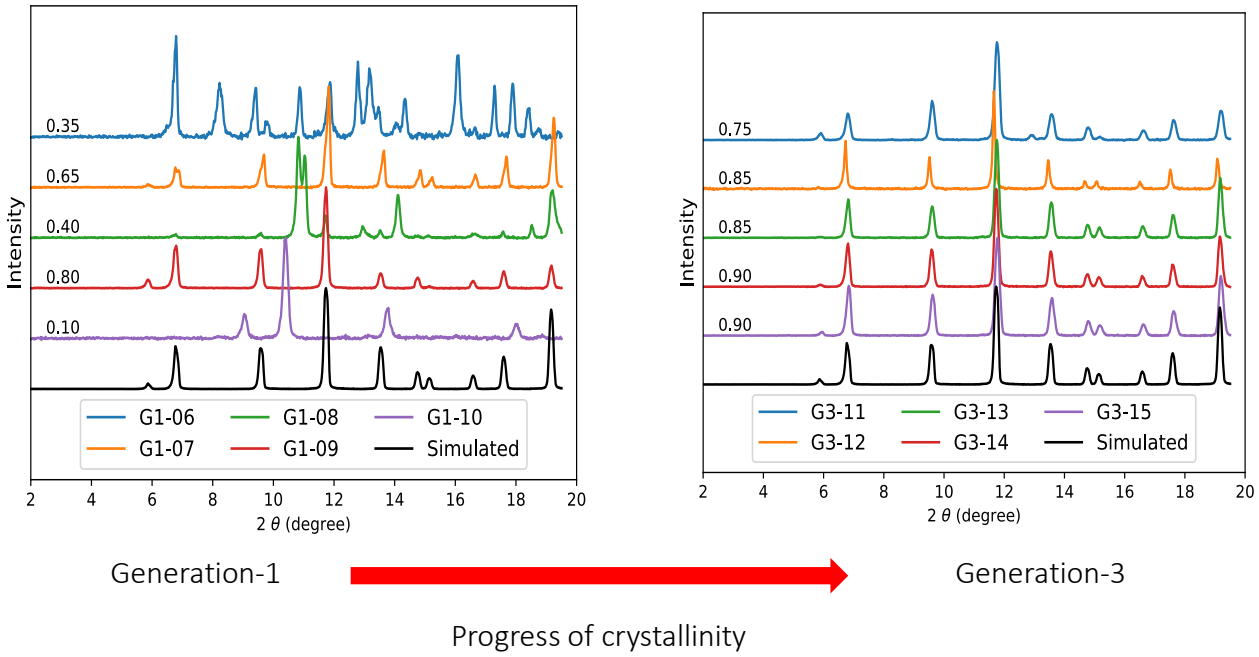

Figure 2.3: Improvement in crystallinity from generation-1 to generation-3

the time consuming process of collecting isotherms and the preference to have a faster and facile assessment of samples.

We thus ranked the experiments or the HKUST-1 samples based on their crystallinity, phase purity and BET surface area. This ranking is fed to the genetic algorithm to generate a new generation of thirty synthetic conditions. Subsequently, the new generation of synthetic conditions from GA is synthesized with HT robot and characterized. This procedure continues until it satisfies the objective function of the GA. All the data generated in the synthesis procedure is used to train a machine learning model to assess the importance of synthetic variables.

With this work flow, we proceeded to search the optimal synthetic condition of HKUST-1. The figures shows the PXRD patterns that were collected for all 120 samples from three generations. The overall improvement in crystallinity and phase purity can be observed as the generations progressed from generation 1 to generation 3. We selected the top five crystalline and phase pure samples from all three generations and whose BET surface areas on analysis revealed a wide range of surface areas. Amongst which, the HKUST-1 sample with the highest BET surface area reported to date was present. Table 2.2 presents the synthetic conditions and the corresponding BET surface area of the top five crystalline and phase pure samples.

Sample	BET [m^2g^{-1}]	H_2O [ml]	DMF [ml]	EtOH [ml]	MeOH [ml]	iPrOH [ml]	Reactants Ratio	Temperature [°C]	Microwave Power [W]	Reaction Time [mins]
1	367	0.5	0.0	5.0	0.0	1.0	0.9	120	174	58
2	526	0.5	1.0	0.0	4.0	0.0	1.8	176	246	44
3	935	0.0	4.5	0.0	0.0	0.0	1.8	123	200	7
4	1596	0.0	4.0	0.0	0.0	2.0	0.8	200	240	60
5	2045	0.5	2.5	2.0	0.0	0.0	1.5	140	200	20

Table 2.2. The synthetic conditions and the BET surface areas of the top five samples with the highest crystallinity

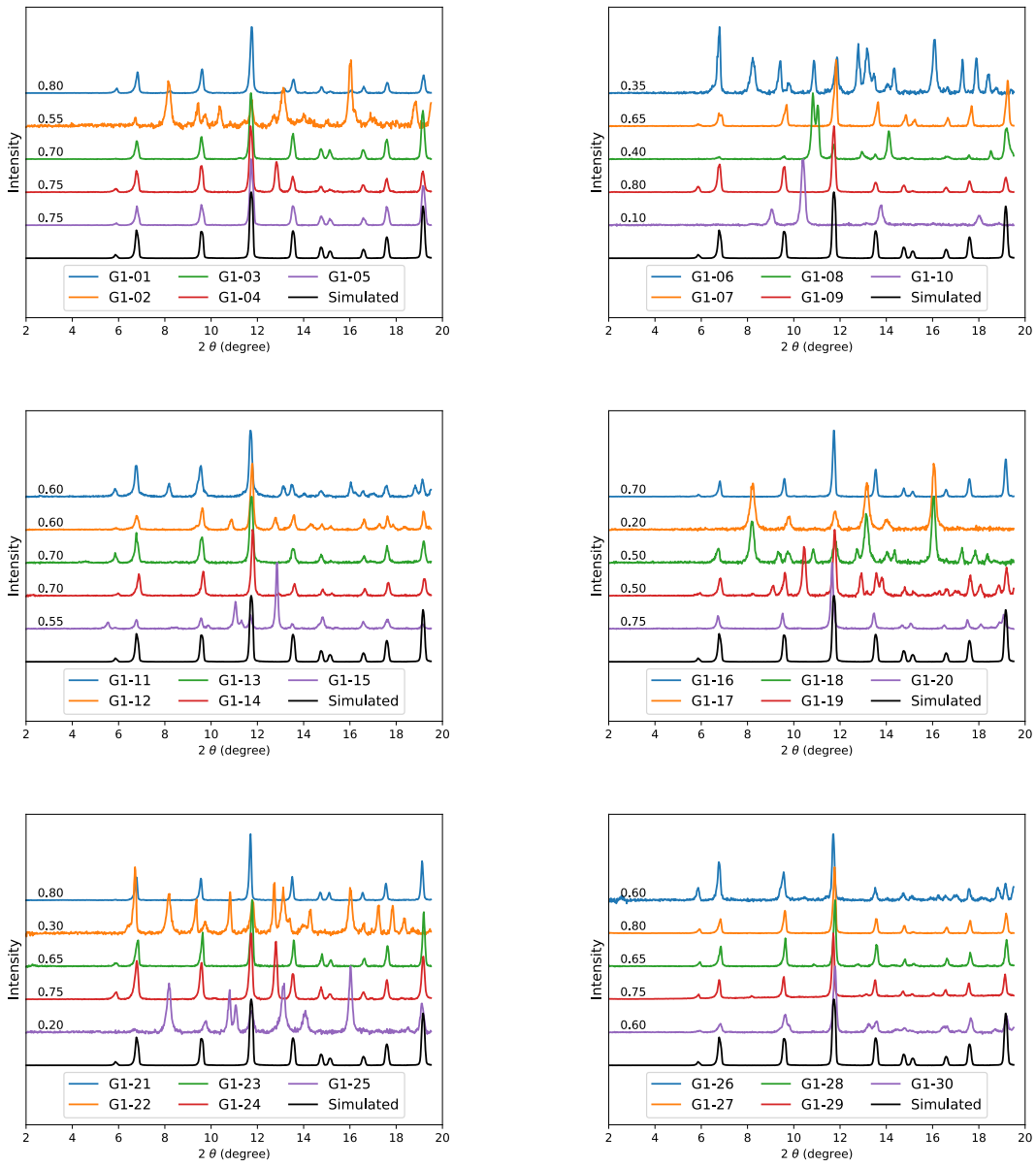

Figure 2.4: The PXRDs of all samples in the first generation (G-1) of genetic algorithm optimization of Cu-HKUST-1

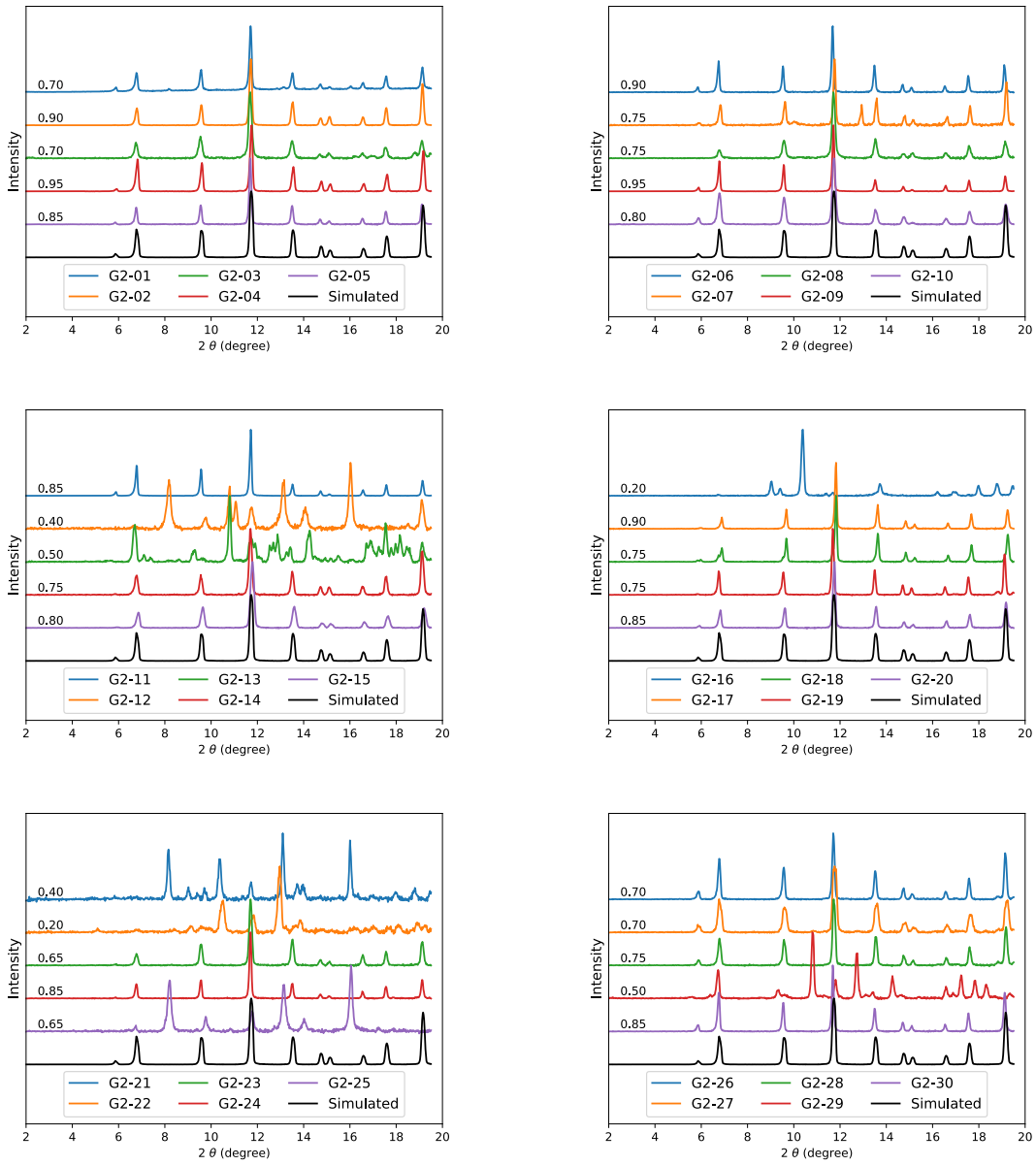

Figure 2.5: The PXRDs of all samples in the second generation (G-2) of genetic algorithm optimization of Cu-HKUST-1

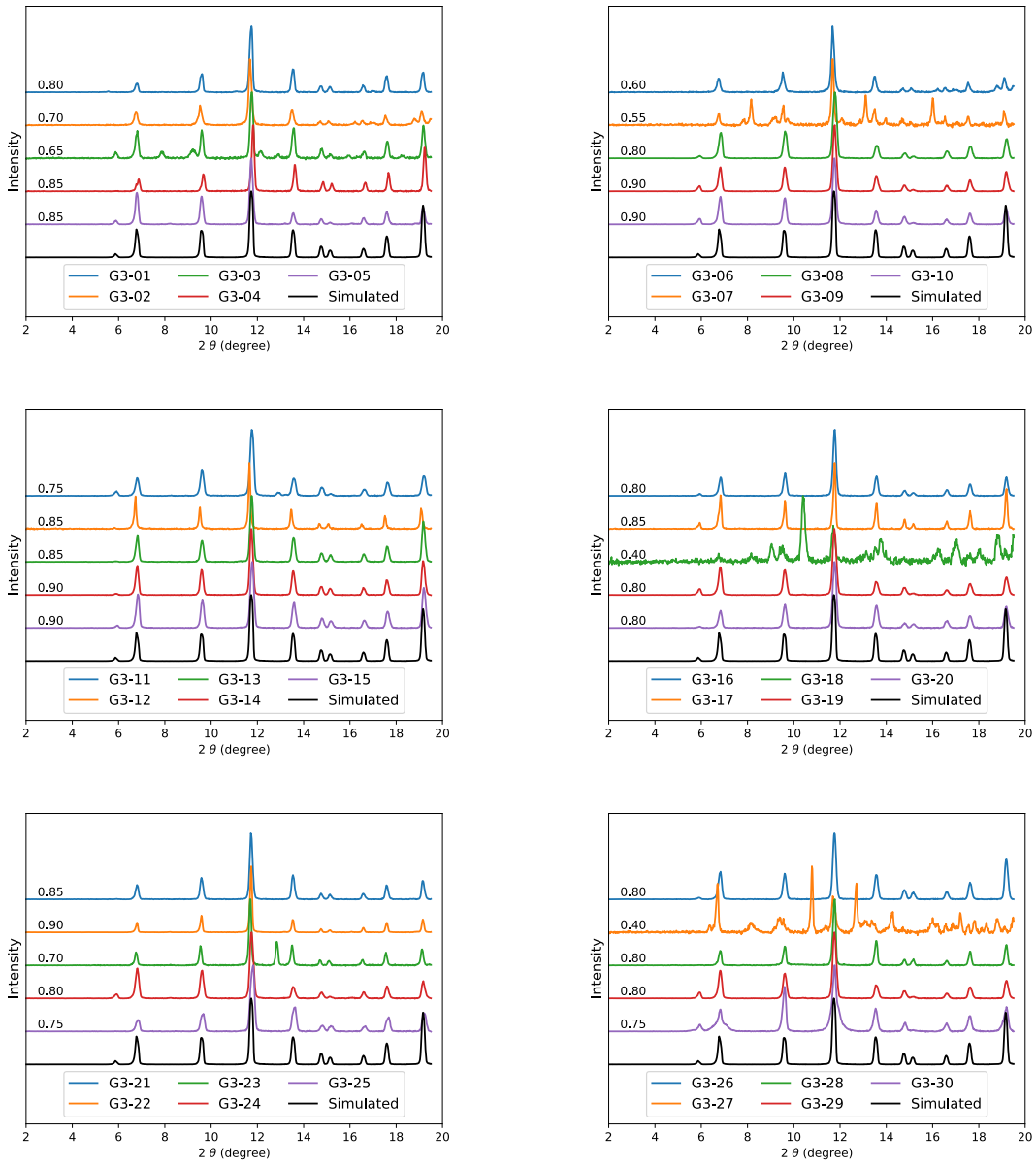

Figure 2.6: The PXRDs of all samples in the third generation (G-3) of genetic algorithm optimization of Cu-HKUST-1

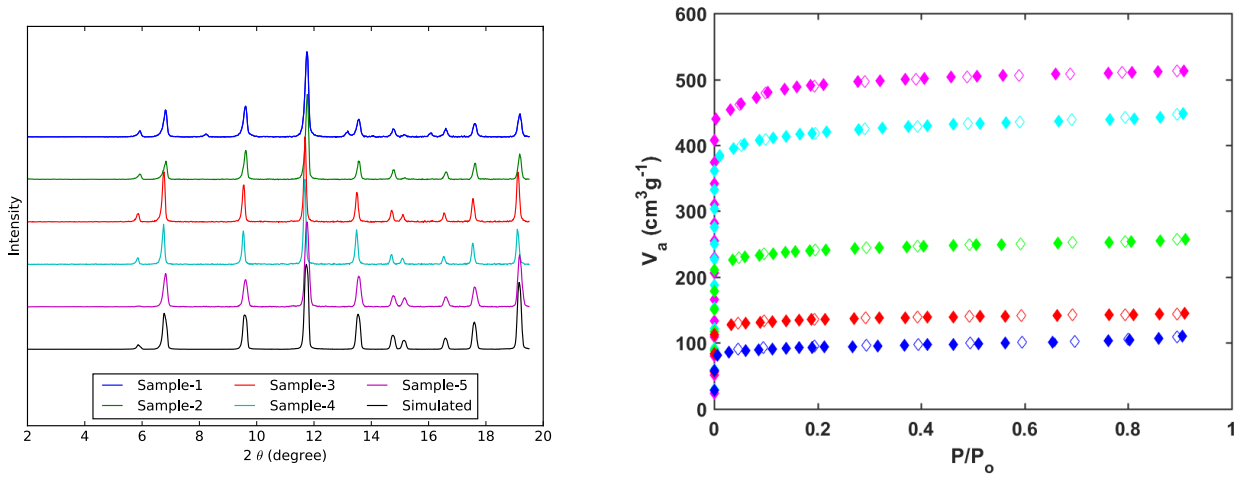

Figure 2.7: The PXRD patterns and N_2 isotherms@77 K plots collected for the top 5 samples with highest crystallinity and phase purity

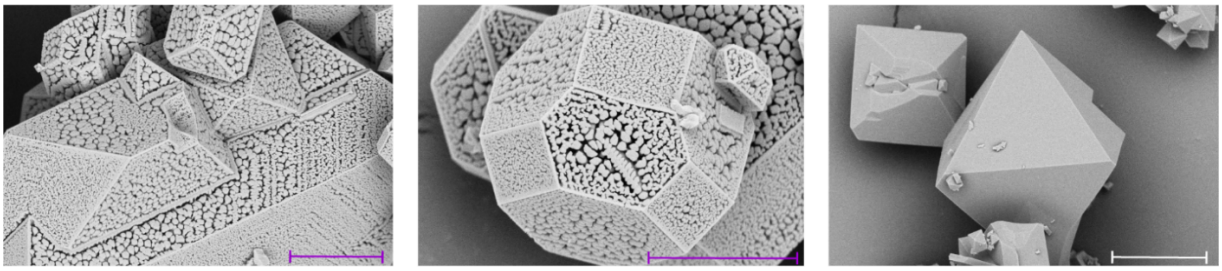

Figure 2.8: Scanning electron micrograph of three Cu-HKUST-1 samples with highest crystallinity and phase purity.

All these samples have high crystallinity but show a wide range of surface areas. Scale bars for sample 1, sample 3 and sample 5 show 5 µm, 4 µm, and 10 µm respectively. (HKUST = Hong Kong University of Science and Technology)

In addition, to PXRD and BET surface areas characterisation the samples were characterized based on SEM images, FT-IR spectra, TGA and elemental analysis. From the SEM micrographs, it is evident that the HKUST-1 samples with low BET surface area exhibit possible crystal intergrowth. Whereas, the samples with higher BET surface area are larger and lacked such morphological features. Although the SEM micrographs of the five samples displayed differences in the morphology of the crystals, the other characterization results which were collected showed no differences.

First, the FTIR spectra was collected for all the five samples. The bands observed in the region of 1500 - 1700 cm^{-1} which is observed in all the five MOFs can be assigned to the asymmetric stretching vibration due to the coordination of the carboxylate group of the BTC ligand and the bands observed in the region

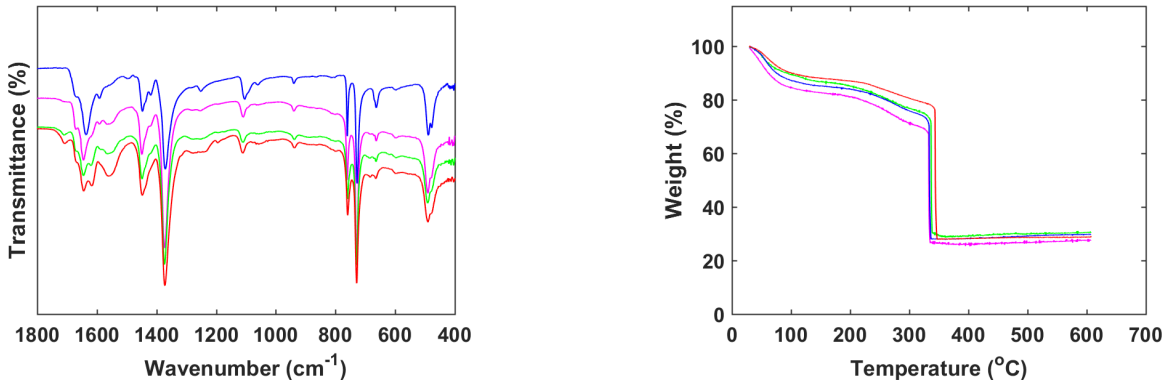

Figure 2.9: FT-IR spectra and TGA profiles of top five HKUST-1 samples with highest crystallinity and phase purity

of 1500 - 1300 cm^{-1} can be assigned to the symmetric stretching vibrations. The IR bands observed around 1450 cm^{-1} could be attributed to the stretching and deformation modes of the benzene ring. The distinct IR band observed at 493 cm^{-1} relates to the vibrational mode involving the Cu centre[140,141].

Second, the TGA analysis revealed the percent of weight loss in all the five MOFs on exposure to air and upon heating from room temperature to 600°C. The TGA curves exhibit several steps of weight losses. The initial two weight losses from 30−90°C and from 90−270°C can be correlated to removal of moisture and solvent molecules. Further which, a sharp decrease in weight is observed which is attributed to the decomposition of the ligand. On further increase in temperature, there is no weight change with respect to the temperature.

	Chemical formula	Element	Calculated	Found
Sample 1	$[Cu_3C_{18}O_{15}H_{12}]\cdot(EtOH)\cdot(iPOH)\cdot 3(H_2O)$	H	3.93	4.01
		C	33.72	32.99
Sample 3	$[Cu_3C_{18}O_{15}H_{12}]\cdot(DMF)\cdot(iPOH)\cdot 3(H_2O)$	H	3.93	3.17
		C	34.06	33.84
		N	1.65	1.78
Sample 4	$[Cu_3C_{18}O_{15}H_{12}]\cdot 2(DMF)\cdot 2(H_2O)$	H	3.59	3.34
		C	34.27	34.07
		N	3.33	3.29
Sample 5	$[Cu_3C_{18}O_{15}H_{12}]\cdot 3(DMF)\cdot 2(H_2O)$	H	3.93	3.86
		C	36.18	35.86
		N	4.68	4.44

Table 2.3: Elemental analysis results of top five HKUST-1 samples with highest crytsallinity and phase purity

The common practice is to publish only the successful and optimized synthetic condition which yielded the MOF with highest crystallinity, phase purity and/or BET surface area. The chemical intuition gained from performing several hundreds or thousands of experiments is not well explained in publications. This results in the high probability of non-transfer of chemical intuition to researchers from other research groups or to researchers within the same research group. Alternatively, in this work, we not only publish but also analyse our data of more than 120 partially successful and failed synthetic conditions. The objective of such analysis was to quantify the relative importance of the synthesis variables. It was performed with random forest model, a machine learning technique. For further details, the reader is referred to the publication version of this work[142].

2.3. Application of chemical intuition to accelerate the synthesis of Zn-HKUST-1

Interestingly, the results of the probed experimental parameters and their impact on crystallinity and phase purity from machine learning agrees with the empirical guidelines of MOF synthesis. It shows the robustness of our approach and also displays that we were able to capture and quantify the chemical intuition that an experimental MOF chemist will possess. For instance, previous studies[14,143-145] on HKUST-1 MOFs indicate the importance of reactant ratio, temperature and polar solvents on nucleation, crystal growth which is resonated in our results also.

Sample	H_2O	DMF	EtOH	MeOH	iPrOH	Reactants Ratio	Temperature	Microwave power	Reaction time
1	0.0	5.5	0.0	0.0	0.5	1	102	155	29
2	3.0	0.0	2.5	0.0	0.0	1.5	171	150	5
3	0.0	2.5	0.0	0.0	3.0	1	100	250	19

Table 2.4: Three synthetic conditions which yielded crystals of Zn-HKUST-1

In addition to the Cu version of HKUST-1, Zn, Co and Ni polymorph versions of HKUST-1 are also synthesized and reported in the literature. The Zn version of HKUST-1 is less stable and collapses upon removal of solvent molecules[146,147]. The objective of the second case study was to synthesize Zn-HKUST-1 with rational experiments as envisioned in our scheme. The rational experiments should stem from the insights gained by analyzing the Cu-HKUST-1 data.

Through this case study of synthesizing Zn-HKUST-1, we demonstrated the inherent feature and drawback of MOF synthesis and MOF chemistry. The top ten successful synthetic conditions of Cu-HKUST-1 were applied for the synthesis of Zn-HKUST-1. However, none of them were successful in yielding Zn-HKUST-1 crystals. This further reiterates that the chemistry is too specific for a particular MOF and the optimal synthetic conditions are non-transferrable to synthesize another MOF even though it is a polymorph version.

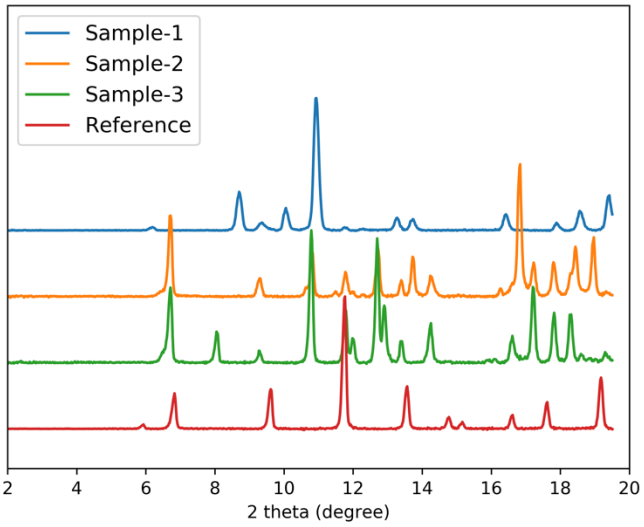

Figure 2.10: PXRD patterns of Zn-HKUST-1 samples.

Further optimization is required to achieve Zn-HKUST-1 samples of highest crystallinity and phase purity

Practically this should require us to perform the optimization of Zn-HKUST-1 synthesis with several experiments. However, our chemical intuition knowledge helped us in assigning the importance of the synthetic variables prior to generating the synthetic conditions of Zn-HKUST-1. As a consequence of which, twenty diverse synthetic conditions were generated and from which, two synthetic conditions yielded Zn-HKUST-1 crystals. We consider the twenty rational experiments to be equivalent to performing several thousands of experiments without chemical intuition.

Thereby, through our HKUST-1 case studies, the objectives for the designed synthetic platform - accelerating the discovery, synthesis of MOFs with rational experiments facilitated by comprehension of the synthetic variables is achieved and illustrated. This study also demonstrates that the captured chemical intuition is not different from the intuition developed by the MOF experimental chemist in the lab after several years of experience with synthesis. Overall, the developed synthetic platform is applicable to synthesize any MOF with any synthesis and optimization problems. We envision that it will promote the acceleration of discovery and synthesis of MOFs.

2.4. Appendix

Corresponding Author	BET (m^2g^{-1})	Synthesis technique	Temp. (°C)	Time (h)	Solvents	Metal, Ligand	Ref.
Ian D. Williams	692	CEH	180	12	H_2O, EtOH	1.8, 1.0 mM	[105]
Bein T	N/A	High-throughput CEH	180	16	H_2O, EtOH	0.3 g, 0.2 g	[148]
M. Douglas LeVan	921	CEH	85	24	DMF, H_2O, EtOH	10 g, 5 g	[149]
R. Staudt	1270	Basolite™ C300	N/A	N/A	N/A	N/A	[150]
	1555						
Stefan Kaskel	1239	Reflux	N/A	N/A	N/A	N/A	[151]
Stefan Kaskel	1370	CEH	100	24	DMF, H_2O, EtOH	3.5 g, 2.1 g	[152]
Johan A. Martens	999	Freeze drying	-196	N/A	EtOH	1.2 g, 0.6 g	[153]
Hua Kuo	1055	CEH	110	18	DMF, H_2O, EtOH	6 g, 3 g	[154]
Sasidhar Gumma	1663	CEH	100	10	DMF, H_2O, EtOH	2.1 g, 1.0 g	[155]
J. Karl Johnson	1482	CEH	85	18	DMF, EtOH	2.0 g, 1.0 g	[156]
	698		85	20		2.0 g, 1.0 g	
Omar M. Yaghi	1507	CEH	85	24	DMF, H_2O, EtOH	10 g, 5 g	[134]
Philip L. Llewellyn	1850	CEH	N/A	N/A	N/A	N/A	[157]
Stefan Kaskel	1502	CEH	120	24	H_2O, EtOH	3.5 g, 2.1 g	[158]
Stefan Kaskel	1340	CEH	100	20	H_2O, EtOH	3.5 g, 2.1 g	[159]
Florian O. R. L. Mertens	418	CEH	25	N/A	N/A	N/A	[160]
	435		60				
	603		100				
Zhong Li	1568.5	CEH	110	24	H_2O, EtOH	0.71 g, 0.42 g	[161]
Darren Bradshaw	1403	RT synthesis	N/A	N/A	N/A	N/A	[162]
	1436						
	1514						
	1763						
	1560						
	1749						
	1680	Basolite™ C300					
Ling-Guang Qiu	1326	CEH	120	12	H_2O, EtOH	1.09 g, 0.525 g	[163]
Ralph T. Yang	1150	CEH	85	20	DMF, H_2O, EtOH	1.0 g, 0.5 g	[164]
Omar M. Yaghi	1944	CEH	85	24	DMF, H_2O, EtOH	10 g, 5 g	[165]
Zifeng Yan	1922	CEH	75	24	DMF	5 g, 2.5 g	[166]
Ana M. Afonso	1068	CEH	110	24	H_2O, EtOH	1.25 g, 0.63 g	[167]
R. Chirone	680	CEH	85	21	DMF, H_2O, EtOH	20 g, 10 g	[168]
Xiaolei Fan	1507	CEH	100	N/A	H_2O, EtOH	0.87 g, 0.42 g	[169]
Jessica Semanscin	964.5	CEH	150	18	H_2O, EtOH	108, 49 g	[170]
Omar M. Yaghi	1781	CEH	85	24	DMF, H_2O, EtOH	10 g, 5 g	[171]
Ulrich Müller	1154	EC	N/A	N/A	N/A	N/A	[172]
Alex Wagener	1510	CEH	120	14	EtOH	1.75 g, 0.84 g	[173]
	1253	Reflux	120	14	N/A	N/A	
	1624	EC	N/A	N/A	N/A	N/A	
Michael Mehring	1143	CEH	120	24	H_2O, EtOH	0.9 g, 0.5 g	[174]

	1321	MW	180	0.3	H_2O, EtOH	0.9 g, 0.5 g	
	1206	US	25	1	N/A	0.2 g, 0.13 g	
	1253	MC	25	N/A	No solvent	N/A	
	1119	EC	40	N/A	N/A	N/A	
	897	Reflux	N/A	N/A	N/A	1 g, 0.7 g	
Jong-San Chang	1392	MW	140	N/A	H_2O, EtOH	3.6, 2 mmol	[175]
Ralph T. Yang	1296	CEH	85	20	DMF, H_2O, EtOH	10.0 g, 5.0 g	[176]
Xia Jiang	1100	US	N/A	N/A	N/A	N/A	[177]
Alexandra Navrotsky	1775.6	CEH	85	20	DMF, H_2O, EtOH	3:2 molar ratio	[146]
Nak Cheon Jeong	1740	CEH	80	20	DMF, H_2O, EtOH	0.87 g, 0.22 g	[178]
Chenguang Liu	1103.7	CEH	120	24	H_2O, EtOH	1.5, 1.0 mmol	[145]
Praveen K. Thallapally	2014	RT synthesis	25	24	MeOH	20, 10 mmol	[179]
Sasidhar Gumma	857	CEH	140	64	DMF, H_2O, EtOH	4.4 g, 1.9 g	[180]
Tao Wu	1292.3	CEH	85	3h	MeOH, C_2H_6	N/A	[181]

Table A2.1: A literature summary of some of the BET surface areas of HKUST-1 and the corresponding synthetic technique and conditions

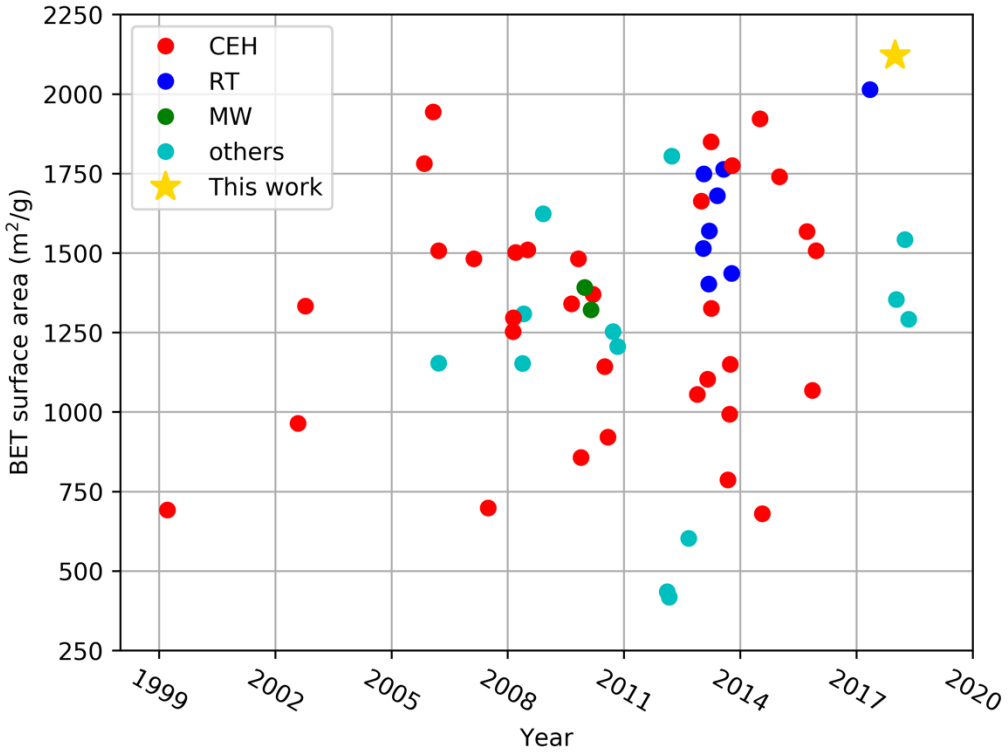

Figure A2.1: Timeline plot of some of the reported BET surface areas of Cu-HKUST-1

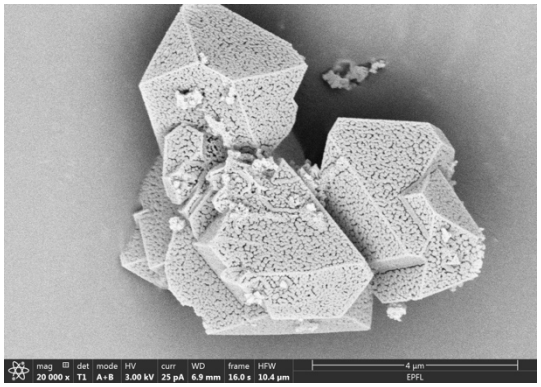

(a)

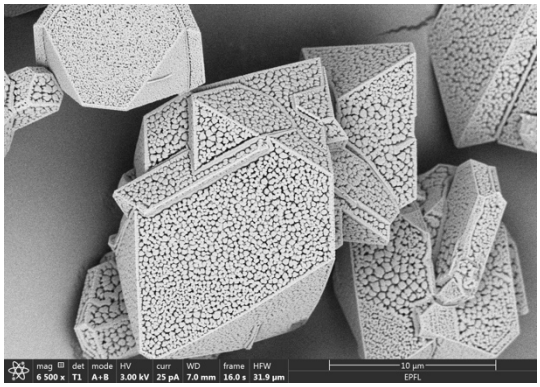

(b)

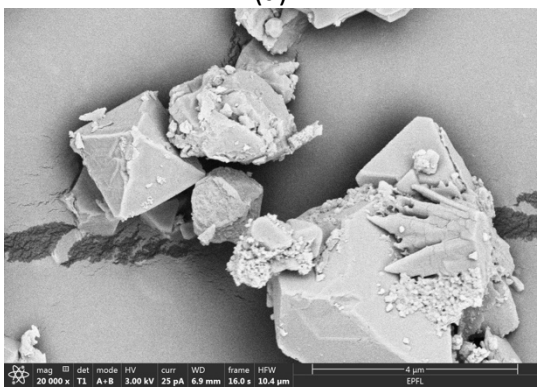

(c)

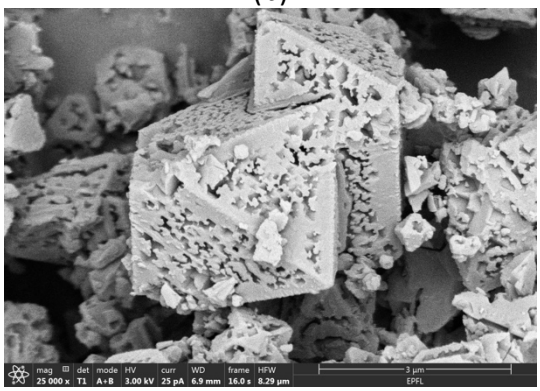

(d)

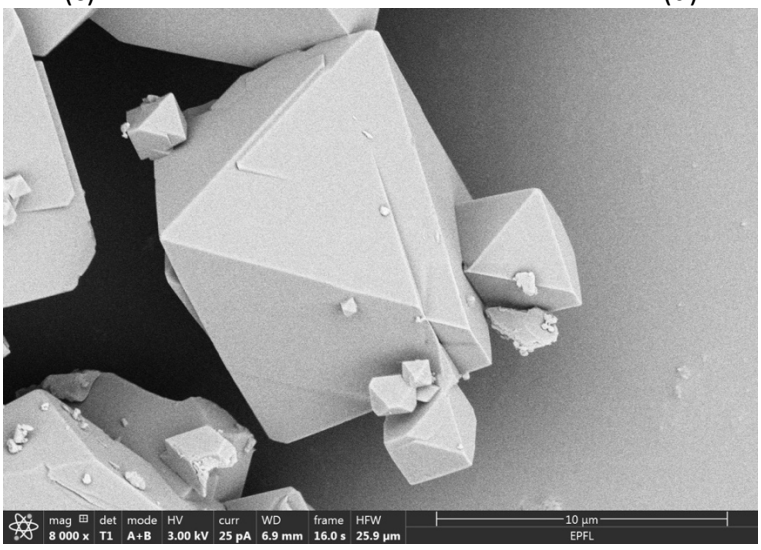

(e)

Figure A2.2: More SEM images of the five samples with high crystallinity based on powder X-ray diffraction but wide range of BET (300-2121$\mathbf{m^2g^{-1}}$). (a), (b), (c), (d) and (e) are corresponding to sample 1 to 5, respectively

Accuracy and reproducibility of experiments

The robotic platform provides a consistent synthesis protocol and a good control over the synthesis variables and reaction conditions. We automated the synthesis with programming the synthesis steps in the Chemspeed AutoSuite software. As it can be seen in Figure the amount of solvents and the solids (metal salt and the ligand) dispensed (refer to the numbers under the columns "actual volume", "actual quantity") on the robotic platform nearly match with the programmed amounts (refer to the numbers under the columns "entered volume", "entered quantity") for the solid dispensers and perfectly match for the liquid dispensers. This reveal the high accuracy and control over the synthesis variables and conditions. To further investigate the reproducibility of the reaction outcomes, we performed synthesis of Cu-HKUST-1 for two of the discussed samples in the main manuscript and measured their BET surface area and collected their PXRDs.

Sample	BET $[m^2g^{-1}]$				Average
	Measurement 1	Measurement 2	Measurement 3	Measurement 4	
4	1585	1646	1549	1607	1596
5	2011	1947	2101	2121	2045

Table A2.2: The measured BET surface area of the repeated experiments of two of the samples discussed in this work

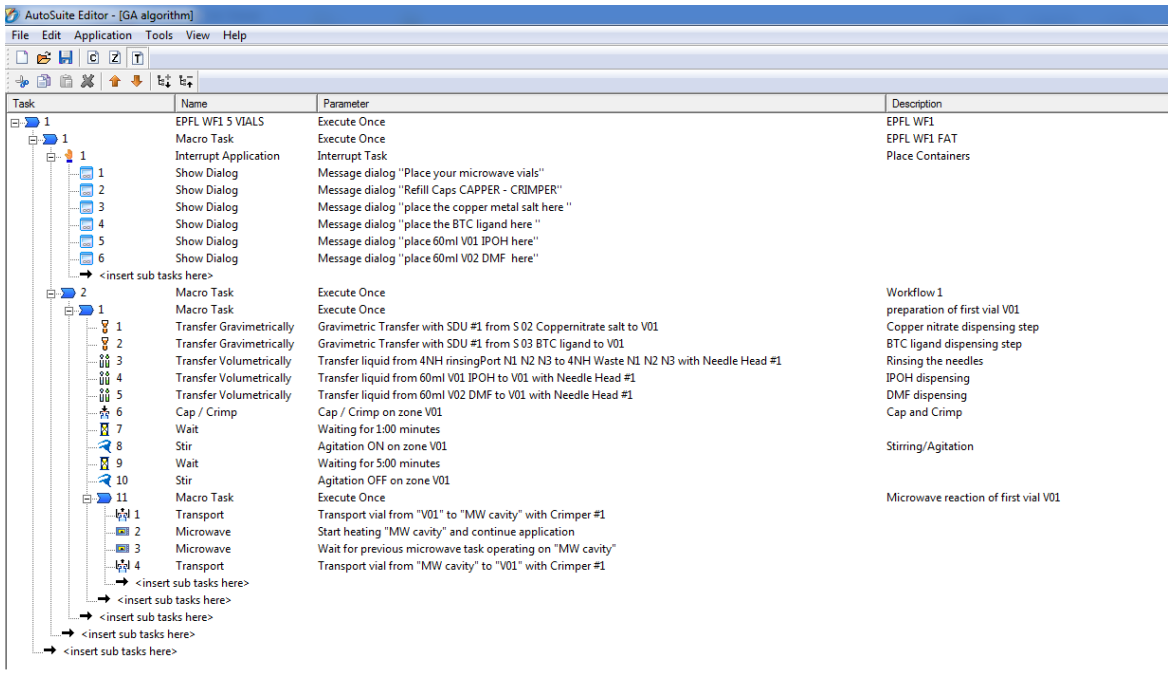

Figure A2.3: A screenshot of the algorithm that was programmed with the Chemspeed AutoSuite software for the automated robotic synthesis of a specific HKUST-1 MOF showing the synthesis steps

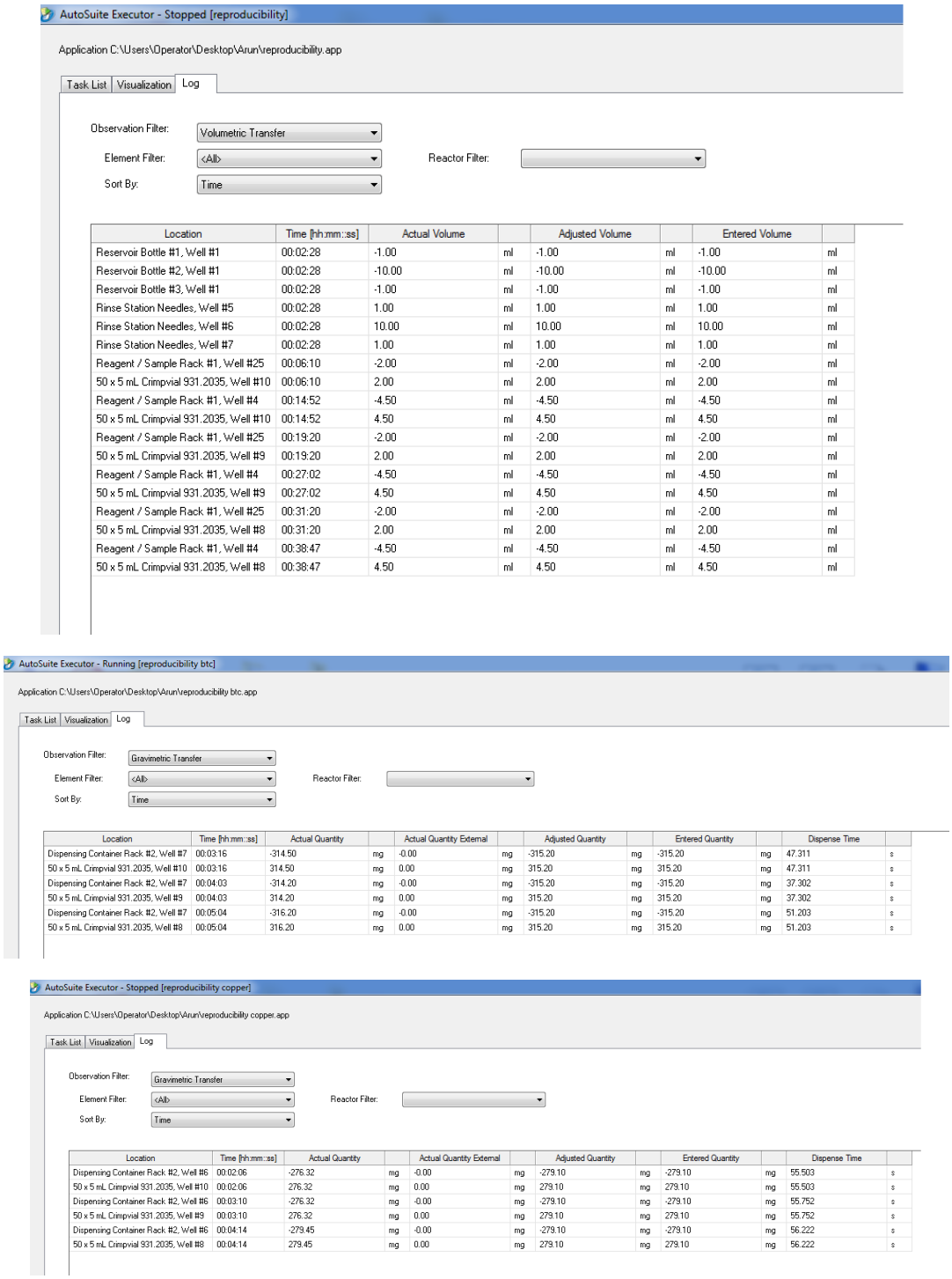

Figure A2.4: Screenshots of the log files of the solvent dispenser and the solid dispenser for one HKUST-1 MOF synthetic reaction performed thrice. Well #10, #9, #8 refer to the microwave reaction vials placed in the aforementioned wells

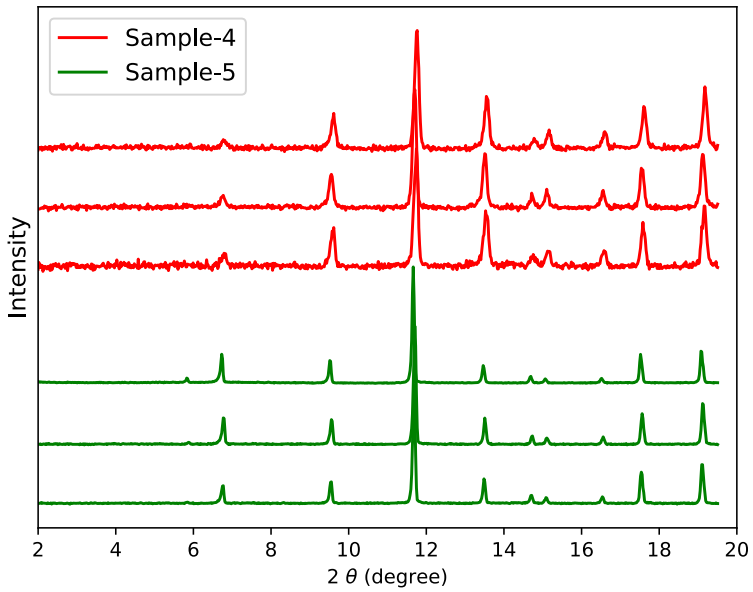

Figure A2.5: The PXRD patterns of sample 4 and 5, repeated three times to evaluate the reproducibility of the synthesis and measurements

Chapter 3 Synthesis and validation of applicability of metal-organic frameworks for wet flue gas CO_2 capture

Abstract

Metal-organic framework materials are promising solid adsorbent materials for carbon capture application. However, their performance is significantly affected when they are subjected to wet flue gasses like postcombustion flue gas. This is due to the competition amongst water and CO_2 for the same adsorption site. To address this, we developed a class of MOFs with a specific structural feature that bestows the MOFs with hydrophobicity and continual selectivity for CO_2 over N_2 in the presence of water. Furthermore, there exists no competition amongst water and CO_2. We have illustrated this with the design, synthesis, extensive characterization and performance assessment of two representative MOFs, which includes a new MOF. Through which, we validate the predictions made from simulations and computations.

3.1. Introduction

The introduction chapter of this doctoral thesis elucidates the importance of reducing anthropogenic CO_2 emissions. It emphasizes on how CCS is one of the viable options to combat this challenge. Also, it introduces the different carbon capture processes and technologies. Amongst which, adsorption with solid adsorbent materials has sparked the research interests. In that context, traditional adsorbents like zeolites and activated carbons are introduced with their merits and demerits. Furthermore, a class of nanoporous metal-organic framework (MOFs) materials is introduced based on which this doctoral thesis is developed.

Additionally, an overview with examples for the different strategies such as open metal sites, surface functionalization, catenation, flexible and MOFs with anions that are pursued to test MOFs as solid adsorbent materials for carbon capture is described. It concludes by emphasizing the water impediment that MOF materials faces on exposure to wet flue gasses which results in either structural or performance related deterioration like capacity, selectivity. Thereby, outlining the second research objective of this doctoral thesis work which is to develop MOFs that can capture CO_2 efficiently in the presence of water. Ideally and more specifically, it is desired to develop MOFs with structural features that does not promote competition amongst water and CO_2 for the same adsorption site.

This chapter of the thesis illustrates on how we address the water impediment challenge through the design, development and assessment of water stable MOFs that contain a specific structural feature for carbon capture from postcombustion flue gas. The work involves the synergistic combination of computations and experiments. A structural feature for MOFs design was identified based on the computational studies. First, an evaluation of hypothetical MOFs for their postcombustion carbon capture performance was performed. Second, several CO_2 adsorption sites were identified and subsequently, the structural features of the adsorption sites were analysed for their similarities. It yielded in the identification of three motifs which were further analysed for their water and CO_2 affinities.

Amongst them, the structural motif of a parallel layer of aromatic rings with an interatomic distance of 7 A° was identified to impart hydrophobicity to the MOF upon incorporation. In addition to imparting hydrophobicity, it also endows continual selectivity of the MOF for CO_2 over N_2 in the presence of water. It is predicted that CO_2 preferentially adsorbs between the parallel layers of aromatic rings whilst water is not adsorbed owing to the hydrophobicity. Thus, the adsorbed CO_2 is insulated from water with no competition amongst them. This entire process of mining and extracting the similarities in the structural features of adsorption sites is heavily inspired from the rational design of drug molecules. Wherein, the extracted structural feature of the adsorption site is called as pharmacophore and owing to which, we labelled our structural feature as adsorbaphore. The readers who are further interested in details of the computations and simulations are referred to the paper version of this work[182] as this chapter focuses on the experimental work.

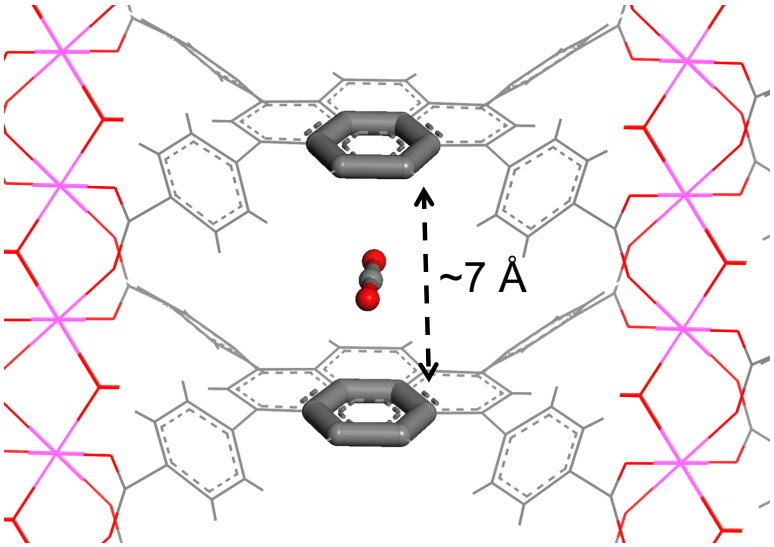

Figure 3.1: The adsorbaphore containing parallel aromatic rings with an interatomic distance of approximately 7 A°

3.2 Synthesis of Al-PMOF and Al-PyrMOF

With the adsorbaphore as the target design, a sub class of hypothetical MOFs was generated with aluminium as the choice of metal. Aluminium was chosen due to its abundant nature and the high thermal, hydrolytic stability that it bestows to the MOF upon coordination with a carboxylate moiety of the organic ligand. The reasoning behind the selection of metal that is earth abundant metal and which gives stability can be found in the introduction chapter of this thesis. We then synthesized two MOFs Al-PMOF and Al-PyrMOF which according to predictions has water frustrating properties and has the ideal adsorbaphore interatomic distance of 6.5 - 7 A°. The MOFs are based on one-dimensional rods of Al(iii) linked by TCPP (tetrakis(4-carboxyphenyl)porphyrin) to yield Al-PMOF and with TBAPy (1,3,6,8-tetrakis(*p*-benzoic acid)pyrene) ligand to yield Al-PyrMOF, respectively. The resultant MOFs are three-dimensional and non-interpenetrated crystalline structures.

Literature review enabled us to identify that Al-PMOF was reported previously for hydrogen production through photo catalysis[183]. Hitherto, the MOF has not been investigated for its carbon capture performance. Unlike, Al-PMOF, Al-PyrMOF has not been previously reported. The two MOFs were synthesized under solvothermal conditions.

3.2.1. Synthesis of [Al-PMOF]·guest molecules

The chemicals were purchased from the commercial suppliers and used without further purification: $AlCl_3 \cdot 6H_2O$ (Aldrich), H_6TCPP (TCI), DMF (Roth), Acetone (Aldrich). The synthesis

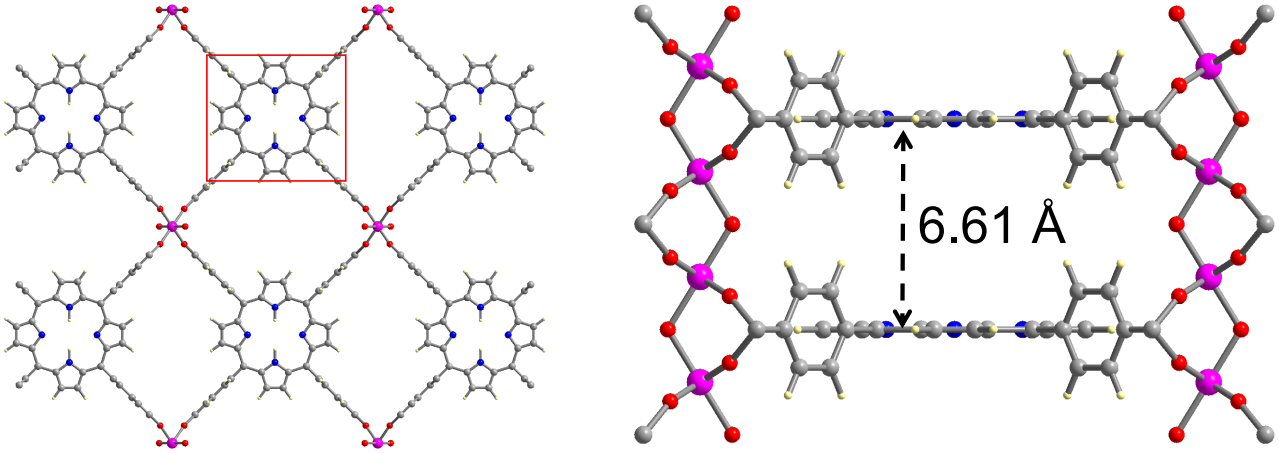

Figure 3.2: Ball-and-stick representation of the structures of [Al-PMOF].

The orientation of the tetra carboxylate ligands around the Al(iii) rods results in the generation of the three-dimensional non-interpenetrated structures containing the adsorbaphore (red box). Atom colour code: pink, Al; grey, C; blue, N; red, O; pale yellow, H

procedure was adapted from the literature[183]. 100 mg (0.126 mmol) of H_6TCPP and 60 mg (0.25 mmol) of $AlCl_3 \cdot 6H_2O$ were introduced into 10 mL of deionized water. The suspension was stirred for 10 minutes at room temperature and heated in an oven at 180°C for 16 hours with a heating rate of 3°C per minute. The solution was allowed to cool with a cooling rate 1.5°C per minute. The solid was recovered by filtration, washed 3 times with DMF (3 × 80 mL) and once with acetone (1 × 80 mL) in order to remove the unreacted H_6TCPP. After drying, the as-made [Al-PMOF]·guest molecules or $[Al_2(OH)_2(H_2TCPP)]$·guest molecules, was obtained as a reddish brown solid powder in a 40% yield. Anal. Calculated for Al-PMOF·$5H_2O$: C, 59.75; H, 3.97; N, 5.80. Found: C, 60.01; H, 4.00; N, 5.51

3.2.2. Synthesis of [Al-PyrMOF]·guest molecules

The chemicals were purchased from the commercial suppliers and used without further purification: $Al(NO_3)_3 \cdot 9H_2O$ (Alfa Aesar), DMF (Roth), Dioxane (Aldrich), Acetone (Aldrich), concentrated HCl (Aldrich). The synthesis of the ligand H_4TBAPy was adapted from[184]. A mixture of $Al(NO_3)_3 \cdot 9H_2O$ 12 mg (0.03 mmol) and H_4TBAPy 10 mg (0.015 mmol) was introduced into 4 mL of DMF/Dioxane/H_2O (ratio 2/1/1) solvent mixture and to which 10 μL of concentrated HCl (0.116 mmol) was added. The vial was heated at 85°C for 12 h with a heating rate of 0.1°C per minute and then cooled to room temperature at a rate of 0.2°C per minute. The solid was recovered by filtration, washed with DMF in order to remove any recrystallized H_4TBAPy. After drying, the as-made [Al-PyrMOF]·guest or $[Al_2(OH)_2(TBAPy)]$·guest molecules, was obtained as a yellow solid powder in a 28% yield. Anal. Calculated for $[Al_2(OH)_2(TBAPy)] \cdot 4DMF \cdot 3H_2O$: C, 60.43; H, 5.25; N, 5.03. Found: C, 59.92; H, 5.12; N, 5.21

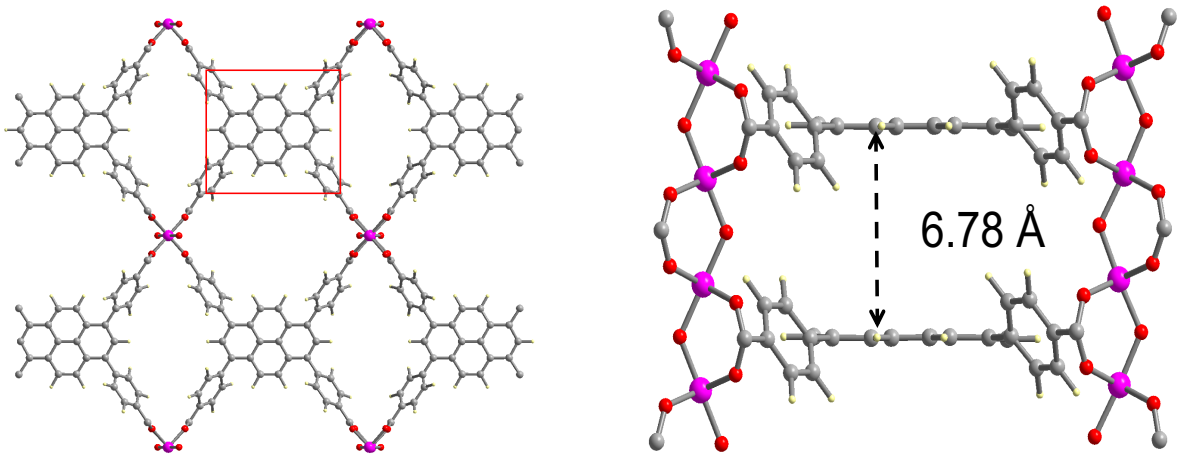

Figure 3.3: Ball-and-stick representation of the structures of [Al-PyrMOF].

The orientation of the tetra carboxylate ligands around the Al(iii) rods results in the generation of the three-dimensional non-interpenetrated structures containing the adsorbaphore (red box). Atom colour code: pink, Al; grey, C; blue, N; red, O; pale yellow, H

3.2.3. Activation protocol

The MOFs were activated with the following protocol: 20 mg of the as-made MOF were immersed in acetone for 72 hours to facilitate the exchange of solvent molecules occluded in the pores of the framework. The MOF powder was then filtered, dried at ambient conditions and heated (for removal of solvent molecules) at 170°C under secondary vacuum for 12 hours. This procedure leads in the generation of activated Al-PyrMOF and Al-PMOF and it was followed prior to adsorption measurements (N_2,CO_2,H_2O vapour isotherms) in-situ CO_2 gas loading powder X-ray diffraction, ^{13}C NMR and breakthrough experiments.

3.3. Characterization of Al-PMOF and Al-PyrMOF

The MOFs were characterized for their crystallinity, phase purity, thermal stability, completeness of activation protocol, morphology, porosity and enthalpy of adsorption.

3.3.1. Laboratory X-ray powder diffraction

The first characterization step was to collect X-ray diffraction patterns to assess the crystallinity and phase purity of MOFs. Since, the synthetic conditions yielded powder MOFs we collected powder X-ray diffraction patterns (PXRD).

Laboratory powder X-ray diffraction (PXRD) patterns shown in Figure 3.4 were carried out on a Bruker D8 Advance with TWIN/TWIN optics and a LYNXEYE XE detector, equipped with a robotic sample changer. The samples were loaded on low background silicon crystal sample holders and the PXRD data was collected throughout a 2θ range of 2–20° using a copper (Cu) X–ray source. The background was subtracted for all

the PXRD plots presented in this work. The sample holders were rotated about their central axis during data collection to improve statistics.

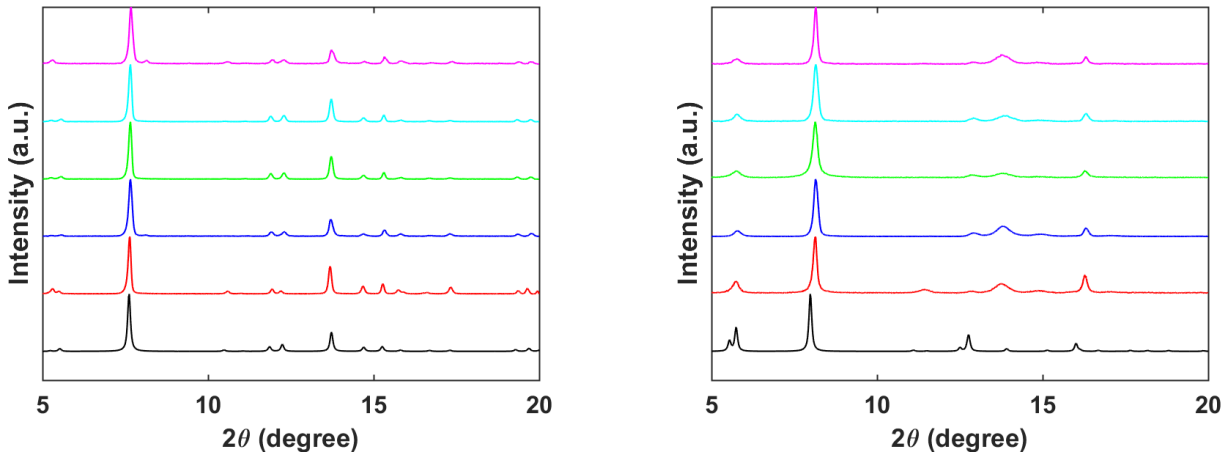

Figure 3.4: Laboratory powder X-ray diffraction (PXRD) patterns of [Al-PMOF] and [Al-PyrMOF].

Black, simulated; red, as-synthesized material; blue, acetone-exchanged material; green, activated material; sky blue, activated material immersed in liquid water for 7 days; pink, activated material exposed to a controlled atmosphere of nitric acid vapour for 3 h

All measurements were performed at room temperature. Figure 3.4 shows that the as synthesized MOFs are crystalline and phase pure as the powder pattern is in concordance with the simulated pattern. Furthermore, the MOFs are stable as the PXRD patterns are largely retained upon acetone exchange, activation and immersion in liquid water for a week. In addition, the MOFs are stable upon exposure to acidic vapours in a controlled environment for three hours.

3.3.2. In-situ variable temperature- Synchrotron X-ray powder diffraction experiment

was performed at BM31 of the Swiss-Norwegian Beamlines of ESRF (Grenoble, France), using a wavelength of 0.5008 Å. For the variable temperature PXRD (VTPXRD) experiments, thermal stability of the MOFs was measured up to 350 °C by using a temperature controlled hot air blower for the as-made powder MOF samples loaded in 0.5 mm quartz-capillaries and mounted on a standard Huber goniometer head and the corresponding PXRD patterns were recorded as a function of temperature.

The MOFs are stable up to the measured temperature of 350°C. The considerable changes observed in the relative intensities are owed to the loss of the occluded solvent molecules. The absence of large shifts of the reflections confirms the rigidity/robustness of the framework. The PXRD based stability results is in line with what was mentioned earlier in this chapter with regard to the stability that aluminium imparts.

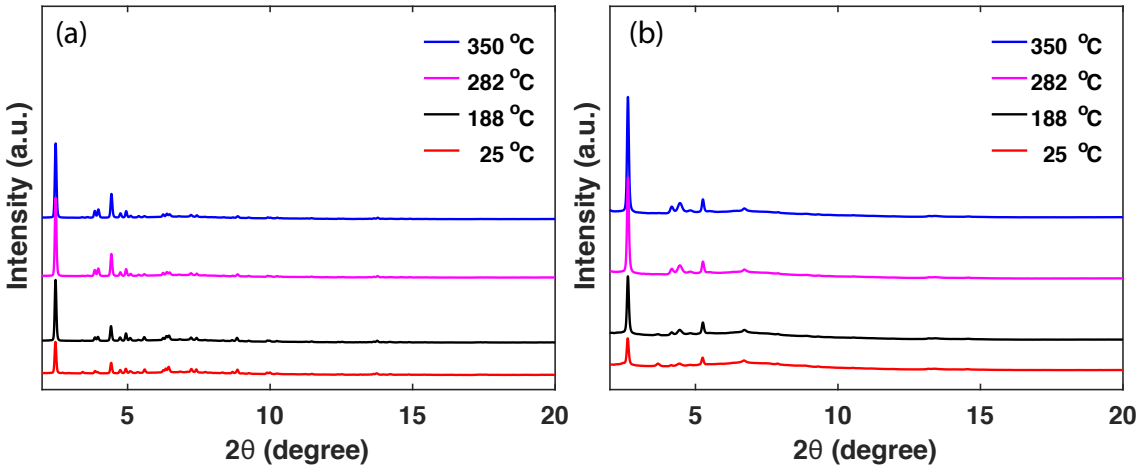

Figure 3.5: Synchrotron in-situ variable temperature X-ray powder diffraction plots. a) Al-PMOF, and b) Al-PyrMOF

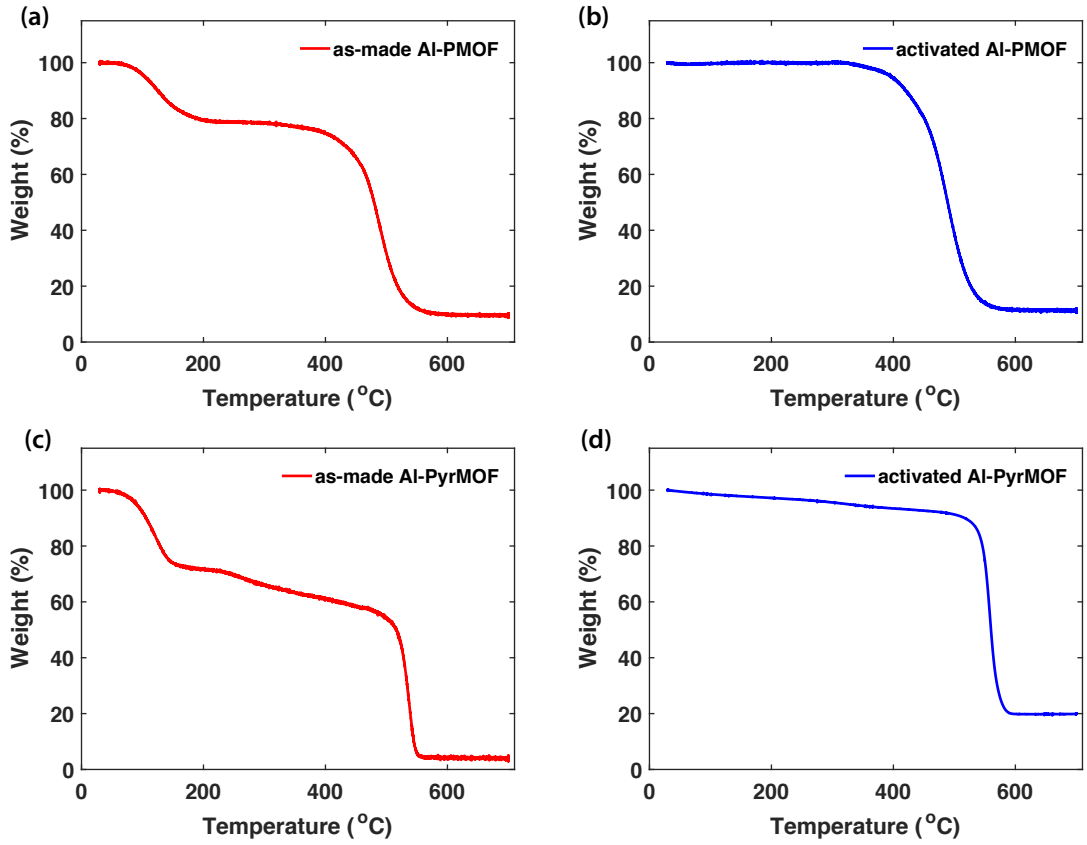

Figure 3.6: Thermogravimetric analysis (TGA) data curves of (a) as-made [Al-PMOF]·guest molecules, (b) activated Al-PMOF, (c) as-made [Al-PyrMOF]·guest molecules, and (d) activated Al-PyrMOF

3.3.3. Thermal Gravimetric Analysis (TGA)

To further assess the thermal stability of MOFs, thermal gravimetric analysis was performed. The TGA data were collected using a PerkinElmer instrument. The temperature range maintained for the measurements was 30 to 700 °C with a heating rate of 5°C per min and cooling rate was 20 °C per minute under air. The microbalance allowed the measurement of the sample's weight with an accuracy of ± 0.001 mg.
From the TGA profiles, it can be concluded that the observed weight losses as a function of temperature in the as made samples can be correlated to the loss of solvent molecules. Whilst, the activated MOFs lack such step wise weight losses which establishes the fact that the developed activation protocol is efficient in removing the occluded solvent molecules from the pore channels.

3.3.4. Fourier transform-infra red (FT-IR) spectroscopy

The completeness of activation protocol can be also studied with Fourier transform-infra-red spectroscopy experiments. The FTIR spectra will display the vibrations of the functional groups of the solvent molecules if they are present in MOF.
The FT-IR spectra shown in this work were collected at room temperature from 400-1800 cm^{-1} with the Perkin Elmer instrument Spectrum 100 for Al-PMOF and Al-PyrMOF MOFs. The band at

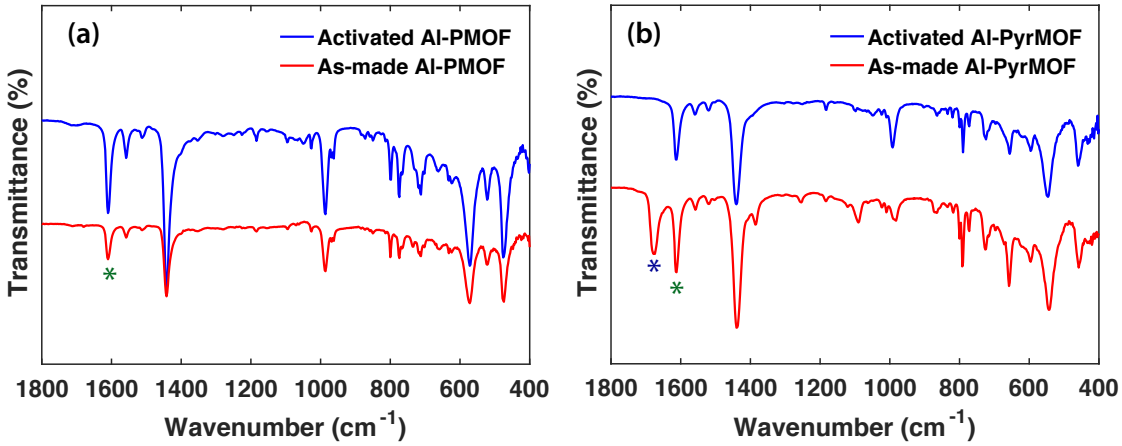

Figure 3.7: FTIR spectra of the as-made and activated (a) Al-PMOF, and (b) Al-PyrMOF from 400-1800 cm^{-1}

1608 cm^{-1} (marked as green asterisk) which is observed in both the MOFs can be assigned to the asymmetric stretching vibration due to the coordination of the carboxylate group with the Al^{3+} ions[185]. The band observed at 1680 cm^{-1} for Al-PyrMOF spectra is assigned to the C=O stretching vibration of the occluded DMF solvent molecules in the frameworks (marked as indigo colour asterisk in b). However, the band disappears in the spectra of the activated Al-PyrMOF. Thereby, reaffirming that the activation conditions of 170°C for 12 hours under vacuum is sufficient to afford a desolvated structure.

3.3.5. Morphology characterization

Having established the activation protocol and validated its efficiency through TGA and FT-IR analysis of the activated samples, we then collected scanning electron microscopy images of the as made and activated samples. The objective here was to identify any morphological changes that could be inflicted in the sample due to activation under electron microscopy.

The scanning electron microscope (SEM) micrographs were collected using the FEI Teneo SEM instrument. For SEM, the MOF samples were prepared by dusting them on a carbon tape which was pasted on a sample holder. Prior to imaging, the samples were coated with Iridium for 7 nm thickness to make them conductive. Close observation of SEM images of the as made and activated MOFs indicates that there are no major morphological changes upon activation. This is in line with our VTPRXD and PXRD results which established that there is no structural change upon activation.

3.3.6. Porosity

The CO_2 (293 K, 303 K, and 313 K) and N_2 (77 K, 313 K) isotherms shown in this work were collected by gravimetric method using an IGA system (Intelligent Gravimetric Analyser, Hiden Isochema Ltd., Warrington, UK). The water vapour sorption isotherms (313 K) were measured using the BELSORP aqua system (MicrotracBEL Corp., Osaka, Japan).

The first objective of the porosity characterization experiments was to determine the pore volume and BET surface area from the N_2 isotherms collected at 77 K. The MOFs displayed type I isotherm according to the IUPAC classification of isotherms and displayed permanent porosity. The total pore volume ($cm^3\ g^{-1}$) was determined from the N_2 isotherm (77 K at $P/P_0 = 0.9$) based on Gurvich-rule, which gave 0.54 $cm^3\ g^{-1}$ and 0.48 $cm^3\ g^{-1}$ for Al-PMOF and Al-PyrMOF, respectively. The BET surface area of Al-PMOF and Al-PyrMOF were determined to be as 1376 and 1109 m^2g^{-1}.

Then we proceeded to collect the single component isotherms of CO_2 and N_2 at 313 K, the post combustion flue gas temperature. We show that the experimental and predicted isotherms are in good agreement. While theory predicts slightly higher adsorption in each material at lower temperatures of 293 and 303 K, the similar slopes on the log-log plots demonstrate their affinities are the same at low loading. It also shows that MOFs are porous to CO_2 and has negligible or dismal uptake of N_2 which is the major component of the post combustion flue gas stream.

Likewise, the water vapour isotherms were collected at 313 K displayed type V isotherms displaying negligible uptake of water even at high relative humidity. The PXRD patterns which were collected after the exposure to water vapour re-establish that the MOFs are hydrophobic and the crystallinity is retained without being affected by water.

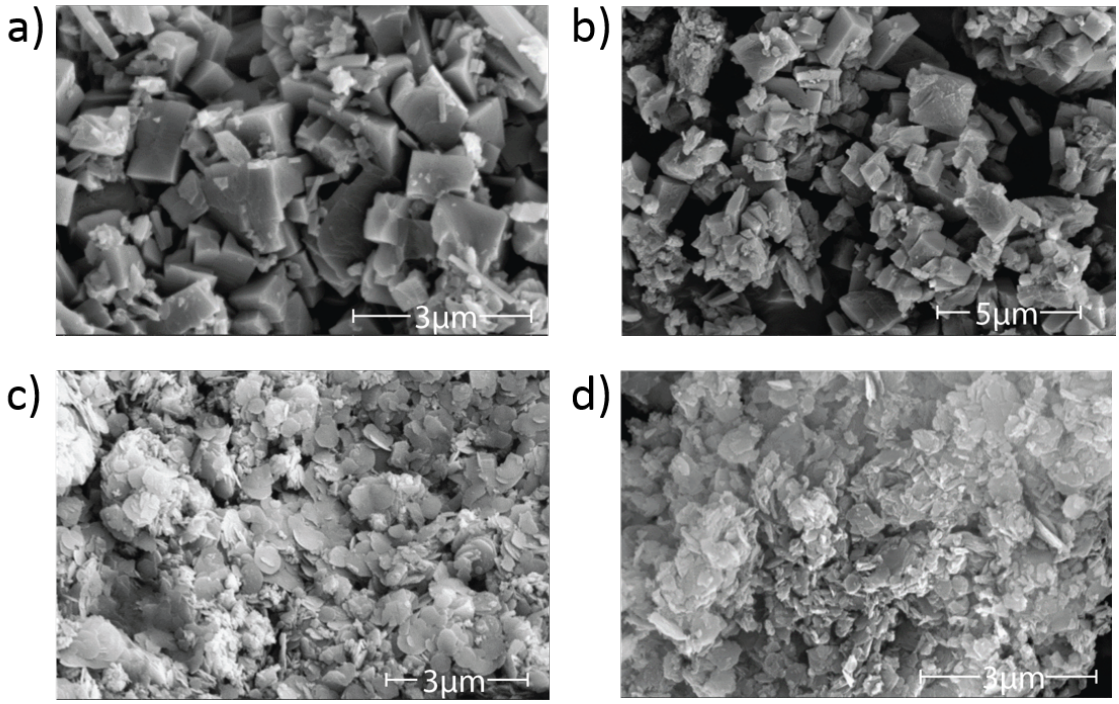

Figure 3.8: SEM images of a) as made [Al-PMOF]·guest molecules, b) activated Al-PMOF, c) as made [Al-PyrMOF]·guest molecules, and d) activated [Al-PyrMOF]

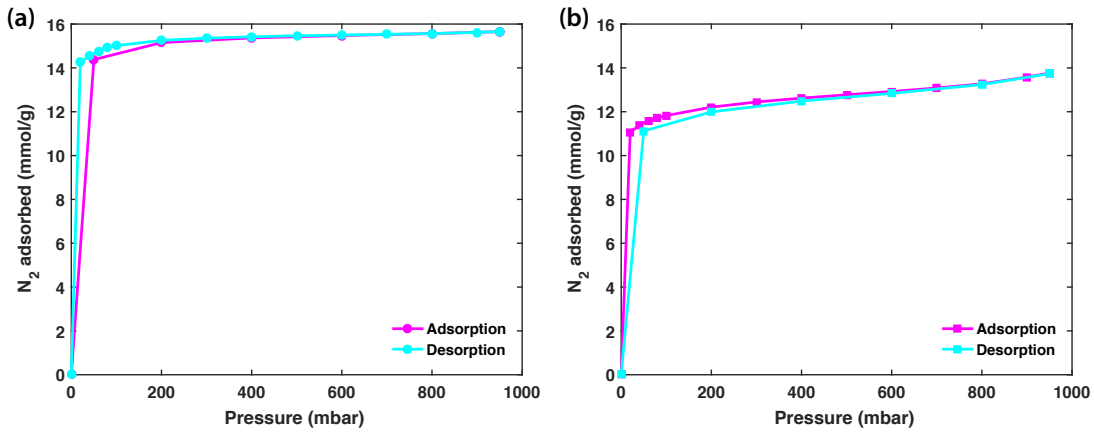

Figure 3.9: N_2 sorption isotherms collected at 77 K for (a) activated Al-PMOF, and (b) Al-PyrMOF

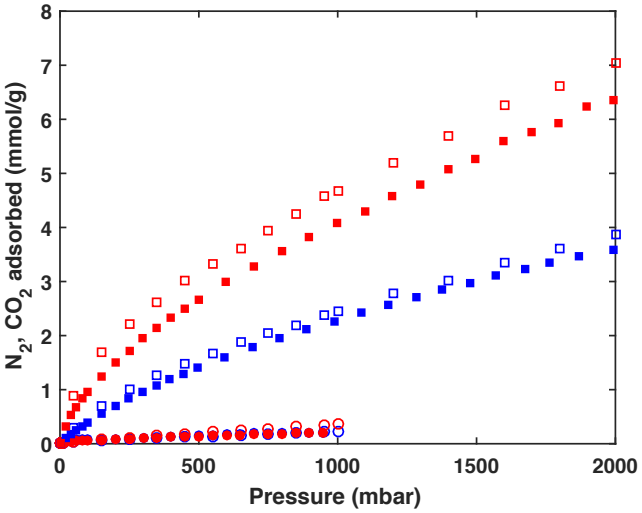

Figure 3.10: Experimental (filled) and computational (open) single-component adsorption isotherms for CO_2 (squares) and N_2 (circles) adsorption collected on activated Al-PMOF (red) and Al-PyrMOF (blue) at 313 K

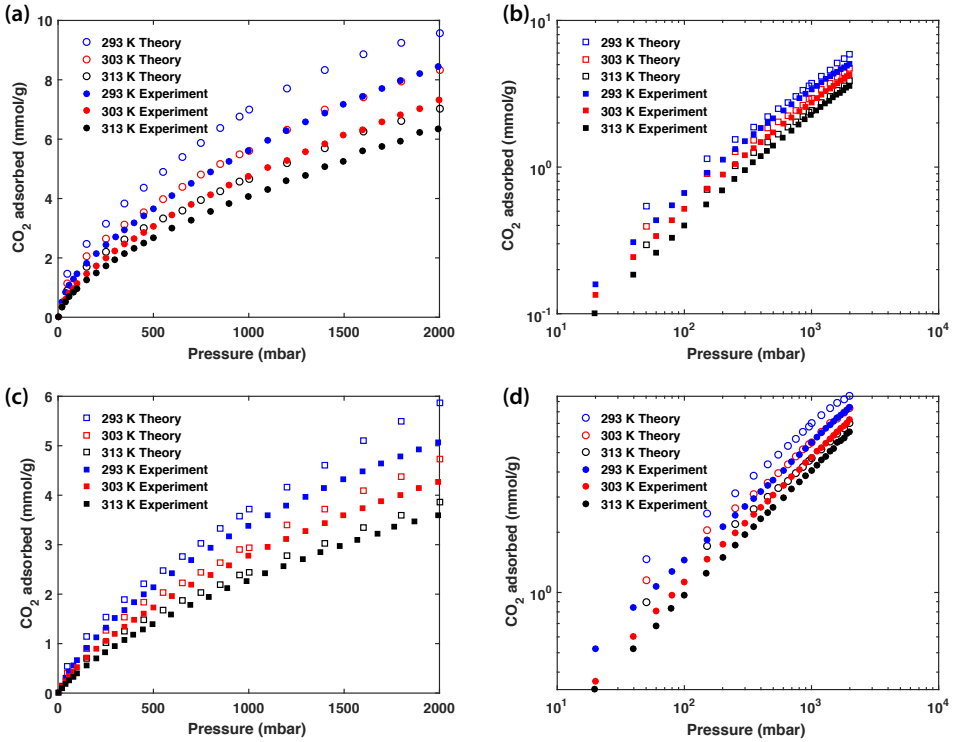

Figure 3.11: CO_2 adsorption isotherms of (a) Al-PMOF and (b) Al-PMOF adsorption on a log-log scale, (c) Al-PyrMOF and (d) Al-PyrMOF on a log-log scale

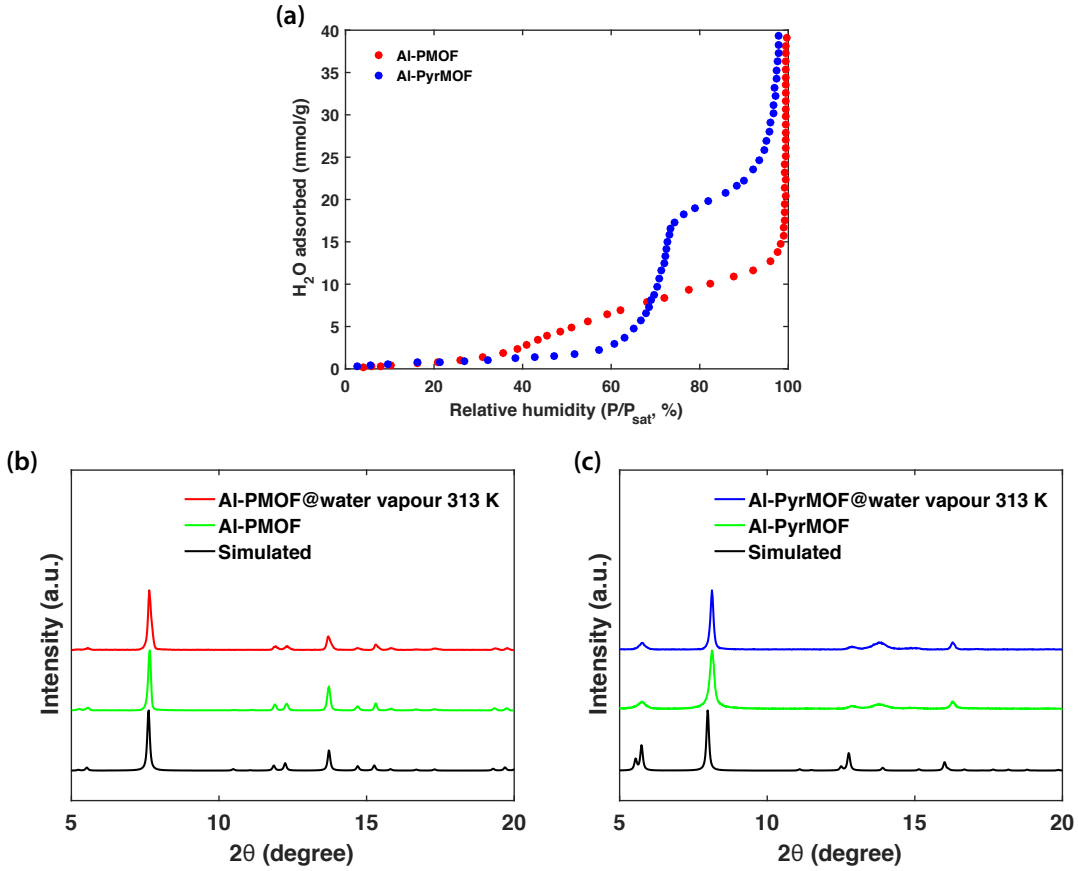

Figure 3.12: (a) H_2O vapour isotherms collected at 313 K for activated Al-PMOF, and Al-PyrMOF displaying type V isotherm. (b) Al-PMOF and (c) Al-PyrMOF PXRD patterns were collected after the isotherm measurements

From the CO_2 adsorption isotherms collected at 293 K and 303 K, the isosteric heat of adsorption representing the average binding energy of the adsorbing gas molecules at a specific surface coverage (n) were calculated based on Clausius-Clapeyron equation. The results are in agreement with the thermodynamics of adsorption as the heat of adsorption decreases with increasing amount of CO_2 adsorbed.

3.4. Siting of CO_2

By establishing the synthetic conditions and characterization of MOFs, we then performed the challenging experiments to experimentally identify the binding sites of CO_2, water. Through these studies the objective is to show that CO_2 preferentially adsorbs in the adsorbaphore and thereby validate the computational predictions.

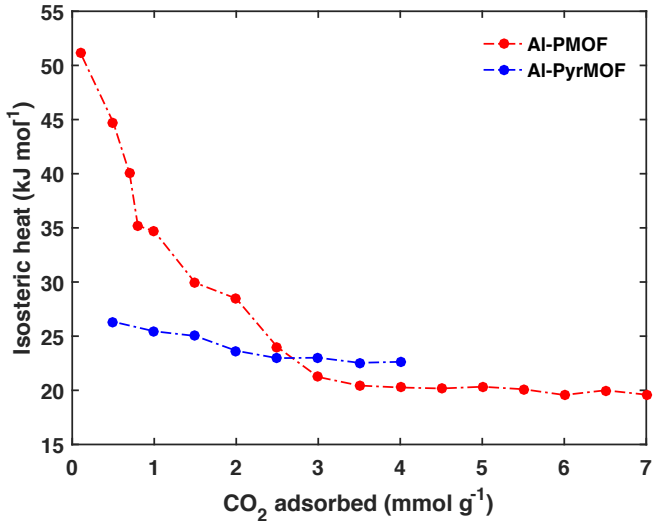

Figure 3.13: Isosteric heat of adsorption plotted as a function of excess adsorbed amount of CO_2 for Al-PMOF, and Al-PyrMOF

3.4.1. *In-situ* synchrotron CO_2 loading powder X-ray diffraction experiments

In-situ CO_2 loading synchrotron X-ray powder diffraction was performed at BM31 of the Swiss-Norwegian Beamlines of ESRF (Grenoble, France), using a wavelength of 0.5008 Å. Previously activated samples were loaded into 0.5 mm quartz-capillaries on a home-made gas cell mounted on a standard Huber goniometer head. Rietveld refinements attempting to locate guest molecules in complex structures are challenging, and high counting statistics are required. Therefore, we chose a Mar345 area detector which allows measuring the entire Debye-Scherrer ring.

Prior to gas loading, the gas line was evacuated and flushed various times with Helium. The diffraction patterns of the activated MOFs loaded with 400 mbar Helium (heat transfer medium) pressure were collected over the entire temperature range in order to detect structural changes unrelated to the subsequent gas-loading, such as intensity changes due to quenching of potential structural disorder or polymorphic transformations at low temperature. The equilibrated gas loading of CO_2 was performed at 2-5 mbar in 400 mbar Helium at 313K, then rapidly quenched to 120 K. We expect the CO_2 molecules to be trapped in their original adsorption sites. The cooling to 120 K was performed to reduce the thermal vibrations of CO_2. Two-dimensional diffraction images were integrated using Bubble[186] and refined with the Rietveld method using the software TOPAS.[187]

The localization gas molecules in host frameworks is by no means routine diffraction work, given the lack of "contrast" between a potentially additionally disordered guest and the host. Nevertheless, in structures of low to medium complexity Fourier analysis directly allows determining the position of molecules such as CO_2 if they are sufficiently localized, without the

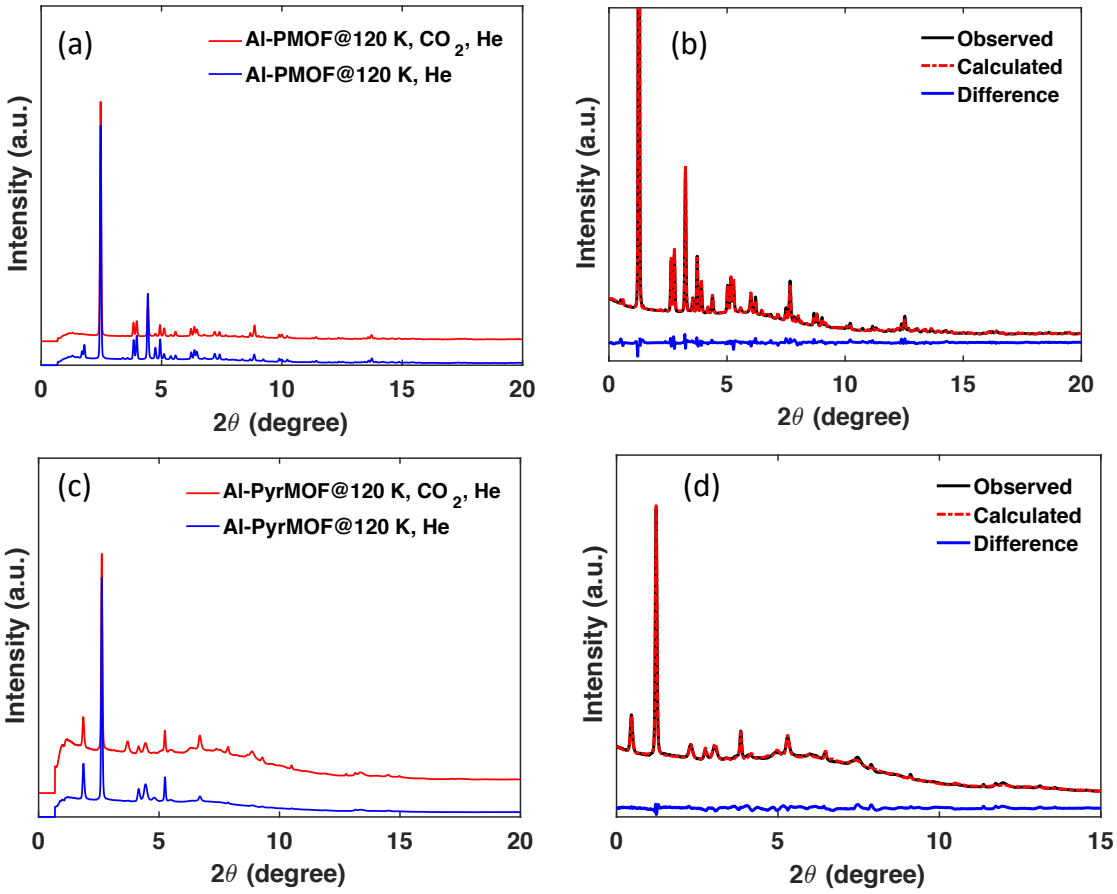

Figure 3.14: Synchrotron data plot (λ=0.5008 Å) of activated and in-situ He and CO_2 loaded (a) (Al-PMOF) at 120K, (b) Rietveld plot for CO_2 loaded Al-PMOF (2 mbar@400 mbar Helium) (c) (Al-PyrMOF) at 120 K and (d) Rietveld plot for CO_2 loaded Al-PyrMOF (5 mbar@400 mbar Helium)

need of global optimization (neither theoretical nor on experimental data), provided the sample quality is high enough and the acquired intensities are high and accurate. This has been shown multiple times for MOFs[188] and related materials such as Zeolites[189] and has also been directly compared to show agreement with neutron powder diffraction data.[190]

3.4.2. Rietveld refinement and localization of CO_2 from *in-situ* gas loading experiments

In Al-PMOF, CO_2 sorption sites could be identified based on Fourier difference maps generated by Rietveld refinement. Furthermore, CO_2 localization is facilitated due to the light elements, low disorder, high degree of crystallinity defining the host framework Al-PMOF and resulting good data quality. Al-PMOF was refined with the Rietveld method at 120 K under 400 mbar He-pressure using 5 distance and 3 angle restraints to stabilize the ligand. Fourier difference analyses indicated that activation was nearly complete.

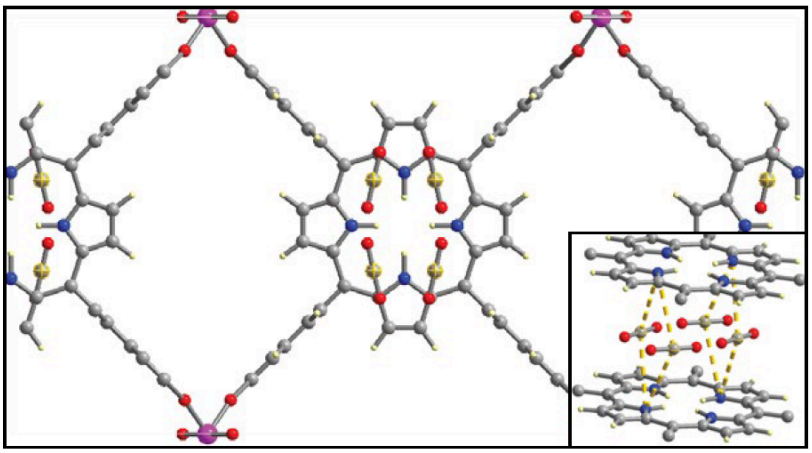

Figure 3.15: Rietveld refinement of the X-ray diffraction data revealed that CO_2 binding in [Al-PMOF] occurs between the porphyrin cores—that is, in the adsorbaphore

The obtained refined, activated and bare framework was used as a starting model to locate the primary sorption site for CO_2 in the framework of Al-PMOF, upon equilibrated gas loading of 2 mbar CO_2 in 400mbar Helium at 313 K which was then cooled to 120 K. The cooling to 120 K was performed to reduce the thermal vibrations of CO_2. Despite the relatively weak differences in diffraction intensities upon gas loading this primary site could be identified without the help of computational modelling. Strong discrete difference peaks were found in the Fourier map at positions located between porphyrin rings, i.e. close to those occupied by remnant water molecules.

The distances between these electron densities amounted to approx. 2.2 Å *before* refinement, indicative of the interatomic oxygen-distances in the CO_2 molecule. In order to stabilize the model during least squares refinement, a rigid body was inserted into the guest structure to describe the CO_2 molecule. For this rigid body, 3 parameters each were refined for translation and rotation, one C-O distance, one occupancy and one common displacement parameter. Data were modelled within the range 1.4 – 25 °2θ (1.1 Å).

In the final refinement, 6 shape parameters of the Thompson-Cox-Hastings pseudo-Voigt function were refined, as well as the detector-zero shift. All atomic positions and structural parameters were refined, stabilized by 2 distance and 1 angle restraints (Al-O octahedral chain) and 5 distance and 4 angle restraints for the cyclic group. This group was flattened additionally. Appropriate weights were applied. One common thermal displacement parameter was assigned to the cyclic group, the porphyrin ring, Al, O and the rigid CO_2 molecule. The porphyrin ring was not additionally restrained. The resulting structural model is shown in Figure 3.15 depicting the position of the adsorbed CO_2 molecule in Al-PMOF.

	a(Å)	b (Å)	c (Å)	V (Å^3)	Rwp %	Rwp bgd %	Chi^^{2}
Al-PMOF@120 K He	31.923(4)	6.597(1)	16.912(3)	3561.6(4)	2.6	11.3	247
Al-PMOF@120 K CO_2, He	31.984(3)	6.606(3)	16.950(1)	3575.7(3)	2.9	9.7	552
Al-PyrMOF@130 K He	30.83(4)	6.61(6)	15.56(4)	3172.2(3)	3.0	27	237
Al-PyrMOF@120 K CO_2, He	30.78(2)	6.63(7)	15.59(3)	3182.3(2)	2.6	18	49

Table 3:1: Lattice parameters and agreement factors for Al-PMOF and Al-PyrMOF dosed with Helium and/or CO_2 for in-situ CO_2 localization experiments

While the CO_2 molecule comes to lie close to the mirror plane on the general position, it is disordered around a 2-fold axis parallel to *c* as well as a mirror plane perpendicular to this axis, resulting in 4-fold disorder around the 2-fold Wyckoff position 2*c* of higher symmetry *mmm*. The occupancy of this disordered site was refined to 28 %, corresponding to 1.1 CO_2 molecules per porphyrin ring. We point out that a second sorption site is barely visible in the difference maps, running parallel to the chains of Al-octahedra. Our attempts to model this site was hampered due to the low occupancy (2 %) and ambiguities in the interpretation. These results confirm the preferential adsorption of CO_2 in the adsorbaphore.

The starting model of Al-PyrMOF was derived from the published indium-analogue[184] by placing Al on the In-site. Anisotropic line broadening in Al-PyrMOF was modelled using the Stephens model for the orthorhombic crystal system.[191] The associated parameters were refined in a profile fit along with lattice parameters and zero error, as well as 4 peak shape parameters of the TCHZ function implemented in TOPAS. All shape parameters (Stephens's model, TCHZ) were then fixed prior to Rietveld refinement. Data were modelled within the range 1.4 – 17 °2θ (1.7 Å).

One benzene group was treated as a rigid body to model disorder with one common C-C distance (refined to 1.38). 3 translations and 3 rotations were refined for the Benzene ring. 2 distance restraints to stabilize distances between the benzene ring and the Al-O chain. 1 common displacement parameter for all C atoms of benzene. The occupancy of the rigid body was corrected for the Wyckoff multiplicity of the special position the ring is lying on. The central fragment of the ligand was fixed to the position on the mirror plane perpendicular to the *b*-axis. 4 CO_2 molecules were refined as rigid bodies. C-O distances were fixed to 1.16 Å. Rigid CO_2 molecules were kept free, i.e. 4*3 translational and 4*3 rotational parameters per molecule. One common isotropic displacement parameter per CO_2 and 1 occupancy (corrected for special positions) of the rigid body were refined additionally. In the final refinement, the background was refined with a Chebyshev polynomial as well as the initially determined peak shape parameters and the 7 parameters of the Stephens model.

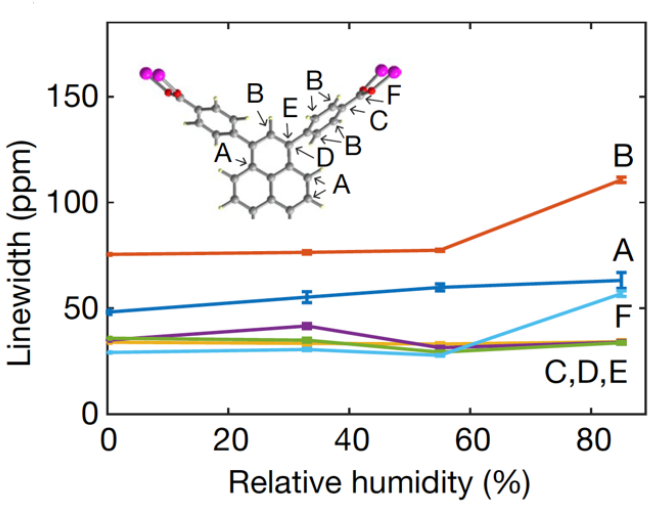

Figure 3.16: The linewidth of each carbon peak of the TBAPy ligand in [Al-PyrMOF] in the ^{13}C cross-polarization MAS spectrum, plotted as a function of relative humidity. Each carbon atom in the ligand is labelled in the inset

3.5. Siting of water

The localizing of water molecules in Al-PyrMOF was performed with solid state nuclear magnetic resonance (NMR) experiments. Under magic angle spinning (MAS), high-resolution ^{13}C NMR chemical shifts are very sensitive to changes in the chemical environment.

3.5.1. Experimental details and results

The solid-state NMR experiments shown in Figure 3.16 were recorded at 9.39 T using a Chemagnetics 3.2 mm probe with the sample spinning at 8 kHz. ^{13}C MOF spectra were obtained using cross polarization (CP) to excite and detect ^{13}C nuclei with a contact time of 2 ms. The ^{13}C NMR spectra of Al-PyrMOF and Al-PMOF shows the assignment of the peaks to specific atoms on the MOF. The solid-state NMR spectra shown in Extended data Fig. 8 are assigned by using the CASTEP density function theory (DFT) package[192-194] that uses the gauge including projector augmented wave (GIPAW) algorithm, permitting the reconstruction of the all-electron wave function within an external magnetic field. To calculate the NMR shifts, we used the Perdew-Burke-Emzerhof (PBE) general gradient approximation (GGA) with ultra-soft pseudopotentials and 0.1 k points $Å^{-3}$. We optimized the chemical shift by converging against the plane-wave cutoff energy to gain an approximation of the chemical shifts relative to each other. The calculation gives many similar chemical shifts across the unit cell, so we broadened the peaks with a 1 ppm Lorenztian function which allowed us to compare to the experimental spectrum.

The presence of adsorbed water at framework sites is assessed by examination of the MOF CPMAS spectra as a function of humidity. The ^{13}C line shapes, linewidths and chemical shifts are similar between activated materials and those exposed to 33% RH and 55% RH. At 85% RH values, we observed a change in peaks

associated with the benzoate and carbonyl parts of the Al-PyrMOF. These shift changes are consistent with literature values obtained when these functional groups hydrate,[195] according to the CASTEP simulations discussed earlier. However, no structural change is observed in PXRD as a function of RH. This confirms that the adsorbaphore itself is not a preferential adsorption site for water.

3.6. Effect of water on CO_2 adsorption

The simulations predict that the adsorbed CO_2 in the adsorbaphore of the MOF is well insulated from water. To confirm and validate this, we performed ^{13}C NMR experiments as the adsorbed CO_2 is sensitive to its local chemical environment. Therefore, any minute disruptions in the local chemical environment is reflected in the chemical shifts and line broadening.

3.6.1 Experimental details and results

To study the influence of H_2O on the NMR line shape of $^{13}CO_2$ in Al-PyrMOF we packed a solid-state NMR rotor and left it inside a home-built humidity chamber. The chamber was designed to be as small as possible while still allowing gas and vacuum ports to be added. The relative humidity (%RH) was changed by adding different saturated salt solutions to the bottom of the chamber and then placing the NMR rotor on a perforated platform just above the solution. This ensures the sample sits inside the vapor above the liquid where the RH value is known. We studied 33% (MgCl), 55% ($Mg(NO_3)_2$) and 85% (KNO_3) RH points using this method.

All measurements were performed using samples left in the humidity chamber for 24 hours at a desired RH value. We studied both the CP-MAS spectrum of the MOF, as well as the static spectrum of $^{13}CO_2$ gas dosed into the MOF after subjecting the material to a given humidity. The CO_2 loading was done using a home built *in-situ* setup with a lecture bottle of $^{13}CO_2$ connected to a regulator which is attached to a line that was fed into the bore of the magnet into a high-pressure liquid NMR tube. The pressure was measured using a dual capacitance manometer pressure gauge from MKS. The line was evacuated using an Edwards oil pump, then dosed to a given pressure using a regulator. We used a one pulse-acquire experiment to collect static ^{13}C spectra of $^{13}CO_2$ at different pressures, with the NMR experiments obtained at 16.44 T using a Bruker BBO 700 MHz S4 5 mm liquid state NMR probe.

The ^{13}C direct acquisition experiments are shown in for Al-PMOF and Al-PyrMOF. Solid CO_2 has a linewidth of 350 ppm characterized by an axially symmetric chemical shift power pattern.[196] In the spectra shown in Figure 3.18 we observe this $^{13}CO_2$ powder pattern, yet there is some motional narrowing to yield a line shape intermediate between solid and gaseous CO_2. As the pressure increases, the line shape narrows for Al-PMOF and Al-PyrMOF, as shown in Figure 3.18 (a) and (b), respectively.

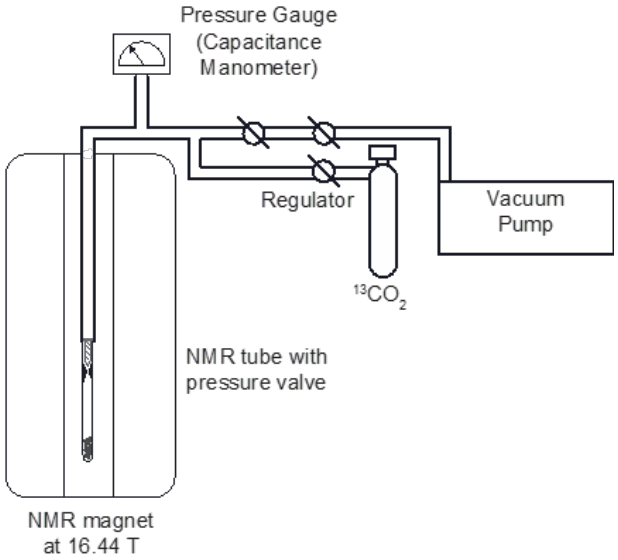

Figure 3.17: Diagram of our home-built apparatus for dosing materials with ^{13}C labelled CO_2 for in-situ measurements

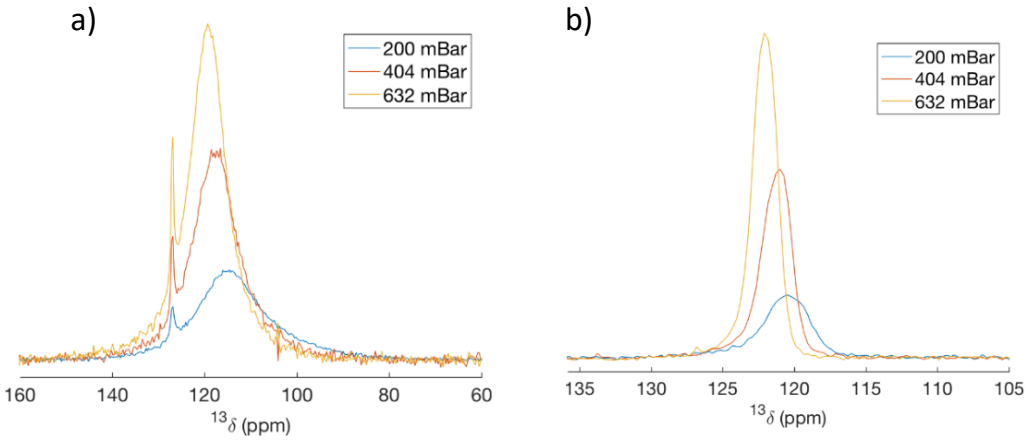

Figure 3.18: The solid-state NMR spectra recorded for activated a) Al-PMOF, b) Al-PyrMOF loaded in-situ with CO_2 at 200 mbar, 404 mbar and 632 mbar

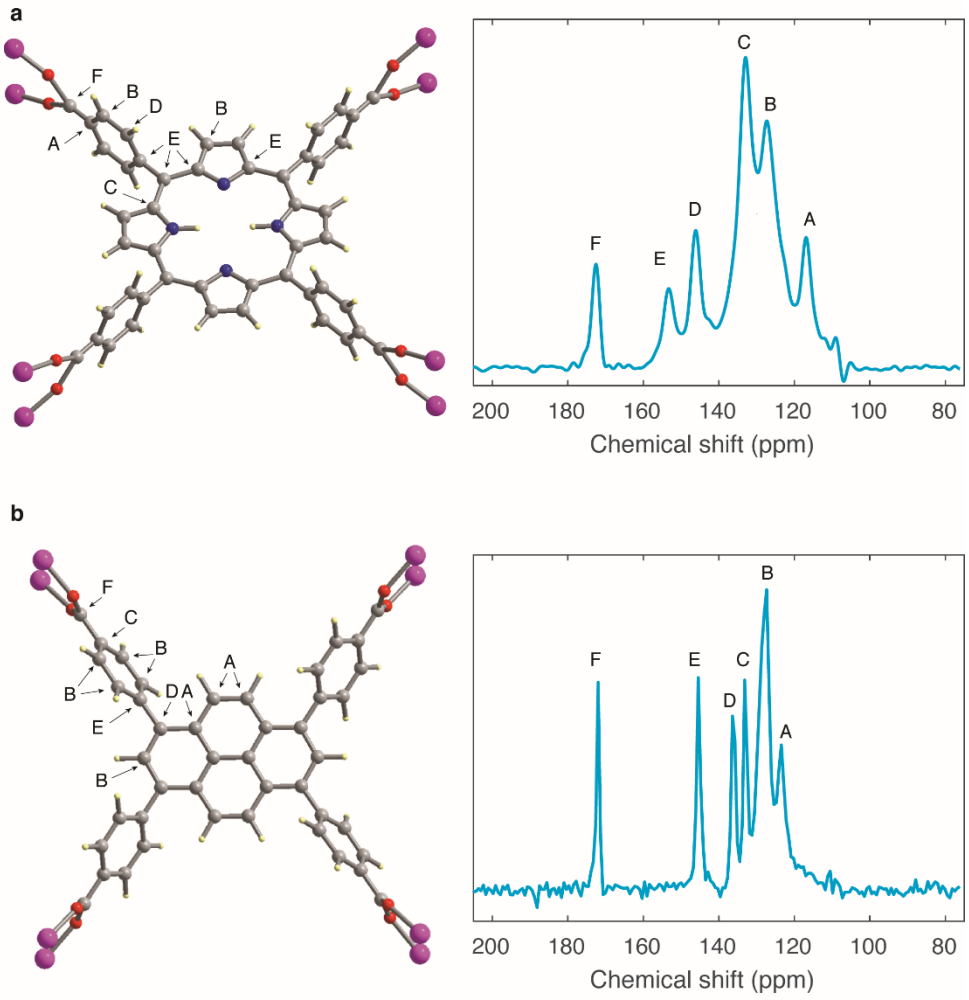

Figure 3.19: ^{13}C cross-polarization MAS spectrum of Al-PMOF (a) and Al-PyrMOF (b) recorded at 9.39 T with sample spinning at 8 kHz; the contact time for the cross-polarization experiment was 2 ms. The letters labelling the peaks of the spectra correspond to the labels on the carbon atoms in the structures on the left

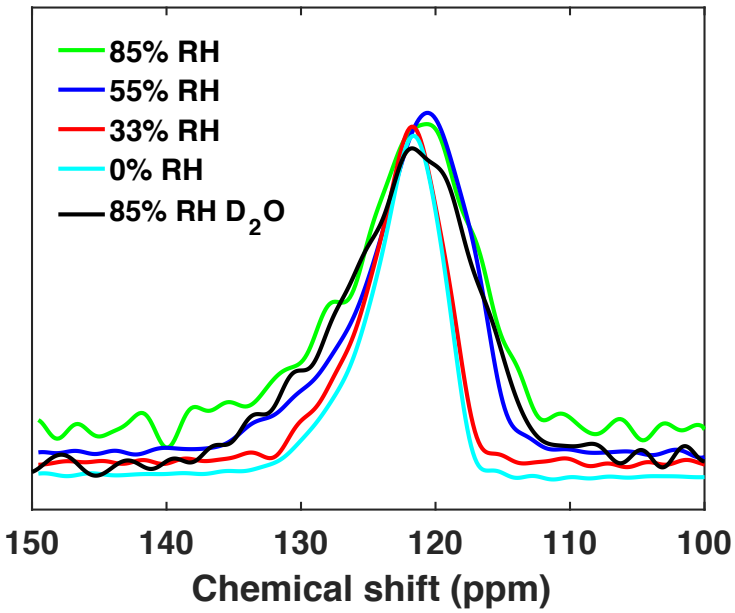

Figure 3.20: Chemical shift of $^{13}CO_2$ loaded in Al-PyrMOF, plotted against relative humidity (RH)

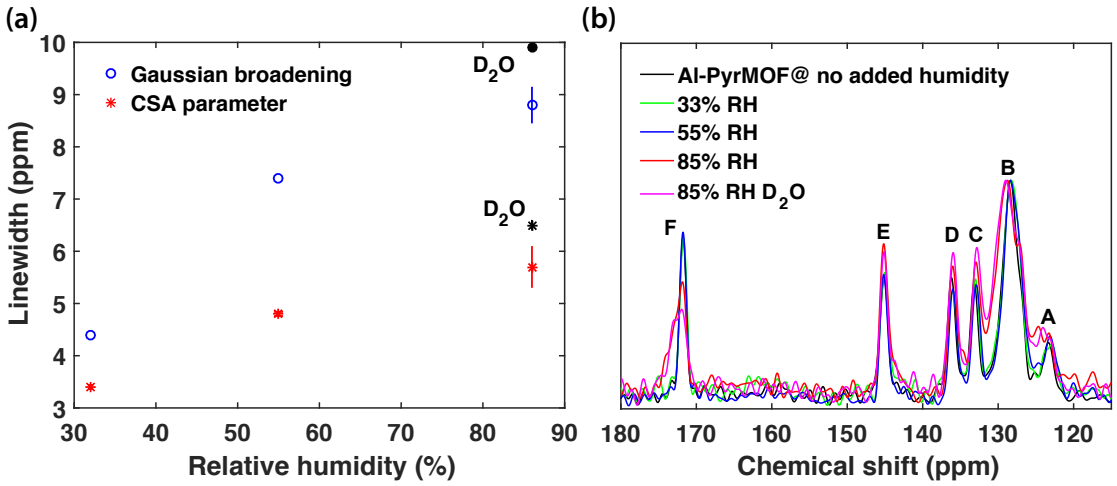

Figure 3.21: a) Linewidth vs relative humidity of $^{13}CO_2$ static spectrum fit of Al-PyrMOF with either Gaussian broadening or CSA as free parameters in the fit and b) 13C CP-MAS spectrum of Al-PyrMOF recorded at 16.34 T with sample spinning at 15 kHz, the contact time for the CP experiment was 2 ms

Between each measurement we heated Al-PyrMOF to 100°C for 1 hour to ensure no residual humidity or CO_2 still bound to the framework. We found that all NMR linewidths remained unchanged for the no

added humidity (activated MOF) and 33% added RH MOF. This was true for both the ^{13}C CP-MAS spectrum of the MOF and the ^{13}C static spectrum of the $^{13}CO_2$ gas dosed into the MOF. At 85% RH values, the $^{13}CO_2$ peak broadens. This broadening may be attributed to increased dipolar interactions (e.g. ^{1}H-^{13}C between H_2O and $^{13}CO_2$) or decreased motional averaging of the $^{13}CO_2$ CSA, which is axial for CO_2 molecules.

We fit (DMFIT[197]) the $^{13}CO_2$ line shape to the known shift parameters with a Gaussian broadening function to extract the contributions of each as the RH values increased, shown in (Figure 3.21(a)). The role of dipolar broadening vis-à-vis motional effects was assessed by first determining the line shape parameters for the freshly activated MOF. We then fixed the parameters of the CSA and let the Gaussian line shape vary as a function of humidity. We then repeated this but with the Gaussian line shape fixed and the CSA $\delta_{parallel}$ and $\delta_{perpendicular}$ terms allowed to vary. We could not unequivocally say that the CSA or the Gaussian parameter varies more than the other in the presence of H_2O.

In order to further investigate the line broadening mechanism, we repeated the humidity dosing experiment but with a saturated solution of D_2O. As ^{2}H has a lower gyromagnetic ratio the ^{2}H-^{13}C dipolar coupling is greatly diminished and if dipolar interactions dominate the observed $^{13}CO_2$ line shapes the observed spectrum would be considerably narrower. In fact, we observed comparable linewidths for both D_2O and H_2O. We conclude that the changes in linewidth for adsorbed $^{13}CO_2$ arises from reduced averaging of the CSA of the CO_2 molecule in the presence of water adsorbed at framework sites. It confirms that water has limited effect on the adsorption of CO_2 in Al-PyrMOF.

3.7. Performance testing

The multicomponent post combustion flue gas mixture simulations predicted that the water has minimal influence on the capture capacity of Al-PMOF and even increase in capacity for Al-PyrMOF. To confirm this, two independent sets of breakthrough experiments were carried out. The initial experiments were carried out at University of Granada, and the more extensive cycling experiments and comparison with reference materials was conducted at Heriot-Watt University in Edinburgh.

3.7.1. Initial experiments

The mixed-gas breakthrough experiments were performed with the activated MOF powder c.a. 300 mg which was packed in a stainless steel chromatographic column of length 20 cm and inner diameter 0.5 cm. The ends of the column were sealed with glass wool.

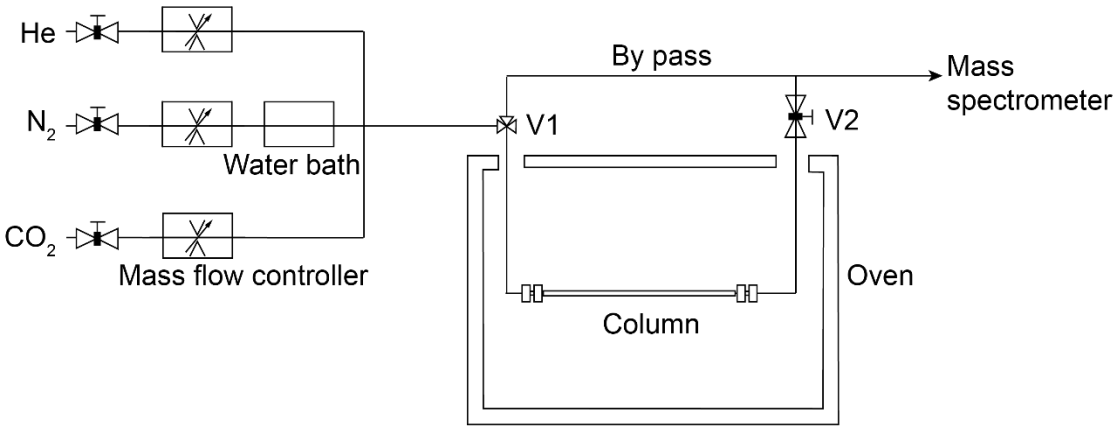

Figure 3.22: Diagram of the setup used for breakthrough experiments

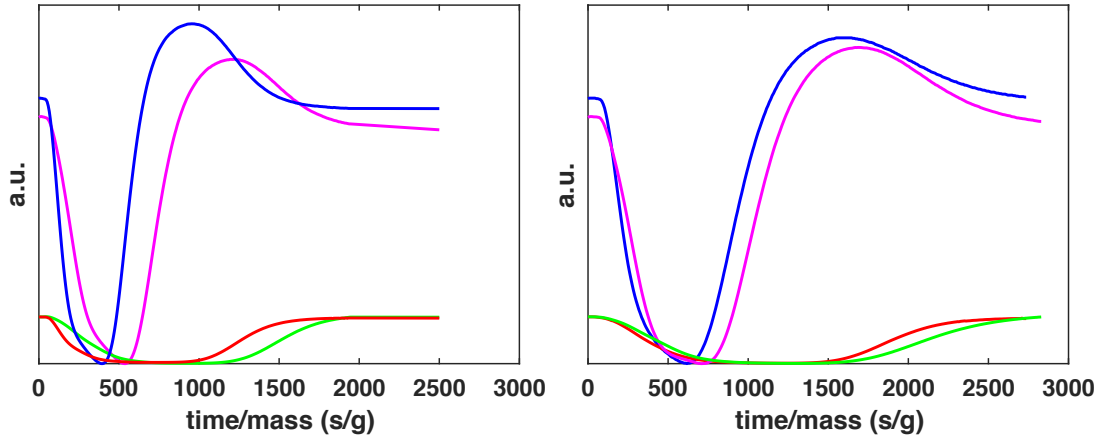

Figure 3.23: Adsorption breakthrough test for Al-PyrMOF (left) and Al-PMOF (right) with 10 ml/min at 313 K, 1 bar and 0.366 g and 0.272 g sample, respectively. Colour coding: (dry) red- CO_2 and blue-N_2, and (wet) green-CO_2 and magenta-N_2

Subsequently, the column was loaded onto a home-made gas setup. To ascertain the irregular packing of the MOF powder and to prevent the clogging of the column, the outlet gas flow rate was measured at regular intervals. The composition of the inlet gas stream was controlled by mass flow controllers. Helium was used as the purging gas before and after the breakthrough experiments with a flow rate of 20 ml min^{-1}. Prior to the breakthrough experiments, the column packed with the activated MOF powder was purged with a Helium flow of 20 ml min^{-1} at 353 K for 6 h to ensure that there were no guest molecules accommodated in the pores of the MOF materials.

To simulate the flue gas composition from a post-combustion coal-fired power plant, a gas mixture with a flow rate of 10 ml min^{-1} and composition of either 85/15 v/v of N_2/CO_2 (dry experiments) or 79:15:6 v/v/v

of $N_2/CO_2/H_2O$ (85% RH, humid experiments) was prepared with the aid of mass flow controllers. The experiments were performed at 313 K and 1 bar. The composition of the outlet gas stream was monitored on a mass spectrometer gas analysis system (Pfeiffer Vacoon) detecting ion peaks at m/z 44 (CO_2), 28 (N_2), 18 (H_2O) and 4 (He). The schematic of the experimental setup is presented in Fig. S2.10. The two valves labelled as V1 and V2 enabled the gas mixture to be fed either through the bypass line, thus isolating the column, or through the reactor. Initially, the flue gas mixture was prepared and fed into the system through the bypass line, and following the stabilization of the corresponding mass spectrometer signals, the valves were turned to direct the feed mixture into the column. After the stabilization of the components MS signals to their corresponding inlet composition values, the breakthrough experiment was considered to be completed.

Figure 3.23 shows the raw breakthrough profiles for Al-PyrMOF and Al-PMOF in dry and wet conditions. The signal is given in arbitrary units, where we have scaled the MS signals for N_2 and CO_2 considering the inlet ratios of N_2:CO_2 for the dry and wet experiments, i.e., 85:15 and 79:15, respectively. The mass spectrometer detects the feed mixture before the valve V1 is turned. Once the valve is turned, it engenders the feed mixture to be directed towards the column thus pushing the helium out of the column. Consequentially, the concentration of the components of the gas mixture decreases and Helium was the only component to be detected until the occurrence of the breakthrough of the first component (N_2). Following this, the breakthrough of CO_2 occurred. The less adsorbed component N_2 breaks first than CO_2 and its breakthrough curve shows the so-called roll-up effect,[198] i.e., the flowrate or concentration of N_2 at the column exit temporarily exceeds the feed one. This is due to the concentration front of N_2 advancing faster through the column than the concentration front of CO_2. However, as the concentration front of N_2 advances further through the column, CO_2 replaces N_2 that was initially adsorbed, i.e. N_2 is desorbed by incoming CO_2, and the aforementioned roll-up effect is observed.

These results confirm that these materials can be used to separate CO_2 from the simulated flue gas mixtures. In the experiments with Al-PyrMOF, CO_2 breaks through earlier than in experiments with Al-PMOF, which corroborates Al-PyrMOF predicted and measured lower capacity versus the Al-PMOF one. Moreover, the dynamic breakthrough of CO_2 is hardly influenced by the presence of H_2O in the experiment with Al-PMOF, whereas it is shifted to higher values with Al-PyrMOF. This observation is in agreement with the predicted performance.

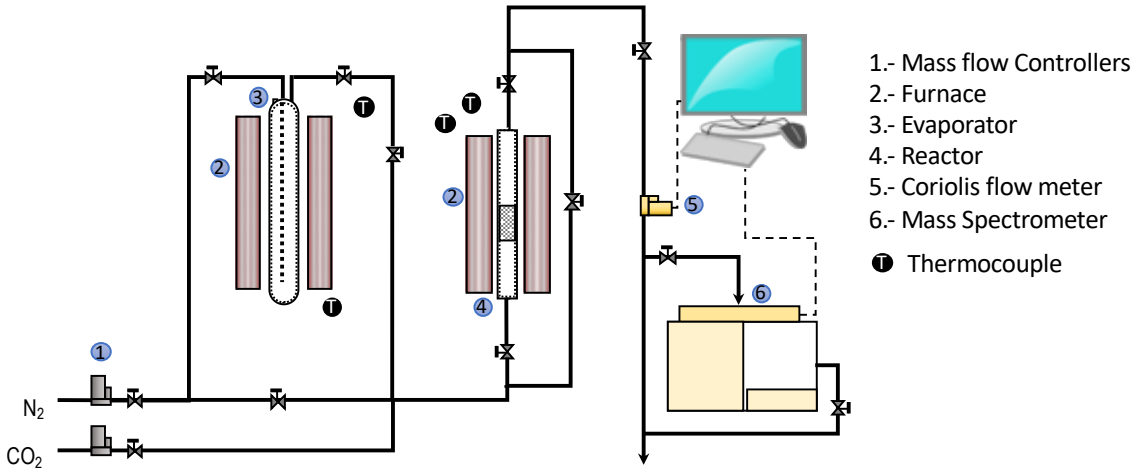

Figure 3.24: Schematic of the experimental setup used for cyclic adsorption-desorption experiments and capture performance evaluation

3.7.2. Cyclic experiments and benchmarking

The cyclic adsorption-desorption experiments were conducted in a purpose-built lab-scale experimental setup which is illustrated in Figure 3.24. The setup consisted of a gas manifold system where two gas lines feed in N_2 and CO_2 so the different gas mixtures can be prepared. A controlled evaporator would allow feeding in a humid gas, i.e. a mixture of N_2, CO_2 and H_2O (vapour) of desired composition. The stainless-steel fixed bed reactor was 7 and 220 mm in diameter and height, respectively, and a series of K-type thermocouples were used to continuously monitor the evaporator and reactor temperatures. The mass flow rate of the outlet stream from the reactor was measured using a Coriolis flow meter, and its composition was monitored by a mass spectrometer which had been previously calibrated with relevant gas mixtures of known composition.

For the adsorption-desorption experiments, the fixed bed reactor was packed with approximately 150 mg of the adsorbent material, i.e., activated Al-PMOF and Al-PyrMOF, and reference samples (activated UiO-66-NH_2, Activated Carbon and Zeolite 13X). Firstly, the adsorbent was dried by flowing N_2 (36 mL min^{-1} STP) for 15 min at atmospheric pressure and either 363K (Al-PyrMOF) or 383K (Al-PMOF, and reference materials). These temperature conditions had been previously identified as the optimum ones for the drying step in order to avoid alteration of the MOF adsorbents structure. The reactor was then allowed to cool down to ambient temperature and isolated from the N_2 flow prior to the adsorption step. During the adsorption step, the bed was heated to 313K under atmospheric pressure (1 bar) and allowed to stabilize. Following this, a gas mixture with a composition of 85:15 v/v N_2/CO_2 at a total flow of 40 ml min^{-1} STP was fed to the reactor (filled with N_2 at the adsorption temperature and pressure) for 20 min. We have tested the reproducibility of our method and comparison of the data showed an absolute error for our reported capture capacity values of $\pm$ 0.02 mmol/g.

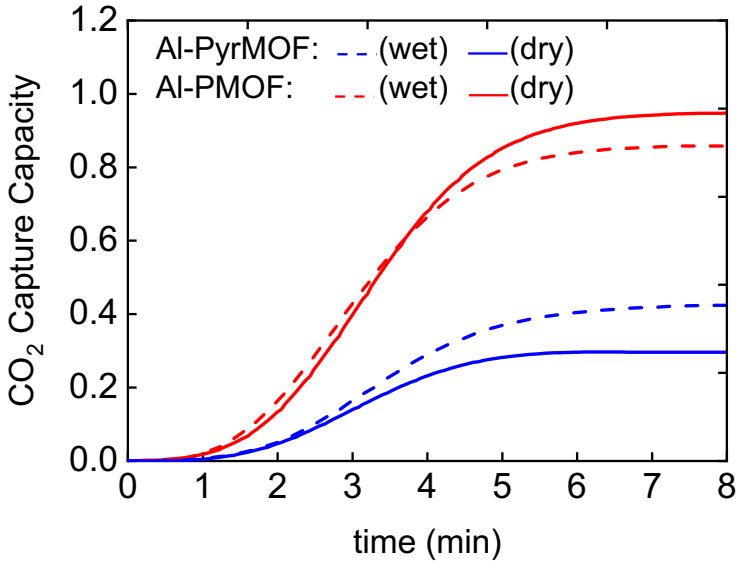

Figure 3.25: CO_2 capture capacity profiles for Al-PyrMOF and Al-PMOF during breakthrough experiments under dry and humid (85% relative humidity) conditions, with 85/15 v/v of N_2/CO_2 (313 K and 1 bar)

The cyclic experiments were performed under wet flue gas conditions, where water vapour at 85% relative humidity was introduced into the flow. After the adsorption step, the reactor was isolated from the feed gas flow and the gas lines were cleaned by flowing N_2 (36 ml min^{-1} STP) through the bypass line for 16 min. The CO_2 concentration was followed and monitored on the

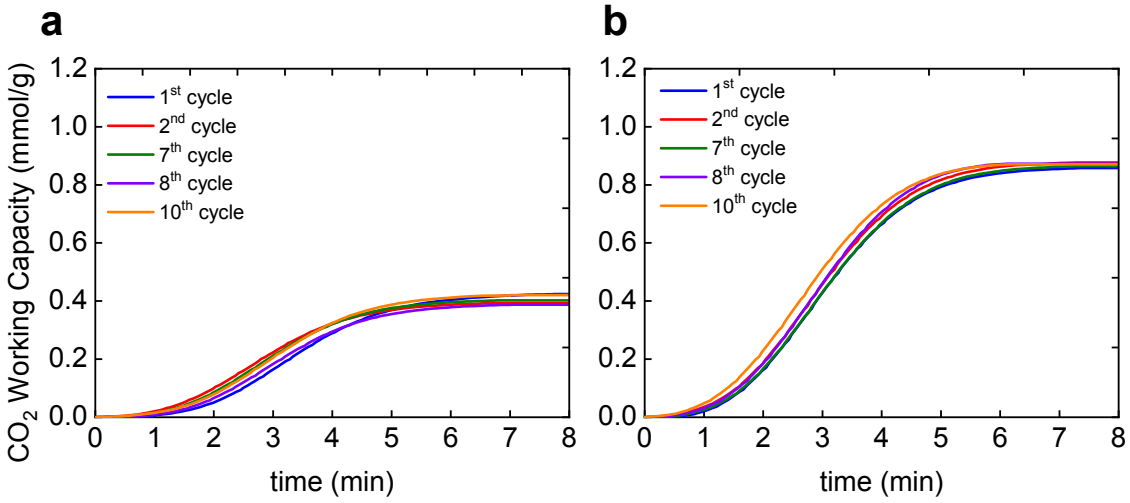

Figure 3.26: CO_2 capture capacity profiles (in mmol/g) for Al-PyrMOF (a) and Al-PMOF (b) during repeated cycling under humid (85%RH) conditions with 85/15 v/v of N_2/CO_2 (313 K and 1 bar)

mass spectrometer to ensure there was no CO_2 left in the line prior to the desorption step. Then, the desorption step followed, and regeneration of the material was achieved by temperature swing where the

reactor was heated under N_2 flow (36 ml min^{-1} STP) to 363K for Al-PyrMOF, and to 383K for Al-PMOF, UiO-66-NH_2, Activated Carbon and Zeolite 13X. On attainment of desorption temperature, the furnace was switched off and the reactor was allowed to cool down. The adsorption step would again follow, and the aforementioned adsorption/desorption procedure was repeated for a number of cycles. Reference UiO-66-NH_2, Activated Carbon, and Zeolite 13X samples were subjected to three consecutive adsorption-desorption cycles and Al-PMOF and Al-PyrMOF samples were subjected to more (ten) number of cycles to ascertain their performance stability after a more extended cycling. The reactor outlet gas composition was continuously monitored over the entire duration of the cyclic experiments and the CO_2 working capacity was determined by applying a mass balance to the reactor, as previously reported.[199-201] Blank experiments under wet and dry conditions were also carried out to account for the intra particle voids and dead space of the bed.

On the basis of the pure component isotherms, one can expect the capture capacity of Al-PMOF to be about more than double the value of the capacity of Al-PyrMOF. Indeed, for dry flue gasses we measure a capacity for Al-PMOF (0.95 mmol/g) and Al-PyrMOF (0.30 mmol/g) which are in good agreement with the pure component isotherms assuming N_2 does not impact the adsorption. In wet flue gasses the simulations predict the capacity of Al-PMOF will decrease slightly, while for Al-PyrMOF an increase of the capacity can be expected. An important practical requirement is that the performance of the materials do not deteriorate upon repeated cycles. We have already established the stability of Al-PMOF and Al-PyrMOF in water and no significant change in capture capacity after 10 adsorption-desorption cycles in humid flue gasses. That Al-PMOF and Al-PyrMOF do not lose capacity upon repeated cycling is an important confirmation of our design principles, in which the effect of water is minimized.

To benchmark the performance of Al-PMOF and Al-PyrMOF, we have compared the capture capacity of these materials in wet and dry flue gasses with a set of reference materials: Zeolite 13X, which is a commercial zeolite and serves as a reference material for carbon capture with zeolites[202]. Zeolite 13X ($Na_{86}[(AlO_2)_{86}(SiO_2)_{106}] \cdot H_2O$) was purchased from ABCR. Activated carbon, an extensively studied material for carbon capture due mainly to its low cost, high surface area, and amenability to pore structure modification and surface functionalization.[69,203] The commercial Activated carbon was supplied by Silcarbon (TH90i) and it is a physically, steam activated coconut-based powdered carbon with a BET surface area of 1305 m^2/g and pore volume of 0.570 cm^3/g.

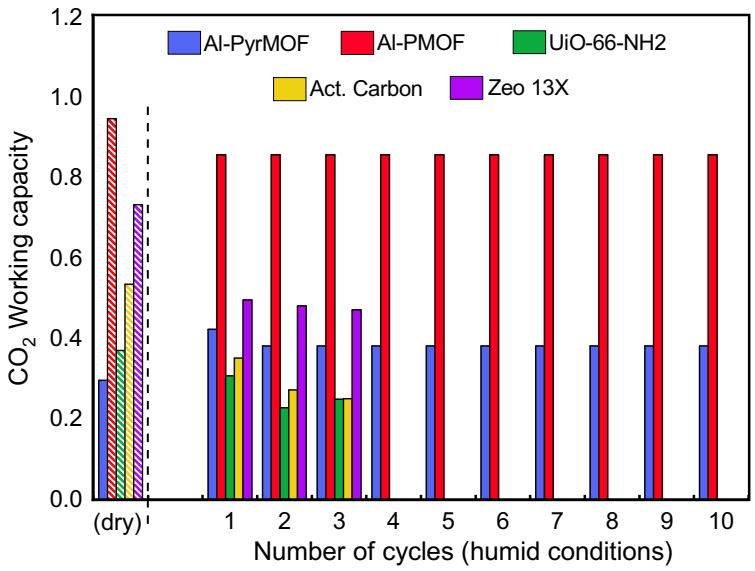

Figure 3.27: Benchmarking the CO_2 working capacity of Al-PyrMOF and Al-PMOF against UiO-66-NH_2, activated carbon and zeolite 13X under dry and humid (85% relative humidity) conditions, with 85/15 v/v of N_2/CO_2 (313 K and 1 bar). For wet flue gases, we studied the performance stability after 3 cycles for reference materials, and after 10 cycles for Al-PyrMOF and Al-PMOF

UiO-66-NH_2, a water stable MOF,[112] where the amines are functional groups that enhance the selectivity. This material is an example of a typical water stable MOF with a promising potential for carbon capture.[204] UiO-66-NH_2 was synthesized by a method adapted by Cavaka *et al*.[112] Briefly, Stock solutions of the zirconium precursor (320 mg of zirconium (IV) chloride ($ZrCl_4$, Aldrich), sonicated in 20 ml of DMF) and ligand (240 mg of 2-aminoterphthalic acid ($H_2BDC\text{-}NH_2$, Aldrich), dissolved in 20 ml DMF) were prepared. 2 ml of each solution was pipetted into 10 x 12ml reactor vials. The reactor vials heated to 120 °C for 48 hours, then cooled at a rate of 0.2 °C min^{-1} to room temperature. The resulting pale-yellow material was combined and washed by centrifuge x 3 with DMF, and x 2 with methanol, and left overnight to dry at room temperature. After methanol exchange, the material was activated under vacuum overnight at 130 °C. The PXRDs of both the as made and activated material agree with literature.

Figure 3.27 shows that for dry flue gasses Al-PyrMOF has the lowest capture capacity and only zeolite 13X approaches the capacity of Al-PMOF. For experiments under humid conditions we see that all reference materials have a significantly lower capacity than under dry conditions. When comparing the materials performance upon several cycles, it is worth highlighting that in the first cycle the material has been fully dried prior to the capture step, whereas in subsequent cycles the samples have been regenerated by temperature swing, i.e., heating to regeneration temperature.

For reference materials, the capacity decreases after repeated exposure to wet flue gas, which is most likely due to the fact that the regeneration temperature is not high enough to fully regenerate the adsorbents within the cycle time. That Al-PMOF even exceeds the capture capacity of zeolite 13X and Al-PyrMOF outperforms reference samples in a wet environment is a very promising result. Also, that Al-PMOF and Al-PyrMOF maintain their working capacity upon cycling at a relatively low regeneration temperature also implies a lower energy demand for the capture process than the one that would be required under higher regeneration temperatures, like in the case of reference materials.

Thus, the second research objective of synthesizing MOFs for energy application like efficient carbon capture in the presence of water is achieved in this work. Herein, computational screening and synthesis of MOFs with the adsorbaphore is linked. The synthetic viability of this linkage and strategy is demonstrated by the design, synthesis, characterization of one new MOF, Al-PyrMOF.

Conclusions and Outlook

Through this doctoral thesis and chapter 2, the potential to accelerate the discovery and synthesis of MOFs was demonstrated with a synthetic platform. The strength of this approach stems from the inclusion of partially successful and failed experiments in the analysis rather than focusing only on successful experiments. This was made possible through the implementation of several robotic experiments and characterization.

The underpinning experimental impetus that was needed for this work to perform several rounds of experiments was appropriately provided through high-throughput robotic synthesis. It comprised of automated handling and gravimetric dispensing of metal salt, ligand and volumetric dispensing of solvents. In addition, all the other activities that were performed on the platform, such as capping and crimping of the reaction vials and transferring the vials to and from the microwave reactor were automated.

The optimal synthetic condition for HKUST-1 reported in this work drastically reduced the synthesis duration when compared with conventional electric heating procedure. Through the combination of microwave chemistry and automated chemistry, the required experimental acceleration for the synthesis of MOFs was achieved. Besides the acceleration, robotic synthesis accounted for the precision over the involved synthetic variables which resulted in reproducibility.

A facile assessment methodology was devised for ranking the numerous HKUST-1 synthetic reactions that were performed in this work. This ranking methodology was devised to assess the crystallinity and phase purity based on the full width at half maximum of the powder X-ray diffraction PXRD peaks of the different HKUST-1 samples. The samples which scored well for their crystallinity and phase purity were further assessed for their porosity with BET surface area assessment. Thereby, each of the synthetic reactions were ranked based on a weighted average of the two scores. It served as the metric for the objective function of the genetic algorithm. This assessment methodology is entirely applicable to all optimization reactions which are typically performed in search of the MOF with the desirable properties – crystallinity, phase purity and porosity.

This work collectively resulted in capturing and quantifying the chemical intuition. The outcome of this approach was reflected in the optimal synthetic condition which yielded HKUST-1 MOF with the highest surface area. This finding is of high interest as the HKUST-1 MOF which was first reported in 1999 and the several ensuing publications in the past two decades reported surface areas of wide variations. This is inclusive of the surface area of the commercially available HKUST-1 Basolite C300 from BASF.

The potential for acceleration of discovery of MOFs was illustrated with the Zn-HKUST-1 synthesis. The captured chemical intuition facilitated us in performing 20 rational synthesis experiments and with which we were able to isolate crystals of Zn-HKUST-1. We predict that without the knowledge gained from the synthesis of Cu-HKUST-1 it would have costed us several hundreds of experiments to isolate Zn-HKUST-1

crystals. Thus, the developed synthetic platform is shown to accelerate the discovery and synthesis of MOFs.

Chapter 3 of this thesis describes on how the second research objective of synthesizing MOFs for efficient carbon capture from wet flue gasses is addressed. It introduces adsorbaphore as a structural feature for CO_2 adsorption which has not been previously reported. Essentially, an adsorbaphore is constituted of two parallel aromatic rings with interatomic spacing of 7 A°. Pragmatically from a synthesis point of view, this was crucial as the target was to synthesis MOFs which includes these motifs rather than a whole MOF. Thereby, it offers the room for flexibility to synthesis and in that way, it complements the versatility and tunability attributes of MOFs.

This was clearly illustrated through the synthesis of two MOFs viz. Al-PMOF and Al-PyrMOF with the adsorbaphore as a structural motif. In particular, Al-PyrMOF has not been previously reported. The MOFs were characterized by PXRD, FT-IR, TGA, SEM, isotherms. A range of challenging characterization techniques varying from bulk to molecular level were utilised to depict the adsorption of CO_2 and CO_2 separation performance as predicted by simulations. The challenging *in-situ* synchrotron gas loading experiment and the refinement analysis showed that CO_2 adsorbs between the aromatic rings of the MOF.

The siting of water and its effect on CO_2 adsorption was performed by the solid state ^{13}C NMR which established that there is no competition amongst water and CO_2 as desired and designed based on predictions. The fixed bed breakthrough experiments demonstrated their separation performance and they outperformed the commercially available adsorbents such as zeolite and activated carbon. Moreover, it is worth highlighting that the CO_2 capture performance of Al-PyrMOF was promoted in the presence of water. As a result, this work distinguished itself from the previously reported screening studies of hypothetical MOFs. Those studies lacked the bridging of computational large-scale screening of hypothetical MOFs and the corresponding experimental synthesis, validation of the predictions.

Future and ongoing work

MOFs of increasing complexity can be synthesized as the next step to further test the robustness of the combinatorial methodology of genetic algorithm and machine learning guided synthesis. Conventionally, MOF structures are comprised of one metal SBU and a ligand. Whereas, the heterogeneity is introduced when the structure has incorporated more than one metal ions or organic ligand. For instance, incorporation of eight distinct ligands within one phase pure structure of a MOF is possible.

Likewise, the introduction of several metals in one structure is possible. These structures with high display of heterogeneity are collectively referred to as multivariate (MTV) MOFs. It will be interesting to observe on how this methodology will function in this particularly more challenging case of crystallization of (MTV) MOFs. In addition, it is well known that titanium based MOFs are very challenging to synthesize due to the oxidation of titanium metal salt during the synthesis. Thus, with this approach attempts can be made to synthesize the highly challenging titanium MOFs.

Natural gas purification and bio gas enhancement would be performed with Al-PMOF and Al-PyrMOF in the presence of water to further demonstrate their carbon capture applicability. The presence of water in natural gas and bio gas has been largely neglected in the current research field of MOFs. In this context, we have performed the experiments of collecting methane isotherms and initial breakthrough measurements for Al-PMOF with wet bio gas. However, further experiments are needed to be performed at different temperatures, compositions, cycling and the same set of experiments for Al-PyrMOF.

In addition, synthesis of MOFs with new adsorbaphores as structural motifs would be synthesized to attain the working capacity higher than Al-PMOF. The initial synthetic attempts to synthesize a MOF m8o82 with aluminium as the metal and organic ligand that is not commercially available. The MOF is predicted to have high working capacity. However, the synthesis attempts in different synthetic conditions were not successful with ligand recrystallizing as the end product.

It is predicted that the choice of metal causes the variation in adsorbaphore distance of the resulting MOF. In consequence, the porosity features and the CO_2 adsorption is expected to differ. In this context, a new gallium based Ga-PyrMOF was synthesized successfully after several synthesis attempts. It requires characterization and analysis to complete the work. Furthermore, the synthesis of more pyrene based MOFs with other metals like iron, scandium, and yttrium is required to validate the predictions.

Literature review made us identify a gallium metal based MIL-120 MOF with an adsorbaphore distance. Based on the reported synthetic conditions, the MOF was successfully reproduced in the lab and it was characterized with XRD, TGA, FT-IR, isotherms. The MOF was synthesized on a large scale and shaped as beads. It needs further work on validation that CO_2 preferentially adsorbs in the adsorbaphore region with XRD and or NMR analysis. In addition, the separation performance can be evaluated with breakthrough experiments. The MOF was also investigated for xenon and krypton separations.

The next step to advance the Al-PMOF and Al-PyrMOF work would be to perform evaluations in an industrial setting, for an overall perspective. To cater to such industrial settings, the MOF synthesis should be accelerated and possibly larger quantities will be required. Whilst, the current procedure used conventional electric heating for synthesis and consumed almost a day for synthesis. The use of an automated, microwave synthesis guided by the synthesis co-finder web application could enable the acceleration of the synthesis. This is an ongoing work in our laboratory in which I contributed by synthesizing Al-PMOF on a gram scale in a high-throughput manner.

The powdered MOFs generated in the gram scale through the aforementioned process should be transformed into more application-oriented form as beads through shape engineering. This is essential as typically, the powdered adsorbents are not favoured in industrial settings due to the challenges involved in transfer and handling of powders, mass loss, clogging, mechanical stability etc.

Ideally, the objective here is to shape them as porous MOF@polymer composite beads with controlled diameters through a phase inversion method. The resultant beads should then be characterized for their porosity and CO_2 uptake with isotherms and separation performance with breakthrough measurements. This is an ongoing work in our laboratory as well. The Al-PMOF synthesized on gram scale was shaped as beads. In addition, unlike the powder MOFs, the beads should enable to devise both fluidised bed and packed bed configuration. This should provide us the information to compare the cycle time, heating and cooling requirements.

Finally, as part of the advancement of the work, diffusion, kinetic studies should be performed to measure the gas diffusion coefficients in Al-PMOF and Al-PyrMOF. This should provide a better understanding of the mass transfer rate and contribute significantly for process designing and modelling of an adsorption column that can meet the specified requirements.

Multisensor arrays constituted of several sensors for the detection of gas/vapours can be referred as electronic noses. They are named this way due to their similarity with the mammalian olfactory system which involves several sensing components to analyse odours. The fundamental working principle of a solid state sensor for the detection of gas or vapour molecules is given as follows. When molecules come into contact with the sensing material, a change in the surface can be observed. It is then recorded as quantifiable signal. The mode of signal transduction can vary depending on the solid sensing material that is employed and its characteristics properties. It can either be optical, electromechanical or electronic.

The application spectra of electronic noses is wide and far reaching. It includes several commercial applications in domestic and industrial sectors such as the pharmaceutical, agricultural, food and several more scientific research sectors. Hitherto, a majority of the devices were based on metal oxides and organic polymers which have their own share of merits and demerits. For example, there are several gas/vapour sensing applications whose technical requirements are out of reach for the existing sensors. This has left a large gap for the development of new materials for solid state gas sensor devices, a gap that could be bridged through the use of MOFs for example.

Several compelling attributes of MOFs were discussed in this thesis. These attributes make MOFs promising materials for (electronic) sensing applications. For instance, to augment the sensitivity of polymer or metal oxide based sensors, pre-adsorption is followed. Herein, the target gas is passed through an adsorbent and upon adsorption, the adsorbent is desorbed releasing a more concentrated target gas. This pre-adsorption step can completely be circumvented if a highly porous MOF is employed as a sensor material. With this in mind and for further details on this burgeoning field of electronic metal-organic framework sensors, the reader is referred to the review by Chidambaram et al[205].

Electronic MOF sensor devices are driven by the changes that MOF sensing layer exhibits in their electrical properties upon interaction with gas or vapour molecules. This can include impedance, capacitance or work function, or resistance. Several intriguing and well demonstrated electronic MOF sensor devices have been reported in the past decade for sensing highly toxic nerve gas agents and ammonia to humidity.

This achievement is commendable whilst MOFs exhibit low conductivity or insulating properties. Moreover, these reports are achieved in spite of the yet to be standardized procedure for the fabrication of MOF films which is on par with the commercial standards. The majority of the work that is reported are based on solution-phase chemistry such as liquid-phase epitaxy or drop-casting of the MOF as a film on substrate[206]. In contrast, well-established techniques for the fabrication of (micro) electronics are based on atomic layer deposition (ALD) and chemical vapour deposition (CVD). Recent studies have also demonstrated CVD based MOF growth on substrates[207,208]. However, these studies, which are proofs of concept, focus on imidazolate based MOFs. It is of greater challenge to extend it to carboxylate ligand based MOFs.

I would like to further work on electronic MOF sensors and MOF sensor arrays as a future research work. These sensors can have MOFs with distinct affinity for target gasses or vapours of varying compositions to give selective detection and discrimination of the analytes. Owing to the promising potential that MOFs exhibits, the sensor configuration is highly flexible. The sensor substrate on which the MOF film will serve as the active sensing layer can vary from quartz crystal microbalance to interdigitated electrodes[209,210]. For instance, the issue of non-conductivity of MOFs can be avoided with quartz crystal microbalance based configurations as it is purely driven by the adsorption induced gravimetric changes as the transduction mechanism. Furthermore, I would like to work on the other pressing issue of standardization of fabrication of MOF films for their incorporation onto substrates.

Bibliography

1 Jacobson, M. Z. Review of solutions to global warming, air pollution, and energy security. *Energy & Environmental Science* **2**, 148-173 (2009).
2 ipcc. https://www.ipcc.ch/site/assets/uploads/2018/03/ipcc_far_wg_I_full_report.pdf
3 Rinscheid, A. & Wüstenhagen, R. Germany's decision to phase out coal by 2038 lags behind citizens' timing preferences. *Nature Energy*, 1-8 (2019).
4 Henson, A. B., Gromski, P. S. & Cronin, L. Designing algorithms to aid discovery by chemical robots. *ACS central science* **4**, 793-804 (2018).
5 Hansen, J., Ruedy, R., Sato, M. & Lo, K. Global surface temperature change. *Reviews of Geophysics* **48** (2010).
6 Kulp, S. A., Strauss, B.H. New elevation data triple estimates of global vulnerability to sea-level rise and coastal flooding. *Nature communications* **10**, doi:10.1038/s41467-019-12808-z.
7 2018, https://www.ipcc.ch/2018/10/08/summary-for-policymakers-of-ipcc-special-report-on-global-warming-of-1-5c-approved-by-governments/
8 He, Y., Zhou, W., Qian, G. & Chen, B. Methane storage in metal–organic frameworks. *Chemical Society Reviews* **43**, 5657-5678 (2014).
9 Berend, S. *Introduction to carbon capture and sequestration*. Vol. 1 (World Scientific, 2014).
10 Metz, B., Davidson, O., de Coninck, H. C., Loos, M., Meyer, L.A.,Eds. Special Report on Carbon Dioxide Capture and Storage Prepared by Working Group III of the Intergovernmental Panel on Climate Change. (2005).
11 Bui, M. *et al.* Carbon capture and storage (CCS): the way forward. *Energy & Environmental Science* **11**, 1062-1176 (2018).
12 MacDowell, N. *et al.* An overview of CO_2 capture technologies. *Energy & Environmental Science* **3**, 1645-1669 (2010).
13 Vitillo, J. G., Smit, B. & Gagliardi, L. ACS Publications, 2017.
14 Schäfer, P., Kapteijn, F., van der Veen, M. A. & Domke, K. F. Understanding the Inhibiting Effect of BTC on CuBTC Growth through Experiment and Modeling. *Crystal Growth & Design* **17**, 5603-5607 (2017).
15 Schoedel, A., Ji, Z. & Yaghi, O. M. The role of metal–organic frameworks in a carbon-neutral energy cycle. *Nature Energy* **1**, 16034 (2016).
16 Benhelal, E., Zahedi, G., Shamsaei, E. & Bahadori, A. Global strategies and potentials to curb CO_2 emissions in cement industry. *Journal of cleaner production* **51**, 142-161 (2013).
17 Fuss, S. *et al.* Betting on negative emissions. *Nature climate change* **4**, 850 (2014).
18 Heuberger, C. F., Staffell, I., Shah, N. & Mac Dowell, N. Quantifying the value of CCS for the future electricity system. *Energy & Environmental Science* **9**, 2497-2510 (2016).
19 Institute, G. C. https://www.globalccsinstitute.com/resources/global-status-report/ accessed in 2019
20 INSTITUTE, G. C. The Global Status of CCS:2017.
21 Consoli, C. P. & Wildgust, N. Current status of global storage resources. *Energy Procedia* **114**, 4623-4628 (2017).

22 IEA. 20 Years of carbon capture and storage: Accelerating future deployment. (Paris, France).
23 Upham, P. & Roberts, T. Public perceptions of CCS: emergent themes in pan-European focus groups and implications for communications. *International Journal of Greenhouse Gas Control* **5**, 1359-1367 (2011).
24 Koelbl, B. S., van den Broek, M. A., Faaij, A. P. & van Vuuren, D. P. Uncertainty in Carbon Capture and Storage (CCS) deployment projections: a cross-model comparison exercise. *Climatic change* **123**, 461-476 (2014).
25 D'Alessandro, D. M., Smit, B. & Long, J. R. Carbon dioxide capture: prospects for new materials. *Angewandte Chemie International Edition* **49**, 6058-6082 (2010).
26 Hu, Z., Wang, Y., Shah, B. B. & Zhao, D. CO_2 Capture in Metal–Organic Framework Adsorbents: An Engineering Perspective. *Advanced Sustainable Systems* **3**, 1800080 (2019).
27 Rubin, E. & De Coninck, H. IPCC special report on carbon dioxide capture and storage. *UK: Cambridge University Press. TNO (2004): Cost Curves for CO_2 Storage, Part* **2**, 14 (2005).
28 Khurana, M. & Farooq, S. Adsorbent screening for postcombustion CO_2 capture: a method relating equilibrium isotherm characteristics to an optimum vacuum swing adsorption process performance. *Industrial & Engineering Chemistry Research* **55**, 2447-2460 (2016).
29 Rochelle, G. T. Amine scrubbing for CO_2 capture. *Science* **325**, 1652-1654 (2009).
30 Jansen, D., Gazzani, M., Manzolini, G., van Dijk, E. & Carbo, M. Pre-combustion CO_2 capture. *International Journal of Greenhouse Gas Control* **40**, 167-187 (2015).
31 Wang, S. *et al.* Advances in high permeability polymer-based membrane materials for CO_2 separations. *Energy & Environmental Science* **9**, 1863-1890 (2016).
32 Stanger, R. *et al.* Oxyfuel combustion for CO_2 capture in power plants. *International Journal of Greenhouse Gas Control* **40**, 55-125 (2015).
33 Sanz-Perez, E. S., Murdock, C. R., Didas, S. A. & Jones, C. W. Direct capture of CO_2 from ambient air. *Chemical reviews* **116**, 11840-11876 (2016).
34 Zulfiqar, S., Sarwar, M. I. & Mecerreyes, D. Polymeric ionic liquids for CO_2 capture and separation: potential, progress and challenges. *Polymer Chemistry* **6**, 6435-6451 (2015).
35 Bottoms, R. R. Process for separating acidic gases. (1930).
36 Kwak, N.-S., Lee, J. H., Lee, I. Y., Jang, K. R. & Shim, J.-G. A study of the CO_2 capture pilot plant by amine absorption. *Energy* **47**, 41-46 (2012).
37 Oyenekan, B. A. & Rochelle, G. T. Alternative stripper configurations for CO_2 capture by aqueous amines. *AIChE Journal* **53**, 3144-3154 (2007).
38 Mumford, K. A., Wu, Y., Smith, K. H. & Stevens, G. W. Review of solvent based carbon-dioxide capture technologies. *Frontiers of Chemical Science and Engineering* **9**, 125-141 (2015).
39 Dave, N. *et al.* CO_2 capture by aqueous amines and aqueous ammonia–A Comparison. *Energy Procedia* **1**, 949-954 (2009).
40 Niu, Z., Guo, Y., Zeng, Q. & Lin, W. A novel process for capturing carbon dioxide using aqueous ammonia. *Fuel processing technology* **108**, 154-162 (2013).
41 Cullinane, J. T. & Rochelle, G. T. Carbon dioxide absorption with aqueous potassium carbonate promoted by piperazine. *Chemical Engineering Science* **59**, 3619-3630 (2004).

42 Mohammed, I. Y., Samah, M., Mohamed, A. & Sabina, G. Comparison of SelexolTM and rectisol® technologies in an integrated gasification Combined cycle (IGCC) Plant for clean energy production. *Int. J. Eng. Res* **3**, 742-744 (2014).
43 Burr, B. & Lyddon, L. in *87th Annual Gas Processors Association Convention, Grapevine, TX, March.* 2-5.
44 Wang, Q., Luo, J., Zhong, Z. & Borgna, A. CO_2 capture by solid adsorbents and their applications: current status and new trends. *Energy & Environmental Science* **4**, 42-55 (2011).
45 Samanta, A., Zhao, A., Shimizu, G. K., Sarkar, P. & Gupta, R. Post-combustion CO_2 capture using solid sorbents: a review. *Industrial & Engineering Chemistry Research* **51**, 1438-1463 (2011).
46 Choi, S., Drese, J. H. & Jones, C. W. Adsorbent materials for carbon dioxide capture from large anthropogenic point sources. *ChemSusChem: Chemistry & Sustainability Energy & Materials* **2**, 796-854 (2009).
47 Sumida, K. *et al.* Carbon dioxide capture in metal–organic frameworks. *Chemical reviews* **112**, 724-781 (2011).
48 Kikkinides, E. S., Yang, R. & Cho, S. Concentration and recovery of carbon dioxide from flue gas by pressure swing adsorption. *Industrial & Engineering Chemistry Research* **32**, 2714-2720 (1993).
49 Chue, K., Kim, J., Yoo, Y., Cho, S. & Yang, R. Comparison of activated carbon and zeolite 13X for CO_2 recovery from flue gas by pressure swing adsorption. *Industrial & Engineering Chemistry Research* **34**, 591-598 (1995).
50 Garcia, S., Gil, M., Pis, J., Rubiera, F. & Pevida, C. Cyclic operation of a fixed-bed pressure and temperature swing process for CO_2 capture: Experimental and statistical analysis. *International Journal of Greenhouse Gas Control* **12**, 35-43 (2013).
51 Marx, D., Joss, L., Hefti, M. & Mazzotti, M. Temperature swing adsorption for postcombustion CO_2 capture: single-and multicolumn experiments and simulations. *Industrial & Engineering Chemistry Research* **55**, 1401-1412 (2016).
52 Joss, L., Gazzani, M. & Mazzotti, M. Rational design of temperature swing adsorption cycles for post-combustion CO_2 capture. *Chemical Engineering Science* **158**, 381-394 (2017).
53 Plaza, M., García, S., Rubiera, F., Pis, J. & Pevida, C. Post-combustion CO_2 capture with a commercial activated carbon: comparison of different regeneration strategies. *Chemical Engineering Journal* **163**, 41-47 (2010).
54 Merel, J., Clausse, M. & Meunier, F. Experimental investigation on CO_2 post−combustion capture by indirect thermal swing adsorption using 13X and 5A zeolites. *Industrial & Engineering Chemistry Research* **47**, 209-215 (2008).
55 Zaabout, A. *et al.* Thermodynamic assessment of the swing adsorption reactor cluster (SARC) concept for post-combustion CO_2 capture. *International Journal of Greenhouse Gas Control* **60**, 74-92 (2017).
56 Schell, J., Casas, N. & Mazzotti, M. Pre-combustion CO_2 capture for IGCC plants by an adsorption process. *Energy Procedia* **1**, 655-660 (2009).
57 Lin, L.-C. *et al.* In silico screening of carbon-capture materials. *Nature materials* **11**, 633 (2012).
58 Huck, J. M. *et al.* Evaluating different classes of porous materials for carbon capture. *Energy & Environmental Science* **7**, 4132-4146 (2014).

59 *International Zeolite Association*, http://www.iza-structure.org/
60 Kim, J., Lin, L.-C., Swisher, J. A., Haranczyk, M. & Smit, B. Predicting large CO_2 adsorption in aluminosilicate zeolites for postcombustion carbon dioxide capture. *Journal of the American Chemical Society* **134**, 18940-18943 (2012).
61 Grajciar, L. *et al.* Controlling the adsorption enthalpy of CO_2 in zeolites by framework topology and composition. *ChemSusChem* **5**, 2011-2022 (2012).
62 Bae, T.-H. *et al.* Evaluation of cation-exchanged zeolite adsorbents for post-combustion carbon dioxide capture. *Energy & Environmental Science* **6**, 128-138 (2013).
63 Lozinska, M. M. *et al.* Cation gating and relocation during the highly selective "trapdoor" adsorption of CO_2 on univalent cation forms of zeolite rho. *Chemistry of Materials* **26**, 2052-2061 (2014).
64 Siriwardane, R. V., Shen, M.-S., Fisher, E. P. & Losch, J. Adsorption of CO_2 on zeolites at moderate temperatures. *Energy & Fuels* **19**, 1153-1159 (2005).
65 Harlick, P. J. & Tezel, F. H. An experimental adsorbent screening study for CO_2 removal from N_2. *Microporous and Mesoporous Materials* **76**, 71-79 (2004).
66 Hauchhum, L. & Mahanta, P. Carbon dioxide adsorption on zeolites and activated carbon by pressure swing adsorption in a fixed bed. *International Journal of Energy and Environmental Engineering* **5**, 349-356 (2014).
67 Brandani, F. & Ruthven, D. M. The effect of water on the adsorption of CO_2 and C_3H_8 on type X zeolites. *Industrial & engineering chemistry research* **43**, 8339-8344 (2004).
68 Sircar, S., Golden, T. & Rao, M. Activated carbon for gas separation and storage. *Carbon* **34**, 1-12 (1996).
69 Creamer, A. E. & Gao, B. Carbon-based adsorbents for postcombustion CO_2 capture: a critical review. *Environmental science & technology* **50**, 7276-7289 (2016).
70 Maciá-Agulló, J., Moore, B., Cazorla-Amorós, D. & Linares-Solano, A. Activation of coal tar pitch carbon fibres: Physical activation vs. chemical activation. *Carbon* **42**, 1367-1370 (2004).
71 Williams, P. T. & Reed, A. R. Development of activated carbon pore structure via physical and chemical activation of biomass fibre waste. *Biomass and Bioenergy* **30**, 144-152 (2006).
72 Kacem, M., Pellerano, M. & Delebarre, A. Pressure swing adsorption for CO_2/N_2 and CO_2/CH_4 separation: Comparison between activated carbons and zeolites performances. *Fuel Processing Technology* **138**, 271-283 (2015).
73 Zhang, Z., Zhang, W., Chen, X., Xia, Q. & Li, Z. Adsorption of CO_2 on zeolite 13X and activated carbon with higher surface area. *Separation Science and Technology* **45**, 710-719 (2010).
74 Siriwardane, R. V., Shen, M.-S., Fisher, E. P. & Poston, J. A. Adsorption of CO_2 on molecular sieves and activated carbon. *Energy & Fuels* **15**, 279-284 (2001).
75 Kim, J.-H. *et al.* Adsorption equilibria of water vapor on alumina, zeolite 13X, and a zeolite X/activated carbon composite. *Journal of Chemical & Engineering Data* **48**, 137-141 (2003).
76 Shafeeyan, M. S., Daud, W. M. A. W., Houshmand, A. & Shamiri, A. A review on surface modification of activated carbon for carbon dioxide adsorption. *Journal of Analytical and Applied Pyrolysis* **89**, 143-151 (2010).

77 Figueiredo, J. L., Pereira, M., Freitas, M. & Orfao, J. Modification of the surface chemistry of activated carbons. *carbon* **37**, 1379-1389 (1999).
78 Pevida, C. *et al.* Surface modification of activated carbons for CO_2 capture. *Applied Surface Science* **254**, 7165-7172 (2008).
79 Furukawa, H., Cordova, K. E., O'Keeffe, M. & Yaghi, O. M. The chemistry and applications of metal-organic frameworks. *Science* **341**, 1230444 (2013).
80 Zhou, H.-C., Long, J. R. & Yaghi, O. M. ACS Publications, 2012.
81 Maurin, G., Serre, C., Cooper, A. & Férey, G. The new age of MOFs and of their porous-related solids. *Chemical Society Reviews* **46**, 3104-3107 (2017).
82 Yaghi, O. M. ACS Publications, 2016.
83 Lee, Y.-R., Kim, J. & Ahn, W.-S. Synthesis of metal-organic frameworks: A mini review. *Korean Journal of Chemical Engineering* **30**, 1667-1680 (2013).
84 Stock, N. & Biswas, S. Synthesis of metal-organic frameworks (MOFs): routes to various MOF topologies, morphologies, and composites. *Chemical reviews* **112**, 933-969 (2011).
85 Stock, N. High-throughput investigations employing solvothermal syntheses. *Microporous and mesoporous materials* **129**, 287-295 (2010).
86 Banerjee, R. *et al.* High-throughput synthesis of zeolitic imidazolate frameworks and application to CO2 capture. *Science* **319**, 939-943 (2008).
87 Bauer, S. *et al.* High-throughput assisted rationalization of the formation of metal organic frameworks in the iron (III) aminoterephthalate solvothermal system. *Inorganic chemistry* **47**, 7568-7576 (2008).
88 Ahnfeldt, T. *et al.* Synthesis and modification of a functionalized 3D open-framework structure with MIL-53 topology. *Inorganic chemistry* **48**, 3057-3064 (2009).
89 Volkringer, C. *et al.* High-throughput aided synthesis of the porous metal− organic framework-type aluminum pyromellitate, MIL-121, with extra carboxylic acid functionalization. *Inorganic chemistry* **49**, 9852-9862 (2010).
90 Reinsch, H. *et al.* A new aluminium-based microporous metal–organic framework: Al (BTB)(BTB= 1, 3, 5-benzenetrisbenzoate). *Microporous and mesoporous materials* **157**, 50-55 (2012).
91 Sonnauer, A. *et al.* Giant Pores in a Chromium 2, 6-Naphthalenedicarboxylate Open-Framework Structure with MIL-101 Topology. *Angewandte Chemie International Edition* **48**, 3791-3794 (2009).
92 Maniam, P. & Stock, N. Investigation of porous Ni-based metal–organic frameworks containing paddle-wheel type inorganic building units via high-throughput methods. *Inorganic chemistry* **50**, 5085-5097 (2011).
93 Sumida, K. *et al.* Hydrogen storage and carbon dioxide capture in an iron-based sodalite-type metal–organic framework (Fe-BTT) discovered via high-throughput methods. *Chemical Science* **1**, 184-191 (2010).
94 Kelty, M. *et al.* High-throughput synthesis and characterization of nanocrystalline porphyrinic zirconium metal–organic frameworks. *Chemical Communications* **52**, 7854-7857 (2016).
95 Lu, W. *et al.* Tuning the structure and function of metal–organic frameworks via linker design. *Chemical Society Reviews* **43**, 5561-5593 (2014).

96 Moghadam, P. Z. *et al.* Development of a Cambridge Structural Database subset: a collection of metal–organic frameworks for past, present, and future. *Chemistry of Materials* **29**, 2618-2625 (2017).
97 Hönicke, I. M. *et al.* Balancing Mechanical Stability and Ultrahigh Porosity in Crystalline Framework Materials. *Angewandte Chemie International Edition* **57**, 13780-13783 (2018).
98 Farha, O. K. *et al.* Metal–organic framework materials with ultrahigh surface areas: is the sky the limit? *Journal of the American Chemical Society* **134**, 15016-15021 (2012).
99 Ding, M., Flaig, R. W., Jiang, H.-L. & Yaghi, O. M. Carbon capture and conversion using metal–organic frameworks and MOF-based materials. *Chemical Society Reviews* **48**, 2783-2828 (2019).
100 Belmabkhout, Y., Guillerm, V. & Eddaoudi, M. Low concentration CO_2 capture using physical adsorbents: Are metal–organic frameworks becoming the new benchmark materials? *Chemical Engineering Journal* **296**, 386-397 (2016).
101 Lin, Y., Kong, C., Zhang, Q. & Chen, L. Metal-organic frameworks for carbon dioxide capture and methane storage. *Advanced Energy Materials* **7**, 1601296 (2017).
102 Yu, J. *et al.* CO_2 capture and separations using MOFs: computational and experimental studies. *Chemical reviews* **117**, 9674-9754 (2017).
103 Li, H. *et al.* Recent advances in gas storage and separation using metal–organic frameworks. *Materials Today* **21**, 108-121 (2018).
104 Trickett, C. A. *et al.* The chemistry of metal–organic frameworks for CO_2 capture, regeneration and conversion. *Nature Reviews Materials* **2**, 17045 (2017).
105 Chui, S. S.-Y., Lo, S. M.-F., Charmant, J. P., Orpen, A. G. & Williams, I. D. A chemically functionalizable nanoporous material $[Cu_3(TMA)_2(H_2O)_3]$ n. *Science* **283**, 1148-1150 (1999).
106 Férey, G. *et al.* A hybrid solid with giant pores prepared by a combination of targeted chemistry, simulation, and powder diffraction. *Angewandte Chemie International Edition* **43**, 6296-6301 (2004).
107 Férey, G. *et al.* A chromium terephthalate-based solid with unusually large pore volumes and surface area. *Science* **309**, 2040-2042 (2005).
108 Rosi, N. L. *et al.* Rod packings and metal− organic frameworks constructed from rod-shaped secondary building units. *Journal of the American Chemical Society* **127**, 1504-1518 (2005).
109 Britt, D., Furukawa, H., Wang, B., Glover, T. G. & Yaghi, O. M. Highly efficient separation of carbon dioxide by a metal-organic framework replete with open metal sites. *Proceedings of the National Academy of Sciences* **106**, 20637-20640 (2009).
110 Kizzie, A. C., Wong-Foy, A. G. & Matzger, A. J. Effect of humidity on the performance of microporous coordination polymers as adsorbents for CO_2 capture. *Langmuir* **27**, 6368-6373 (2011).
111 Yu, J. & Balbuena, P. B. Water effects on postcombustion CO_2 capture in Mg-MOF-74. *The Journal of Physical Chemistry C* **117**, 3383-3388 (2013).
112 Cavka, J. H. *et al.* A New Zirconium Inorganic Building Brick Forming Metal Organic Frameworks with Exceptional Stability. *J. Am. Chem. Soc.* **130**, 13850-13851, doi:10.1021/ja8057953 (2008).

113 Biswas, S. & Van Der Voort, P. A general strategy for the synthesis of functionalised UiO-66 frameworks: characterisation, stability and CO_2 adsorption properties. *European Journal of Inorganic Chemistry* **2013**, 2154-2160 (2013).
114 Cmarik, G. E., Kim, M., Cohen, S. M. & Walton, K. S. Tuning the adsorption properties of UiO-66 via ligand functionalization. *Langmuir* **28**, 15606-15613 (2012).
115 Si, X. *et al.* High and selective CO_2 uptake, H_2 storage and methanol sensing on the amine-decorated 12-connected MOF CAU-1. *Energy & Environmental Science* **4**, 4522-4527 (2011).
116 An, J., Geib, S. J. & Rosi, N. L. High and selective CO_2 uptake in a cobalt adeninate metal− organic framework exhibiting pyrimidine-and amino-decorated pores. *Journal of the American Chemical Society* **132**, 38-39 (2009).
117 Demessence, A., D'Alessandro, D. M., Foo, M. L. & Long, J. R. Strong CO_2 binding in a water-stable, triazolate-bridged metal− organic framework functionalized with ethylenediamine. *Journal of the American Chemical Society* **131**, 8784-8786 (2009).
118 McDonald, T. M., D'Alessandro, D. M., Krishna, R. & Long, J. R. Enhanced carbon dioxide capture upon incorporation of N, N'-dimethylethylenediamine in the metal–organic framework CuBTTri. *Chemical Science* **2**, 2022-2028 (2011).
119 Mulfort, K. L., Farha, O. K., Malliakas, C. D., Kanatzidis, M. G. & Hupp, J. T. An interpenetrated framework material with hysteretic CO_2 uptake. *Chemistry–A European Journal* **16**, 276-281 (2010).
120 McDonald, T. M. *et al.* Capture of carbon dioxide from air and flue gas in the alkylamine-appended metal–organic framework mmen-Mg_2 (dobpdc). *Journal of the American Chemical Society* **134**, 7056-7065 (2012).
121 McDonald, T. M. *et al.* Cooperative insertion of CO_2 in diamine-appended metal-organic frameworks. *Nature* **519**, 303 (2015).
122 Nugent, P. *et al.* Porous materials with optimal adsorption thermodynamics and kinetics for CO_2 separation. *Nature* **495**, 80 (2013).
123 Shekhah, O. *et al.* Made-to-order metal-organic frameworks for trace carbon dioxide removal and air capture. *Nature communications* **5**, 4228 (2014).
124 Gong, Y.-N., Zhong, D.-C. & Lu, T.-B. Interpenetrating metal–organic frameworks. *CrystEngComm* **18**, 2596-2606 (2016).
125 Serre, C. *et al.* Very Large Breathing Effect in the First Nanoporous Chromium (III)-Based Solids: MIL-53 or CrIII (OH){O_2C− C_6H_4− CO_2}{HO_2C− C_6H_4− CO_2H} x.H_2O y. *Journal of the American chemical society* **124**, 13519-13526 (2002).
126 Yazaydın, A. O. z. r. *et al.* Screening of metal− organic frameworks for carbon dioxide capture from flue gas using a combined experimental and modeling approach. *Journal of the American Chemical Society* **131**, 18198-18199 (2009).
127 Mason, J. A. *et al.* Application of a high-throughput analyzer in evaluating solid adsorbents for post-combustion carbon capture via multicomponent adsorption of CO_2, N_2, and H_2O. *Journal of the American Chemical society* **137**, 4787-4803 (2015).

128 Mason, J. A., Sumida, K., Herm, Z. R., Krishna, R. & Long, J. R. Evaluating metal–organic frameworks for post-combustion carbon dioxide capture via temperature swing adsorption. *Energy & Environmental Science* **4**, 3030-3040 (2011).
129 Soubeyrand-Lenoir, E. *et al.* How water fosters a remarkable 5-fold increase in low-pressure CO_2 uptake within mesoporous MIL-100 (Fe). *Journal of the American Chemical Society* **134**, 10174-10181 (2012).
130 González-Zamora, E. & Ibarra, I. A. CO_2 capture under humid conditions in metal–organic frameworks. *Materials Chemistry Frontiers* **1**, 1471-1484 (2017).
131 Canivet, J., Fateeva, A., Guo, Y., Coasne, B. & Farrusseng, D. Water adsorption in MOFs: fundamentals and applications. *Chemical Society Reviews* **43**, 5594-5617 (2014).
132 Li, H., Eddaoudi, M., Groy, T. L. & Yaghi, O. Establishing microporosity in open metal− organic frameworks: Gas sorption isotherms for Zn (BDC)(BDC= 1, 4-benzenedicarboxylate). *Journal of the American Chemical Society* **120**, 8571-8572 (1998).
133 Li, H., Eddaoudi, M., O'Keeffe, M. & Yaghi, O. M. Design and synthesis of an exceptionally stable and highly porous metal-organic framework. *nature* **402**, 276 (1999).
134 Rowsell, J. L. & Yaghi, O. M. Effects of functionalization, catenation, and variation of the metal oxide and organic linking units on the low-pressure hydrogen adsorption properties of metal− organic frameworks. *Journal of the American Chemical Society* **128**, 1304-1315 (2006).
135 Chae, H. K. *et al.* A route to high surface area, porosity and inclusion of large molecules in crystals. *Nature* **427**, 523 (2004).
136 Benoit, V. *et al.* A promising metal–organic framework (MOF), MIL-96 (Al), for CO_2 separation under humid conditions. *Journal of Materials Chemistry A* **6**, 2081-2090 (2018).
137 Chanut, N. *et al.* Screening the effect of water vapour on gas adsorption performance: application to CO_2 capture from flue gas in metal–organic frameworks. *ChemSusChem* **10**, 1543-1553 (2017).
138 Le, T. C. & Winkler, D. A. Discovery and optimization of materials using evolutionary approaches. *Chemical reviews* **116**, 6107-6132 (2016).
139 Mason, J. A., Veenstra, M. & Long, J. R. Evaluating metal–organic frameworks for natural gas storage. *Chemical Science* **5**, 32-51 (2014).
140 Borfecchia, E. *et al.* Insights into adsorption of NH3 on HKUST-1 metal–organic framework: a multitechnique approach. *The Journal of Physical Chemistry C* **116**, 19839-19850 (2012).
141 Li, L. *et al.* A MOF/graphite oxide hybrid (MOF: HKUST-1) material for the adsorption of methylene blue from aqueous solution. *Journal of Materials Chemistry A* **1**, 10292-10299 (2013).
142 Moosavi, S. M. *et al.* Capturing chemical intuition in synthesis of metal-organic frameworks. *Nature communications* **10**, 1-7 (2019).
143 Zacher, D., Liu, J., Huber, K. & Fischer, R. A. Nanocrystals of $[Cu_3(btc)_2]$(HKUST-1): a combined time-resolved light scattering and scanning electron microscopy study. *Chemical communications*, 1031-1033 (2009).
144 Millange, F. *et al.* Time-Resolved In Situ Diffraction Study of the Solvothermal Crystallization of Some Prototypical Metal–Organic Frameworks. *Angewandte Chemie International Edition* **49**, 763-766 (2010).

145 Wang, F., Guo, H., Chai, Y., Li, Y. & Liu, C. The controlled regulation of morphology and size of HKUST-1 by "coordination modulation method". *Microporous and mesoporous materials* **173**, 181-188 (2013).
146 Bhunia, M. K., Hughes, J. T., Fettinger, J. C. & Navrotsky, A. Thermochemistry of paddle wheel MOFs: Cu-HKUST-1 and Zn-HKUST-1. *Langmuir* **29**, 8140-8145 (2013).
147 Feldblyum, J. I., Liu, M., Gidley, D. W. & Matzger, A. J. Reconciling the discrepancies between crystallographic porosity and guest access as exemplified by Zn-HKUST-1. *Journal of the american chemical society* **133**, 18257-18263 (2011).
148 Biemmi, E., Christian, S., Stock, N. & Bein, T. High-throughput screening of synthesis parameters in the formation of the metal-organic frameworks MOF-5 and HKUST-1. *Microporous and Mesoporous Materials* **117**, 111-117 (2009).
149 Liu, J. *et al.* CO_2/H_2O adsorption equilibrium and rates on metal− organic frameworks: HKUST-1 and Ni/DOBDC. *Langmuir* **26**, 14301-14307 (2010).
150 Möllmer, J., Möller, A., Dreisbach, F., Gläser, R. & Staudt, R. High pressure adsorption of hydrogen, nitrogen, carbon dioxide and methane on the metal–organic framework HKUST-1. *Microporous and Mesoporous Materials* **138**, 140-148 (2011).
151 Krawiec, P. *et al.* Improved Hydrogen Storage in the Metal-Organic Framework $Cu_3(BTC)_2$. *Advanced Engineering Materials* **8**, 293-296 (2006).
152 Klein, N., Henschel, A. & Kaskel, S. n-Butane adsorption on $Cu_3(btc)_2$ and MIL-101. *Microporous and mesoporous materials* **129**, 238-242 (2010).
153 Wee, L. H., Lohe, M. R., Janssens, N., Kaskel, S. & Martens, J. A. Fine tuning of the metal–organic framework $Cu_3(BTC)_2$ HKUST-1 crystal size in the 100 nm to 5 micron range. *Journal of Materials Chemistry* **22**, 13742-13746 (2012).
154 Lin, K.-S., Adhikari, A. K., Ku, C.-N., Chiang, C.-L. & Kuo, H. Synthesis and characterization of porous HKUST-1 metal organic frameworks for hydrogen storage. *International journal of hydrogen energy* **37**, 13865-13871 (2012).
155 Chowdhury, P., Mekala, S., Dreisbach, F. & Gumma, S. Adsorption of CO, CO_2 and CH_4 on Cu-BTC and MIL-101 metal organic frameworks: Effect of open metal sites and adsorbate polarity. *Microporous and Mesoporous Materials* **152**, 246-252 (2012).
156 Liu, J. *et al.* Experimental and theoretical studies of gas adsorption in $Cu_3(BTC)_2$: an effective activation procedure. *The Journal of Physical Chemistry C* **111**, 9305-9313 (2007).
157 Wiersum, A. D., Chang, J.-S., Serre, C. & Llewellyn, P. L. An adsorbent performance indicator as a first step evaluation of novel sorbents for gas separations: application to metal–organic frameworks. *Langmuir* **29**, 3301-3309 (2013).
158 Senkovska, I. & Kaskel, S. High pressure methane adsorption in the metal-organic frameworks $Cu_3(btc)_2$, Zn2(bdc)2dabco, and $Cr_3F(H_2O)_2O(bdc)_3$. *Microporous and Mesoporous Materials* **112**, 108-115 (2008).
159 Küsgens, P. *et al.* Characterization of metal-organic frameworks by water adsorption. *Microporous and Mesoporous Materials* **120**, 325-330 (2009).
160 Münch, A. S. & Mertens, F. O. HKUST-1 as an open metal site gas chromatographic stationary phase—capillary preparation, separation of small hydrocarbons and electron donating

compounds, determination of thermodynamic data. *Journal of Materials Chemistry* **22**, 10228-10234 (2012).

161 Zhao, Z. *et al.* Competitive adsorption and selectivity of benzene and water vapor on the microporous metal organic frameworks (HKUST-1). *Chemical engineering journal* **259**, 79-89 (2015).

162 Huo, J., Brightwell, M., El Hankari, S., Garai, A. & Bradshaw, D. A versatile, industrially relevant, aqueous room temperature synthesis of HKUST-1 with high space-time yield. *Journal of Materials Chemistry A* **1**, 15220-15223 (2013).

163 Ye, S. *et al.* Post-combustion CO_2 capture with the HKUST-1 and MIL-101 (Cr) metal–organic frameworks: Adsorption, separation and regeneration investigations. *Microporous and Mesoporous Materials* **179**, 191-197 (2013).

164 Chen, H., Wang, L., Yang, J. & Yang, R. T. Investigation on hydrogenation of metal–organic frameworks HKUST-1, MIL-53, and ZIF-8 by hydrogen spillover. *The Journal of Physical Chemistry C* **117**, 7565-7576 (2013).

165 Wong-Foy, A. G., Matzger, A. J. & Yaghi, O. M. Exceptional H_2 saturation uptake in microporous metal− organic frameworks. *Journal of the American Chemical Society* **128**, 3494-3495 (2006).

166 Yan, X., Komarneni, S., Zhang, Z. & Yan, Z. Extremely enhanced CO_2 uptake by HKUST-1 metal–organic framework via a simple chemical treatment. *Microporous and mesoporous materials* **183**, 69-73 (2014).

167 Rocío-Bautista, P. *et al.* The metal–organic framework HKUST-1 as efficient sorbent in a vortex-assisted dispersive micro solid-phase extraction of parabens from environmental waters, cosmetic creams, and human urine. *Talanta* **139**, 13-20 (2015).

168 Raganati, F., Gargiulo, V., Ammendola, P., Alfe, M. & Chirone, R. CO_2 capture performance of HKUST-1 in a sound assisted fluidized bed. *Chemical Engineering Journal* **239**, 75-86 (2014).

169 Al-Janabi, N. *et al.* Mapping the Cu-BTC metal–organic framework (HKUST-1) stability envelope in the presence of water vapour for CO_2 adsorption from flue gases. *Chemical Engineering Journal* **281**, 669-677 (2015).

170 Wang, Q. M. *et al.* Metallo-organic molecular sieve for gas separation and purification. *Microporous and mesoporous materials* **55**, 217-230 (2002).

171 Millward, A. R. & Yaghi, O. M. Metal− organic frameworks with exceptionally high capacity for storage of carbon dioxide at room temperature. *Journal of the American Chemical Society* **127**, 17998-17999 (2005).

172 Panella, B., Hirscher, M., Pütter, H. & Müller, U. Hydrogen adsorption in metal–organic frameworks: Cu-MOFs and Zn-MOFs compared. *Advanced Functional Materials* **16**, 520-524 (2006).

173 Hartmann, M. *et al.* Adsorptive separation of isobutene and isobutane on $Cu_3(BTC)_2$. *Langmuir* **24**, 8634-8642 (2008).

174 Schlesinger, M., Schulze, S., Hietschold, M. & Mehring, M. Evaluation of synthetic methods for microporous metal–organic frameworks exemplified by the competitive formation of $[Cu_2(btc)_3(H_2O)_3]$ and $[Cu_2(btc)(OH)(H2O)]$. *Microporous and Mesoporous Materials* **132**, 121-127 (2010).

175 Seo, Y.-K. *et al.* Microwave synthesis of hybrid inorganic–organic materials including porous $Cu_3(BTC)_2$ from Cu (II)-trimesate mixture. *Microporous and Mesoporous Materials* **119**, 331-337 (2009).
176 Li, Y. & Yang, R. T. Hydrogen storage in metal-organic and covalent-organic frameworks by spillover. *AIChE Journal* **54**, 269-279 (2008).
177 Li, Z.-Q. *et al.* Ultrasonic synthesis of the microporous metal–organic framework $Cu_3(BTC)_2$ at ambient temperature and pressure: an efficient and environmentally friendly method. *Materials Letters* **63**, 78-80 (2009).
178 Kim, H. K. *et al.* A Chemical route to activation of open metal sites in the copper-based metal–organic framework materials HKUST-1 and Cu-MOF-2. *Journal of the American Chemical Society* **137**, 10009-10015 (2015).
179 Elsaidi, S. K. *et al.* Xenon recovery at room temperature using metal–organic frameworks. *Chemistry–A European Journal* **23**, 10758-10762 (2017).
180 Chowdhury, P., Bikkina, C., Meister, D., Dreisbach, F. & Gumma, S. Comparison of adsorption isotherms on Cu-BTC metal organic frameworks synthesized from different routes. *Microporous and Mesoporous Materials* **117**, 406-413 (2009).
181 Mu, X., Chen, Y., Lester, E. & Wu, T. Optimized synthesis of nano-scale high quality HKUST-1 under mild conditions and its application in CO_2 capture. *Microporous and Mesoporous Materials* **270**, 249-257 (2018).
182 Boyd, P. G. *et al.* Data-driven design of metal–organic frameworks for wet flue gas CO_2 capture. *Nature* **576**, 253-256 (2019).
183 Fateeva, A. *et al.* A Water-Stable Porphyrin-Based Metal–Organic Framework Active for Visible-Light Photocatalysis. *Angewandte Chemie International Edition* **51**, 7440-7444 (2012).
184 Stylianou, K. C. *et al.* A guest-responsive fluorescent 3D microporous metal− organic framework derived from a long-lifetime pyrene core. *Journal of the American Chemical Society* **132**, 4119-4130 (2010).
185 Krüger, M. *et al.* $[Al_2(OH)_2(TCPB)]$–An Al-MOF based on a tetratopic linker molecule. *Microporous and Mesoporous Materials* **216**, 27-35 (2015).
186 Dyadkin, V., Pattison, P., Dmitriev, V. & Chernyshov, D. A new multipurpose diffractometer PILATUS@SNBL. *J Synchrotron Radiat* **23**, 825-829, doi:10.1107/S1600577516002411 (2016).
187 Coelho, A. A. Whole-profile structure solution from powder diffraction data using simulated annealing. *J. Appl. Crystallogr.* **33**, 899-908, doi:10.1107/S002188980000248x (2000).
188 Carrington, E. J., Vitorica-Yrezabal, I. J. & Brammer, L. Crystallographic studies of gas sorption in metal-organic frameworks. *Acta Crystallographica Section B-Structural Science Crystal Engineering and Materials* **70**, 404-422, doi:10.1107/S2052520614009834 (2014).
189 Smeets, S. *et al.* Locating Organic Guests in Inorganic Host Materials from X-ray Powder Diffraction Data. *J. Am. Chem. Soc.* **138**, 7099-7106, doi:10.1021/jacs.6b02953 (2016).
190 Queen, W. L. *et al.* Comprehensive study of carbon dioxide adsorption in the metal-organic frameworks $M_2(dobdc)$ (M = Mg, Mn, Fe, Co, Ni, Cu, Zn). *Chem. Sci.* **5**, 4569-4581, doi:10.1039/c4sc02064b (2014).

191 Stephens, P. W. Phenomenological model of anisotropic peak broadening in powder diffraction. *J. Appl. Crystallogr.* **32**, 281-289, doi:10.1107/S0021889898006001 (1999).
192 Clark, S. J. *et al.* First principles methods using CASTEP. *Z Kristallogr* **220**, 567-570, doi:10.1524/zkri.220.5.567.65075 (2005).
193 Pickard, C. J. & Mauri, F. All-electron magnetic response with pseudopotentials: NMR chemical shifts. *Physical Review B* **63**, doi:10.1103/PhysRevB.63.245101 (2001).
194 Yates, J. R., Pickard, C. J. & Mauri, F. Calculation of NMR chemical shifts for extended systems using ultrasoft pseudopotentials. *Physical Review B* **76**, doi:10.1103/PhysRevB.76.024401 (2007).
195 Fulmer, G. R. *et al.* NMR Chemical Shifts of Trace Impurities: Common Laboratory Solvents, Organics, and Gases in Deuterated Solvents Relevant to the Organometallic Chemist. *Organometallics* **29**, 2176-2179, doi:10.1021/om100106e (2010).
196 Witherspoon, V. J., Xu, J. & Reimer, J. A. Solid-State NMR Investigations of Carbon Dioxide Gas in Metal-Organic Frameworks: Insights into Molecular Motion and Adsorptive Behavior. *Chemical Reviews* **118**, 10033-10048, doi:10.1021/acs.chemrev.7b00695 (2018).
197 Massiot, D. *et al.* Modelling one- and two-dimensional solid-state NMR spectra. *Magn Reson Chem* **40**, 70-76, doi:10.1002/mrc.984 (2002).
198 Couck, S. *et al.* An Amine-Functionalized MIL-53 Metal-Organic Framework with Large Separation Power for CO_2 and CH_4. *J. Am. Chem. Soc.* **131**, 6326-+, doi:10.1021/ja900555r (2009).
199 Garcia, S. *et al.* Breakthrough adsorption study of a commercial activated carbon for pre-combustion CO_2 capture. *Chemical Engineering Journal* **171**, 549-556, doi:10.1016/j.cej.2011.04.027 (2011).
200 Garcia, S., Gil, M. V., Pis, J. J., Rubiera, F. & Pevida, C. Cyclic operation of a fixed-bed pressure and temperature swing process for CO_2 capture: Experimental and statistical analysis. *Int. J. Greenh. Gas Control* **12**, 35-43, doi:10.1016/j.ijggc.2012.10.018 (2013).
201 Alvarez-Gutierrez, N., Garcia, S., Gil, M. V., Rubiera, F. & Pevida, C. Dynamic Performance of Biomass-Based Carbons for CO_2/CH_4 Separation. Approximation to a Pressure Swing Adsorption Process for Biogas Upgrading. *Energ Fuel* **30**, 5005-5015, doi:10.1021/acs.energyfuels.6b00664 (2016).
202 Li, G. *et al.* Capture of CO_2 from high humidity flue gas by vacuum swing adsorption with zeolite 13X. *Adsorption-Journal of the International Adsorption Society* **14**, 415-422, doi:10.1007/s10450-007-9100-y (2008).
203 Choi, S., Drese, J. H. & Jones, C. W. Adsorbent Materials for Carbon Dioxide Capture from Large Anthropogenic Point Sources. *ChemSusChem* **2**, 796-854, doi:10.1002/cssc.200900036 (2009).
204 Wang, C. H., Liu, X. L., Demir, N. K., Chen, J. P. & Li, K. Applications of water stable metal-organic frameworks. *Chem. Soc. Rev.* **45**, 5107-5134, doi:10.1039/c6cs00362a (2016).
205 Chidambaram, A. & Stylianou, K. C. Electronic metal–organic framework sensors. *Inorganic Chemistry Frontiers* **5**, 979-998 (2018).
206 Stassen, I. *et al.* An updated roadmap for the integration of metal–organic frameworks with electronic devices and chemical sensors. *Chemical Society Reviews* **46**, 3185-3241 (2017).
207 Stassen, I. *et al.* Chemical vapour deposition of zeolitic imidazolate framework thin films. *Nature materials* **15**, 304 (2016).

208 Cruz, A. J. *et al.* An integrated cleanroom process for the vapor-phase deposition of large-area zeolitic imidazolate framework thin films. *Chemistry of Materials* (2019).
209 Sturluson, A. *et al.* Curating metal-organic frameworks to compose robust gas sensor arrays in dilute conditions. (2019).
210 Campbell, M. G., Liu, S. F., Swager, T. M. & Dincă, M. Chemiresistive sensor arrays from conductive 2D metal–organic frameworks. *Journal of the American Chemical Society* **137**, 13780-13783 (2015).

CV

Arunraj Chidambaram

Avenue de Tourbillon 36 B
1950 Sion
Switzerland

+41 786 64 97 36
arunchid92@gmail.com
Skype: arunraj.chidambaram
LinkedIn profile

STRENGTHS

- A chemical engineer with PhD level of experience in applying innovation for solving technical problems
- Versatile with academic and research backgrounds in chemistry and chemical engineering
- Proven track record of transformation of theoretical concepts into new products and/or processes
- Expertise in high-throughput robotic synthesis, characterization experiments and carbon capture
- Solid experience in project management skills
    - Conceptual design, planning, development, testing and writing publications, reports, patents
    - Aptitude for insightful data analysis, interpretation and corresponding plan of design of experiments
- Multitasker with progress and result driven attitude, highly organized and autonomous working style
- Interpersonal skills: successful exhibition of working and contributing individually and as well as in teams
- Team player: 7 years of international R&D work experience with academic and industrial partners
- Strong communication and presentation skills

EDUCATION

2016 – present *Expected April 2020*	**Ecole polytechnique fédérale de Lausanne (EPFL), Lausanne, Switzerland** PhD candidate, Chemistry and Chemical Engineering
Sep 2013 – Nov 2015	**Delft University of Technology (TU Delft), Delft, The Netherlands** Master of Science M.Sc., in Chemical Engineering
Aug 2009 - May 2013	**Anna University, Chennai, India** Bachelor of Technology B. Tech in Chemical Engineering

RESEARCH EXPERIENCE

Doctoral thesis
May 2016 – Jan 2020

Accelerated Discovery of Metal-Organic Frameworks (MOFs) for Energy Related Applications
Laboratory of Molecular Simulations (LSMO). EPFL Valais Wallis, Sion, Switzerland

The main aim of this thesis is to contribute to the development of MOFs as adsorbents for efficient carbon capture from wet flue gas. I designed and developed MOFs which exhibited carbon capture performance better than the commercially available adsorbents like zeolite, activated carbon. This is considered as breakthrough and the work is published in Nature. Furthermore, I mastered the various testing and analyzing experiments and with which I carried out the validation studies and improved the stability and performance of the synthesized adsorbents. In addition, I co-developed a synthetic platform for improving the capacity, efficiency of MOF synthesis.

M.Sc. internship
July – Dec 2015

Testing the chemical resistance of thermoplastic composite pipes
Airborne Oil and Gas, Ijmuiden, The Netherlands

My objective was to devise an assessment methodology to efficiently test the chemical resistance of thermoplastic composite pipes. In a very short timeframe, I identified the possible mechanism through simulations and devised my experiments accordingly. This led for further research work in their R&D group.

M.Sc. thesis
Aug 2014 – May 2015

Synthesis, characterization of 2D nanohybrid materials and their electroanalytical applications
Organic Materials & Interface (OMI) group, Department of Chemical Engineering, TU Delft, The Netherlands

My objective was to establish the synthetic conditions of the highly versatile 2D nanosheets and transform them to diverse nanohybrids. The resultant nanohybrids were analysed and employed as (electro) catalysts to detect wide range of compounds and biomolecules. In a very short timeframe, I amassed the required knowledge of exfoliation of nanosheets, electroanalytical chemistry and developed the projects simultaneously. It resulted in two publications.

M.Sc. project
April – July 2014

Conceptual process and product design project
FrieslandCampina, Bedum, The Netherlands

Our aim here was to design an industrial cleaning mechanism of cheese moulds which is energy efficient and cost-effective for the Dutch dairy cooperative. The proposed product design and the economic, ecological analysis was well received and was considered to lead to significant savings for their dairy plant.

Bachelor thesis
Dec 2012 – June 2013

Fabrication of compact heat exchanger for using phase change materials for thermal management in fuel cells
Centre for Fuel Cell Technology, Indian Institute of Technology Madras (IITM) research park, Chennai, India

Our aim here was to design a heat exchanger that can control the temperature of the air that is supplied to the proton exchange membrane fuel cell stack. We explored the absorption of heat through liquid phase change and solid phase change concepts. The proposed heat exchanger was demonstrated to be efficient in removing the amount of heat that was supplied to the fuel cell stack.

Bachelor projects
August 2011 – June 2012

Targeted drug delivery with nanoparticles and (bio) polymers for cancer cells
Department of Chemical Engineering, SSN college of Engineering, Chennai, India

The objective here was to investigate the encapsulation efficiency of cancer treatment drugs along with nanoparticles in (bio) polymers like chitosan, polylactic acid. They were analysed for their *in-vitro* drug release efficacy. These research works resulted in two publications.

Synthesis of silver nanoparticles using bio extract and its usage in water purification
Department of Chemical Engineering, SSN college of Engineering, Chennai, India

The aim here was to synthesize nanoparticles from bio-sources such as *azadirachta indica* (neem leaves) and characterize them. Furthermore, a filtrate that incorporated the nanoparticles was developed and tested for their antibacterial properties in a drinking water contaminated with E.coli.

TECHNICAL SKILLS

Materials synthesis

- High-throughput experimentation with automated robotic synthesis and screening of materials
- I was the reference person in my PhD research group for high-throughput synthesis
- Microwave, solvothermal and spray drying synthesis
- Exfoliation of layered materials - nanosheets
- Nanoparticle, nanocomposite synthesis

Structure-property relationship of materials

Porosity characterization
- Surface area and porosity analysis – BET surface area, pore volume, gas and vapour isotherms, fixed bed breakthrough experiments, gas phase pulse chromatogram, temperature programmed desorption (TPD)
- I was the reference person in my PhD research group for porosity characterization

Thermal analysis
- Thermal gravimetric analysis (TGA), Differential Scanning calorimetry (DSC)

Crystallinity characterization
- Powder X-ray diffraction (PXRD), variable temperature and *in-situ* gas loading PXRD, Synchrotron experiences

Spectroscopy characterization
- FT-IR, UV-VIS, ICP-AES

Morphology characterization
- Scanning electron microscopy (SEM), zetasizer nano, contact angle measurements

Electro-analytical

- Cyclic voltammetry (CV), differential pulse voltammetry (DPV), electrochemical impedance spectroscopy (EIS)

Software Skills

- **Process design and simulation software** Aspen Hysys, Aspen Plus
- **Other software** Matlab, Latex and Microsoft Office, CheFEM, Mercury
- **Working knowledge** of genetic algorithms and artificial intelligence for synthetic chemistry

Chemical engineering subjects

Mass transfer, downstream separation engineering and process evaluation

PUBLICATIONS & PATENTS

- Boyd, P.G., Chidambaram, A., García-Díez, E. et al. Data-driven design of metal–organic frameworks for wet flue gas CO_2 capture. Nature 576, 253–256 (2019) doi:10.1038/s41586-019-1798-7
- Selective adsorption of carbon dioxide by a metal-organic framework, filed on Apr 20, 2018, EU No. EP 18 168 544.7;
- Moosavi SM, Chidambaram A, Talirz L, Haranczyk M, Stylianou KC, Smit B. Capturing chemical intuition in synthesis of metal-organic frameworks. Nature communications. 2019 Feb 1;10(1):539.
- Shyshkanov S, Nguyen TN, Chidambaram A, Stylianou KC, Dyson PJ. Frustrated Lewis pair-mediated fixation of CO_2 within a metal–organic framework. Chemical Communications. 2019;55(73):10964-7.
- Chidambaram A, Stylianou KC. Electronic metal–organic framework sensors. Inorganic Chemistry Frontiers. 2018;5(5):979-98.
- Gładysiak A, Deeg KS, Dovgaliuk I, Chidambaram A, Ordiz K, Boyd PG, Moosavi SM, Ongari D, Navarro JA, Smit B, Stylianou KC. Biporous Metal–Organic Framework with Tunable CO_2/CH_4 Separation Performance Facilitated by Intrinsic Flexibility. ACS applied materials & interfaces. 2018 Sep 24;10(42):36144-56.
- Nguyen TN, Capano G, Gładysiak A, Ebrahim FM, Eliseeva SV, Chidambaram A, Valizadeh B, Petoud S, Smit B, Stylianou KC. Lanthanide-based near-infrared emitting metal–organic frameworks with tunable excitation wavelengths and high quantum yields. Chemical communications. 2018;54(50):6816-9.
- Dolinska J, Chidambaram A, Adamkiewicz W, Estili M, Lisowski W, Iwan M, Palys B, Sudholter EJ, Marken F, Opallo M, Rassaei L. Synthesis and characterization of porous carbon–MoS_2 nanohybrid materials: electrocatalytic performance towards selected biomolecules. Journal of Materials Chemistry B. 2016;4(8):1448-57.
- Dolinska J, Chidambaram A, Taleat Z, Adamkiewicz W, Lisowski W, Palys B, Holdynski M, Andryszewski T, Sashuk V, Rassaei L, Opallo M. Decoration of MoS_2 nanopetal stacks with positively charged gold nanoparticles for synergistic electrocatalytic oxidation of biologically relevant compounds. Electrochimica Acta. 2015 Nov 10;182:659-67.
- Chidambaram A, Kumar PS, Kumar KS. Kinetics and drug release studies of isoniazid encapsulated with PLA-co-PEG/gold nanoparticles. International Journal of Pharmacy and Pharmaceutical Sciences. 2012;4(4):1-7.
- Kumar KS, Gnanaprakash D, Mayilvaganan K, Chidambaram A, Mohankumar S. Chitosan-gold nanoparticles as delivery systems for curcumin. International Journal of Pharmaceutical Sciences and Research. 2012 Nov 1;3(11):4533.
- Google scholar profile https://scholar.google.ch/citations?user=VUhOkyQAAAAJ&hl=en

SOFT SKILLS

- Strong team player with good communication and networking skills

- Able to communicate research results clearly to the professional community as well as to the laymen public
- Presented my projects in several international research conferences and symposiums
    - MOF 2018, Auckland, New Zealand; International conference on MOF materials
    - EUROMOF 2017, Delft, The Netherlands; European conference on MOF materials
    - Electrochem day 2015, Delft, The Netherlands; Symposium
    - Scientastic 2019, open day scientific outreach to public of Valais; presented my work and demonstrated the working of robotic synthesizer platform in French

LANGUAGE PROFICIENCY

- English: Native or bilingual, medium of instruction in school, college (bachelors)
- French: B2, actively learning French, willingness to learn German